Beatriz Martins de Abreu

Licenciatura em Engenharia de Materiais

Bio-inspired nanocellulose composites systems with structural coloration as optical security features

Dissertação para obtenção do Grau de Mestre em
Engenharia de Materiais

Orientador: Susete Fernandes, Ph.D. Researcher at *DCM, Faculdade de Ciência e Tecnologia-Universidade NOVA de Lisboa*

Co-orientador: Luís Filipe Lopes, Ph.D. Researcher at *Instituto de Higiene e Medicina Tropical - Universidade Nova de Lisboa, GHTM, Centre for Ecology, Evolution and Environmental Changes (CE3C)*

Júri:

Presidente: Doutor João Paulo Miranda Ribeiro Borges, Professor Associado com Agregação, FCT – UNL

Arguente: Doutora Maria Helena Godinho, Professora Associada com Agregação, FCT – UNL

Vogal: Doutora Susete Fernandes, Investigadora em Pós-doutoramento, FCT-UNL

FACULDADE DE CIÊNCIAS E TECNOLOGIA
UNIVERSIDADE NOVA DE LISBOA

Outubro, 2019

Bio-inspired nanocellulose composites systems with structural coloration as optical security features

“Lucky is what happens when preparation meets opportunity”

-Seneca

Acknowledgements

Em primeiro lugar, quero agradecer à nossa instituição, a Faculdade de Ciências e Tecnologia da Universidade Nova de Lisboa, ao Departamento das Ciências dos Materiais e ao CENIMAT

Quero agradecer à minha orientadora, Drª Susete Fernandes por me ter inspirado todos estes anos de faculdade e a quem eu considero uma mentora, devido à determinação e dedicação que se entrega a todos os seus trabalhos. Agradeço ao Dr. Luís Filipe Lopes, por quem tenho muito respeito e consideração, e ao Ricardo Chagas e Diogo Saraiva que foram absolutamente incansáveis e indispensáveis durante estes meses de investigação. Estou também muito grata ao Dr. Pedro Silva e aos restantes investigadores do laboratório pela ajuda, disponibilidade e assistência.

Um obrigada especial à minha família que sempre me fez sentir capaz de conquistar o mundo. Aos meus pais que me deram as bases para ser a pessoa que sou hoje. Ao meu avô Martins, avó Esmeralda e bisavó Rosa que me ensinaram o significado de trabalho, resiliência e humildade. E à minha madrinha que me deve uns Louboutin. A vocês devo-vos muito. Obrigada.

Agradeço ao meu namorado Miguel por me acompanhar lado a lado, todos os dias, independentemente se fazia chuva ou sol. Um agradecimento muito especial aos meus amigos, que também fazem parte da minha família. Sem eles a caminhada teria sido muito mais difícil.

Por último, quero agradecer aos meus companheiros de laboratório por terem dividido comigo o stress, as lágrimas e o suor: Rita, Margarida, Adriana, Bárbara, César, Ana Sofia, Pedro e Lavadinho. Foi reconfortante saber que tínhamos sempre o ombro uns dos outros e que daí se pode levar boas amizades.

Este trabalho foi financiado por fundos concedidos pela FEDER através do Programa COMPETE 2020, Fundos Nacionais, através da FCT – Fundação para a Ciência e Tecnologia e também pelo POR Lisboa2020 ao abrigo dos projetos POCI – 01-0145-FEDER-007688 (Referenciar UID/CTM/50025) e PTDC/CTM-REF/30529/2017 (NanoCell2SEC), e também da rede M-ERA.NET pelo projeto com referência M-ERA-NET2/0007/2016 (CellColor).

Resumo

A falsificação possui um impacto significativo na economia da sociedade, havendo a necessidade constante de atualização dos elementos de segurança baseados em dispositivos com propriedades opticamente variáveis (OVDs). Estes exibem efeitos óticos que podem mudar na presença de estímulos externos (como ângulo de visão ou luz), impossibilitando a sua replicação pelos métodos convencionais.

É possível encontrar na natureza, em animais e plantas, magníficas colorações estruturais possíveis devido à interação da luz com as suas estruturas organizacionais à nanoescala. O principal objetivo deste trabalho é mimicar essas estruturas iridescentes e produzir filmes com coloração estrutural que podem ser usados como OVDs.

As membranas de celulose nanocristalina (CNCss), produzidas a partir de suspensões liotrópicas aquosas, exibem iridescência, reflexão seletiva da luz polarizada circular à esquerda e transmissão seletiva da luz polarizada circular à direita. Estas propriedades óticas extraordinárias tornam as CNCss favoráveis à produção de sistemas com coloração estrutural. No entanto, embora estas características sejam extremamente difíceis de reproduzir por técnicas de impressão, as suas membranas tendem a ser quebradiças limitando assim a sua aplicação.

A alteração da coloração estrutural refletida pelos filmes de celulose nanocristalina, produzida por hidrólise ácida, para o comprimento de onda azul é conseguida substituindo o seu contra-ião por potássio (CNCs-K), produzindo-se assim uma ampla gama de cores usando diferentes proporções de CNCs com o protão como contra-ião (CNCs-H) e CNCs-K. A hidroxipropilcelulose (HPC) adicionada em diferentes concentrações, possibilita o ajuste do comprimento de onda refletido das membranas compósitas, preservando a sua organização estrutural e melhorando sua elasticidade. As membranas obtidas mudam para um acabamento *matte* à medida que a concentração de HPC aumenta.

Este trabalho expõe o potencial da manipulação de cores usando CNCs-K, bem como as suas aplicações em membranas de CNCs-K/HPC, melhorando as propriedades mecânicas e mantendo comprimentos de onda refletidos no intervalo da luz visível. Os resultados obtidos abrem caminho para o uso de sistemas 100% celulósicos de CNCs/HPC em soluções de impressão OVDs.

Palavras-chave: celulose nanocristalina, hidroxipropilcelulose, dispositivos opticamente variáveis, troca iónica, membranas compósitas.

Abstract

Counterfeiting has a tremendous economic impact in our society leading to a constant 'upgrade' of the security systems based on optically variable devices (OVDs). OVDs exhibits various optical effects that can change in the presence of external stimulus (viewing angle or light) making them impossible to replicate.

Magnificent structural coloration found in nature, in animals and plants, is due to interaction between light and the nanoscale organization or their structures. The main goal of this work is to mimic these iridescent structures and produce films with structural coloration that can be used as OVDs.

Cellulose nanocrystals (CNCss) films produced from aqueous lyotropic suspensions, exhibit extraordinary optical properties such as iridescence, selective left circularly polarized light reflection and right circularly polarized light transmission. These assets make CNCss suitable to produce systems with structural coloration. Although these optical features are extremely difficult to reproduce by printing or photocopy techniques the films applications are limited due to their physical brittleness.

In this work a shift to the blue wavelength of the cellulose nanocrystals, obtained by acid hydrolysis, is achieved by changing the CNCss counter-ion to potassium and wide range of colors were obtained using different ratios of CNCs-H and CNCs-K. Thus, when hydroxypropylcellulose (HPC) is added in different concentrations, it was possible to tune the reflected wavelength of the composite films, while preserving their structural organization and improving their elasticity. The obtained films change to a matte finishing as the concentration of HPC increases.

This work presents the potential color manipulation using CNCs-K as well as their applications in CNCs-K/HPC composite films while improving the mechanical properties of the films and maintaining the optical features within the range of the visible spectrum. The results obtained paves the way to the use of all-cellulosic composite systems of CNCs/HPC in OVDs printing solutions.

Keywords: cellulose nanocrystals, hydroxypropylcellulose, optically variable devices, ion exchange, composite films

Table of Content

List of figures

List of tables

Acronyms

AFM	Atomic Force Microscopy
ATR	Attenuated Total Reflectance
$(C_6H_{10}O_5)_n$	Cellulose
CrI	Crystallinity Index
Ch	Cholesteric
CM500	Micronized Cellulose 500 μm
CMC	Microcrystalline Cellulose
CNCs	Cellulose Nanocrystals
CNCs-CM500	Cellulose Nanocrystals produced from Micronized Cellulose 500 μm
CNCs-CMC	Cellulose Nanocrystals produced from Microcrystalline Cellulose
CNCs-H	Protonated CNCs
CNCs-K	Potassium ion exchange CNCs
CNCs-Na	Sodium ion exchange CNCs
DS	Degree of Substitution
DSC	Diferencial Scanning Calorimetry
EA	Elemental Analysis
EISA	Evaporation-induced Self-assembly
FTIR	Fourier Transform Infrared
FWHM	Full Width at Half Maximum
H_2SO_4	Sulfuric Acid
HPC	Hydroxypropylcellulose
ITO	Indium Tin Oxide
LC	Liquid Crystals
LCP	Left-handed Circularly Polarized
N	Nematic
n	Average refractive index
OSD	Optical security device
OVD	Optical variable device

P	Pitch
PEG	Polyethylene Glycol
POM	Polarized Optical Microscopy
RCP	Right-handed Circularly Polarize
SEM	Scanning Electron Microscopy
TEM	Transmission Electron Microscopy
TGA	Thermogravimetric Analysis
UVO	Ultra Violet Ozone
XRD	X-Ray diffraction
λ	Reflected Wavelength

1. Motivation

Counterfeiting and fraud have a tremendous economic impact in our society, translating in financial losses and corruption. It furthermore represents a great threat to the public's safety, through the existence of counterfeit passports (terrorism), forged identity (identity theft), pharmaceutical products (health hazards) and even airplane smuggling (safety issues). Therefore, optical security devices (OSDs), first introduced in 1980, now existent in personal documents and currency, represent one of the most important measures against counterfeiting [1]. OSD possess optical properties that shift with the observation plane and the majority of them are based on fossil fuel derivatives. Some of these features are printing complex images, distinctive typefaces, exclusive colored inks, watermarks, microprinting and unique serial numbers, all easily counterfeited [1]. With accessible technology such as copiers, scanners, high-resolution printers and others, it becomes imperative to continuously produce new features, which are required to be complex, economically viable and difficult to replicate.

As an example of protection features present in currency, **Figure 1.1** illustrates the €10 and €20 banknotes currently in circulation in the European Union where it is possible to observe the watermarks throughout the note, with especially significance in the side bar and in the value number.

Figure 1.1 €10 and €20 banknotes currently in circulation in the European Union where OSDs can be seen (black rectangle). These OSDs present optical color variation dependent of the viewing angle.

According to the Bank of England, in 2017 a volume of 473 thousand counterfeit banknotes were received, equal to 9.98 million pounds sterling where the majority of this were £10 and £20 [2] bank notes. More notes were collected that year than in 2016, with a total of 354 thousand, equivalent to 7.63 million pounds. In Europe, in 2017, a total of 694 thousand counterfeit euro banknotes were seized, and 301 thousand in the first half of 2018 [3].

The necessity of constant 'upgrade' of security features combine with the progress of photonic materials research gave rise to the development of new optically variable devices (OVDs). OVDs exhibit various optical effects, such as color and appearance changes in the presence of external stimulus. For example, they can present color change according to the viewing angle, or by variation of pressure or temperature. These properties are impossible to replicate in common copiers and scanners.

OVDs can be holograms, hidden images and iridescent images [4]. These optical variable devices possess passive optical properties, perceptible to the naked eye, as well as active optical properties, undetectable without the proper equipment or chemicals.

In reality, we are encountered with many natural structural coloration and patterns developed by nature itself, from flower petals, fruits, animal feathers and beetles exoskeleton [5]. These structures have been inspiring us for centuries, including antique civilizations. Ancient gyptians societies, for example, were fascinated by scarabs which was an iconographic and ideological symbol. In point of fact, the Scarabaeidae family includes a huge diversity of species with amazing structural coloration, as the stunning green iridescence in *Gastrophysa viridula*, and optical phenomenon which have been drive plenty scientific research. *Chrysina gloriosa* possesses a metallic green coloration that vanishes when observed using a right circular polarizer

[6]. These characteristics are possible due the nanoscale organization in their exo-cuticle. As an example, *Hoplia coerulea* is a blue scarab who presents structural coloration, fluorescence emission and fluid-induced color and fluorescence change, features originated from a periodic porous multilayer [7].

Cellulose nanocrystals (CNCs) is a nanomaterial with a huge potential to develop enhanced performance materials due to their unique properties as availability, biocompatibility, biodegradability and nontoxicity. CNCs has the capacity to form cholesteric liquid crystalline phases at relatively low concentrations (between 3 w/w% and 7 w/w%) when suspended as colloids in water, whose ordering can be retained in a solid film when the suspension dries. These films exhibit photonic properties including iridescence and selective reflection of left-handed circularly polarized light [8], [9].

Hydroxypropylcellulose (HPC) is a water-soluble cellulose ether. It is a highly used cellulosic derivative and can be found commercially with different viscosity grades and molecular weights. It is used for instance as a binder in pharmaceutical products or thickener in foods and presents a plastic behavior. HPC is capable of forming the lyotropic cholesteric crystalline liquid phase under certain pressure, temperature, and solvent for instance it will self-assembly into a chiral nematic phase between 50–75 w/w% of HPC, when dissolved in water [10] [11]. It was found that HPC is capable of transform energy into motion triggered by humidity when prepared from liquid crystalline solutions, leading the path to a water responsive HPC films [12].

The main goal of this dissertation is to develop optical responsive all-cellulosic composite films with structural coloration that can potentially be used as OVD, inspired in the optical properties of scarabs' exoskeleton. To mimic these iridescent structures, the CNCss from a cholesteric liquid crystalline phase will be produced and used as matrix. In order to improve the mechanical properties and the brittleness of the cellulose nanocrystals films HPC will be introduction to the polymeric system.

This work is structured in four main parts. Firstly, a theoretical framework is presented with the description of the main concepts and related state-of-the-art. The second chapter introduce the materials and procedures executed and the following chapter presents and discusses the obtained results. Lastly, the ending chapter includes the research conclusions and suggestions for future investigation.

2. Introduction

2.1. Bio Inspiration

Living organisms tend to morphologically adapt to the environment that surrounds them, acquiring complex and multifunctional materials. Structural colors developed by nature are an unlimited source of inspiration for developing materials, including in the research field of photonics. These colors are originated from complex interactions between light and sophisticated micro or nanostructures, and differ considerably from other coloration mechanisms such as pigments, dyes, and metals (where the colors are produced by the energy consumption of light) [13]. Structural coloration can be found in lepidopterans, beetles, birds, fishes, and plants [13].

Inspiration to develop complex systems, such as OVDs, can arise from nature. For instance, similar structures can be artificially produced using cellulose nanocrystals (CNCss) with the advantage of being accessible, economical and more environmentally friendly than the materials in current security devices [14][15]. For that reason, efforts have been made to develop biomimetic materials to replicate the structural color of plants, butterflies and beetles derived from this source [16].

2.2. Cellulose and cellulose derivatives

Cellulose, $[C_6H_{10}O_5]_n$ (n = 10,000–15,000 depending on the source material), is the most abundant biopolymer on earth and can be found in the skeleton of plants (cell wall), bacteria and marine animals such as *tunicates* [11], [17], [18]. It is a biodegradable and renewable material, insoluble in most solvents, resistant and cheap. These characteristics make cellulose one of the most studied materials for the replication of natural biomimetism and to develop sustainable materials [19].

Cellulose, or poly(anhydro-β-1,4-glucopyranose), exists in nature as a polydisperse, linear, crystalline (polysaccharide) macromolecule of high molecular weight and degree of polymerization [18]. The repeating unit of the natural polymeric chain is called cellobiose [$C_{12}H_{22}O_{11}$], illustrated in **Figure 2.1**, which makes a β-1,4-glicosidic bond between two glucose units [20] that rotate 180º in relation with one another.

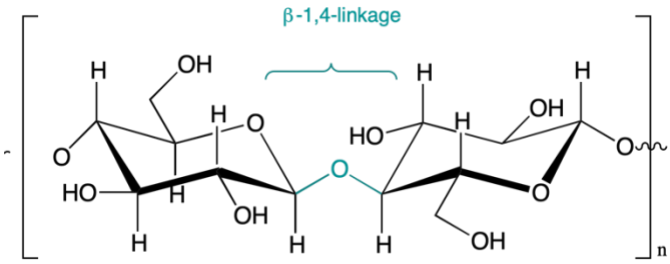

Figure 2.1 Representation of cellulose repeating unit, cellobiose.

Cellulose is a versatile polymer since it is possible to substitute its hydroxyl (OH) groups, by different chemical groups. This explains the wide variety of cellulose derivatives commercially available with different properties [21]. Some derivatives, such as hydroxypropylcellulose (HPC) and ethyl cellulose (EC) have the capacity to form lyotropic chiral nematic (cholesteric) liquid crystals phases [22].

HPC is a highly substituted ether cellulose derivative obtained by replacing hydroxyl groups of the C2, C3 and C6 carbons for hydroxypropyl groups. Due to the presence of both hydrophobic and hydrophilic groups, it has a lower critical solution temperature than cellulose, below 45 ºC [12]. The polymer is soluble in water as well as in polar organic solvents, biodegradable, biocompatible and electroneutral, well suited for pharmaceutical and food applications as thickeners, emulsifiers and encapsulators [12], [23].

Hydroxypropylcellulose forms an ordered cholesteric structure in concentrated aqueous solutions, between 50 and 75 w/w% of HPC [11], [24] and is capable of forming both thermotropic and lyotropic liquid crystalline phases [25].

Since cellulose is an easily modifiable material, it is possible to expand the range of applications by exploring its nano scale high potential. Materials with nanosized structural features ranging from 1 to 100 nm are very appealing for a variety of applications (e.g. electronics, optics, magnetism, energy storage, and electrochemistry) [9].

Fernandes et al. produced iridescent sheared transparent cellulose-based films, with characteristics similar to those found in petals of tulip “Queen of the Night” [26]. The authors succeeded in modulating the mechanical and optical properties of the HPC films by incorporating CNCss in the LC precursor solution of HPC/water.

Bulk cellulose contains highly ordered, crystalline regions along with some disordered (amorphous), depending on its source [19]. Using acid hydrolysis, rising the temperature above room temperature and adding sources of hydrogen, such as sulfuric acid (H_2SO_4) and hydrochloric acid (HCl), is possible to remove the amorphous areas and obtain cellulose nanocrystals (CNCss). The resulting particles, exhibit high specific strength, high Young’s modulus, high surface area, and unique liquid crystalline properties, when compared with the initial cellulose [19]. CNCss, when dispersed in water, self-assembly to a cholesteric phase making them suitable for producing systems with structural color without the need of using a dye [18].

The CNCs’s size, biocompatibility and resistance enables a large range of applications, between material reinforcement as well as pharmaceutical uses. Also, solid films prepared from solvent evaporation of aqueous lyotropic cellulose nanocrystals suspensions exhibit extraordinary optical properties such as iridescence, selective reflection of left circularly polarized light, and transmission of right circularly polarized light [10].

2.3. Liquid Crystals

Liquid Crystals (LCs), or also called ‘mesomorphic phases’, exhibit intermediate phase between solid and liquid [27]. This thermodynamic stable state has the capacity to flow like liquids, yet possess optical properties of the solid such as birefringence [28]. LCs are formed by anisometric molecules or particles, where one or two dimensions are much greater than the third, such as rod-like or disk entities [29].

Liquid crystals can be classified, according to its thermodynamic genesis, as thermotropic, obtained by changing the temperature, and lyotropic, by varying the solute concentration in a specific solvent at constant temperature and pressure. The first ones have become strategic materials in modern information display industry, such as LCDs. while in the later they turn out to be significant in living matter, biological and biomedical science [30].

The mesophases classification were first defined by G. Friedel, in 1922, based on their symmetry, in three main classes: nematic, smectic and cholesteric [27].

Nematic (N) is a “layer-less” structure, where the molecules are aligned on average along a general direction defined by a unit vector ***n***, called director. The direction of ***n*** is arbitrary in

space and it is imposed by minor forces, such as the guiding effect of the walls of the container [27].

Cholesteric (Ch), or chiral nematic liquid crystals (N*), are locally very similar to a nematic phase. Ch is organized by “pseudo-layers”, where each one has its own director axis that rotates a few degrees in relation to the ones immediately below and above it, leading to a helical structure [21]. The cholesteric phase is characterized by the distance required for the director to complete a full turn of 360º, as showed in **Figure 2.2**, normally designated by *P*, the pitch, and its handedness [21].

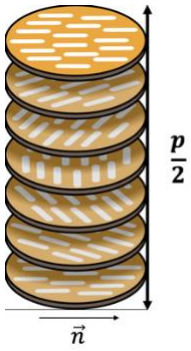

Figure 2.2 Illustration of the organization of molecules of particles in a cholesteric mesophases, where the pitch value represents the distance required for the director to complete a full turn of 360º [82], note that the layers do not represent any discontinuity of the medium.

According to the de Vries equation, (**Equation 1**), the helicoidal pitch, *P*, the average refractive index, *n*, and wavelength λ_0 are related [22] if the incident light is perpendicular to the helical axis:

$$\lambda_0 = nP \qquad \textbf{Equation 1}$$

If θ is the angle between the helix axis and the incident light, and the value of λ_0 is in the range of the visible region of the electromagnetic spectrum and the same light reaches the Ch with an angle (θ) iridescence will appear. The **Equation 1** can be expressed by **Equation 2**, and the wavelength of the reflected light will be dependent on the incident angle and the observed color of the cholesteric will change with it [21][22].

$$\lambda_0 = nPcos\theta \qquad \textbf{Equation 2}$$

In cholesteric structures, the incident circularly polarized light with the same handedness as the cholesteric structure is totally reflected, while opposite handedness is transmitted. Meaning, right circularly polarized (RCP) light will be reflected by cholesteric materials with a right-handed helix, such as HPC aqueous solutions, while left circularly polarized (LCP) light will be reflected by cholesteric materials with a left-handed helix, as is the case with CNCss [22].

2.4. Bio inspiration from optical responsive structures

In Nature, there are several examples that present structural coloration with selective circularly polarized light reflection due to the structure’s helical arrangement. *Cetonia aurata* (Linnaeus, 1758), with bright green coloration, reflects LCP light due to the left-handed organization of the chitin nanorods in the beetles exoskeleton (**Figure 2.3 - (a), (b)**) [29]. However, similar optical phenomenon can be explained by different cholesteric arrangements. For example,

both *Chrysina resplendens* (Boucard, 1875) (scarab, **Figure 2.3 - (c)**) and *Pollia condensate (C. B. Clarke)* (fruit) display coloration when seen under left and right circular polarizers. Yet, while *P. condensata* creates coexisting cellulose-based left and right handed helicoidal structures, the exocuticle of *C. resplendens* only presents left-handed ones (that tend to confine anisotropic layers in between, **Figure 2.3 - (d)**). *Gymnopleurus virens* has the ability to reflect (mainly) left circularly polarized light and not right circularly polarized light and can show blue, green and red iridescence according to the angle view [31]. Different colors are achieved by members of the same species solely by thickness variations of the layered chiral structure.

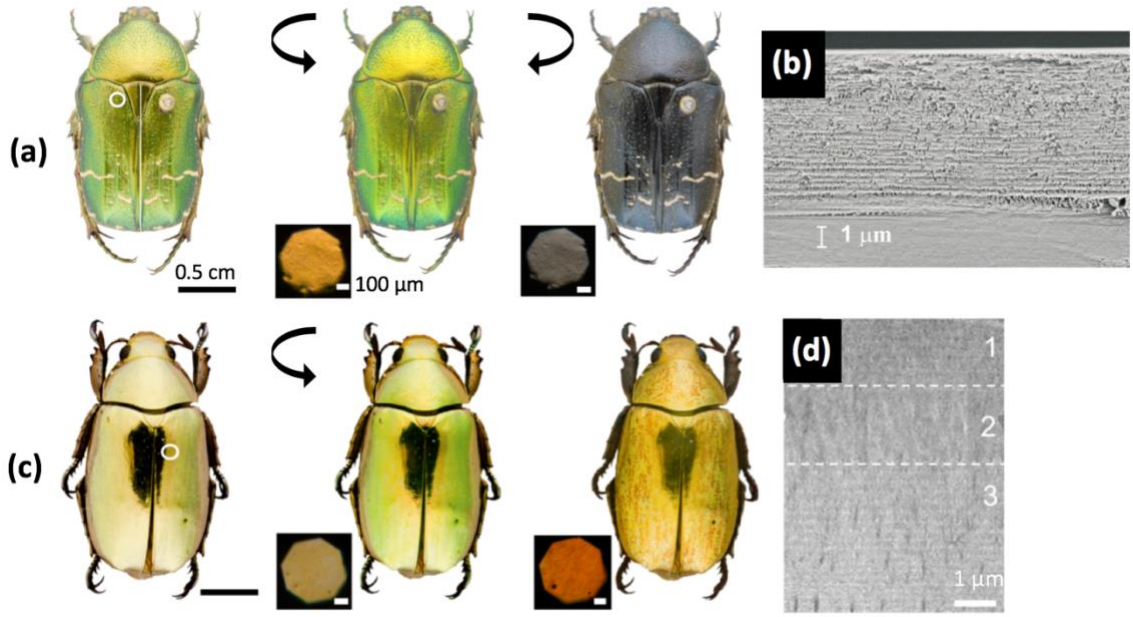

Figure 2.3 Photographs of the beetle *C. aurata* (a) and *C. resplendens* (c) beetles seen under unpolarized light, left and right circular polarize light, respectively. Scanning electron microscopy (SEM) micrograph of a section cut vertically through the cuticle of the *C. aurata* beetle showing the lamellar organization in the exocuticle responsible for its bright coloration Transmission electron microscopy (TEM) micrograph of a section cut vertically through the cuticle of the *C. resplendens* beetle showing two lamellar organizations (1 and 3) separated by an anisotropic layer (2). Reprinted from [29], Copyright 2019, with permission from Elsevier .

Mouchet *et al.* analyzed the natural photonic structures of the male *Hoplia coerulea (Drury, 1773)* scarab beetle and their color changes induced by liquids and vapors contacts [7]. The beetle appeared to have several optical properties combined in a single entity, such as structure coloration, fluid-induced color change, fluorescence emission and fluid-induced fluorescence changes [7][32]. The authors considered that such characteristics, when synthesized artificially, can be possibly used to develop bioinspired functional photonic materials and smart optical coatings.

These are just some examples that can serve as models to develop bio-inspired materials with outstanding optical properties. As described before, is possible to biomimetic these by using from cellulose nanocrystals LCs suspensions. Among others, Dumanli *et al*. [33] produced multi-coloured cholesteric cellulose films by slow evaporation of CNCs suspensions on polystyrene substrates. These films contain multicolored domains and selectively reflected LCP light, as in *Cetonia aurata*. More recently, Zhao *et al*., developed a scalable printing method and produced structurally colored CNCs microfilms arrays [34]. By combining a strong anchoring, of the CNCss to the substrate, with an imposed slow evaporation, where the CNCss self-assembly were not disrupted by shear or “coffee-ring” effects, the result was a highly-ordered, monodomain structure with little to no defects. The authors stated that high surface to volume ratio of the hydrophilicity

of the natural building block allow for a dramatic real-time colorimetric response to changes in relative humidity. This optimized procedure leads to a better reflection of LCP light and transmission of RCP, similarly to what is observed for the beetles in **Figure 2.3** (a)

Fernandes *et al*. reported a cellulose-based photonic structure that reflected both RCP and LCP light, in a mechanism similar to what is observed in the beetles *C. resplendens*, that can be tuned by temperature variation and the application of an external electric field [35]. Wu *et al*. developed a cellulose nanocrystal-based film with left-handed cholesteric photonic structure that mimic the shell of the *Chrysina* beetle [36]. The CNCss/PEGDA layers in the nanocomposite film allows for simultaneous and reversible three-dimensional deformation behavior as well as the shift of the Bragg reflection when exposed to a humid environment. This self-assembled photonic material could be attractive to be used as optical anti-counterfeiting film, tunable bandpass filters, reflectors or polarizers and humidity-responsive sensors.

2.5. CNCss photonic materials

CNCss lyotropic liquid crystalline behavior was reported by Marchessault *et al*. [37], in 1959, and later recognized by Revol [38] as a cholesteric phase. This phase of CNCss suspensions occurs at low critical concentrations of nanoparticles, between 3 w/w% and 7 w/w%. An important work with respect to the development of photonic materials based on CNCss was reported in the late 1990s by Gray and co-workers [39]. Is important to note, that the group of Prof Gray greatly contributed to the optimization of CNCss extraction by understanding the influence of the parameter within the obtained properties.

Recently, MacLachlan and co-workers were able to retain the chiral nematic organization of the CNCss suspension in mesoporous silica solid films by evaporation-induced self-assembly (EISA) [9] and obtained structurally colored glass. With an adapted EISA methodoly, Leng *et al*. obtained highly flexible latex films with tunable structural coloration through CNCss templating [40]. The chiral nematic (N*) structure from the organization of CNCss was retained in the latex film, even after removing the CNCss with alkali treatment, by leading to the preservation of the structural color. The films also exhibited a reversible response to water adsorption and dehydration. Gladman *et al*. inspired by plant architecture, printed composite hydrogel structures that are encoded with localized, anisotropic swelling behavior controlled by the alignment of cellulose fibrils along prescribed four-dimensional printing pathways [41].

The manipulation of the structural coloration is mainly attributed to changes of the helical pitch of the cholesteric structure. For example, the addition of salt increases the ionic strength of the suspension and the electrostatic repulsion between the CNCss is decreased due to the surface charge of the CNCss introduced by the sulfate esters. Thus, yielding a contraction of the helical pitch, promoting a blue-shifted reflectance [9].

In 1996, Dong and Gray revealed that the nature of the counterions also influences other properties of the suspensions [42]. Such as their stability, the temperature dependence of the phase separation and of the cholesteric pitch value, and the redispersability of dried samples made from the suspensions. Cheung *et al*. studied the influence of the counter ion on the surface sulfate esters on the EISA process [43]. In their study, they neutralized acidic CNCss suspensions with different hydroxides and discovered that increasing the size of the cation, a blue shift in the reflected color was observed while increasing the hydrophobicity of the alkylammonium cations led to a red shift of the signal.

Gilman and co-workers developed all-cellulosic films by assembling the CNCss with a minority fraction of high aspect ratio CNCss derived from tunicates (t-CNCss) [44]. These damage tolerant optically active materials reported remarkable enhancement of both mechanical

properties and flexibility. The films also displayed UV reflecting behavior for contents above 5% t- CNCss, which hold potential for protective coatings applications.

2.6. CNCss composite materials: possible OVDs applications

CNCs films developed iridescence, selective reflection, unique morphology, a white light diffraction pattern and the capacity to act as a reinforcement. These features make CNCs suitable for biomimicking materials and be applied as an optically variable device.

As discussed before, OVDs have extraordinary optical properties, such as iridescence that makes them impossible to replicate, an amazing security device and an anti-counterfeiting measure (on money, credit cards and government-issued identification cards).

Andrews and co-workers presented an iridescent fluorescent CNCs film with multiple potential security features: overt security (iridescence) and covert security (selective circular reflection and fluorescence) [45]. Although the produced films covered these three security levels, the system evidenced brittleness. Chindawong and Johannsmann used anisotropic ink based on cholesteric CNCs fraction dispersed in a latex blend for security printing applications [46]. Giese *et al*. synthesized amino resin-cellulose nanocrystals composites with structural coloration that can be manipulated by pressure application [8]. These tunable displaying colors could be imprinted into the composite films for security features, pressure sensors, and decoration. In recent literature it is possible to find information on pigments prepared by dry grinding iridescent CNCs films [34], CNCs doped with active optically response elements [35] or passive elements [36]. However, all these systems are based on fossil fuel-based matrices.

Recently, in 2018, Wang and co-workers produced highly flexible and iridescent CNCs films with humidity and pressure-responsive chromism by introducing glycerol as both plasticizer and hygroscopic agent [47]. The authors evidenced that the additive results in the enhancement of CNCss' mechanical toughness, making it possible to obtain free-standing iridescent CNCs films with tunable structural colors. They succeeded in producing reversible chromism, mimicking the properties of the longhorn beetle *Tmesisternus isabellae (Vollenhoven, 1871).*

Yao *et al*. produced large, flexible, and flat photonic composite films with uniform structured colors from blue to red by assembling poly(ethylene glycol) (PEG) and CNCs [48]. The CNCs/PEG (80/20) composite film demonstrated a reversible and smooth structural color change between green and transparent according to an increase and decrease of relative humidity. They also shown excellent mechanical and thermal properties.

Wan *et al*. presented responsive and flexible photonic papers by mixing waterborne polyurethane (WPU) latex particles with aqueous CNCs suspensions [49]. The CNCs/WPU composite papers exhibit tunable iridescent colors, by adjusting the helical pitch size with different CNCs/WPU ratios, and reversible optical responses to water, wet gas and NaCl solutions. The authors were able to develop colorful patterns on the CNCs/WPU photonic paper that can be made temporary, durable, or even disguisable.

MacLachlan and co-workers reported a series of responsive photonic hydrogels prepared by self-assembly of cellulose nanocrystals with various hydrogel monomers, including acrylamide (AAm), N-isopropylacrylamide (NIPAm), acrylic acid (AAc), 2-hydroxyethylmethacrylate (HEMa), polyethylene glycol dimethacrylate (DiPEGMa), and polyethylene glycol methacrylate (PEGMa) [50]. These presented tunable colors, respond to various stimuli, and interesting mechanical and swelling behavior. It was shown that the hydrogels can be prepared as large, freestanding films and can be photopatterned by incorporate latent images. Their findings can be important for developing sensors and other chiral optoelectronic devices.

Chen *et al*. developed a self-healing and responsive chiral photonic film (SCPF) based on the co-assembly of boronic ester crosslinked poly(vinyl alcohol)-polyacrylamide with CNCss [51]. The reversible covalent bonds of boronic esters groups enables the self-healing of

the photonic material, which allows for the construction of patterns and stacked structures as well as for anchoring on surfaces. A QR code was printed on paper and covered by a thin film of the reported CNCs/polymer composite. It was proven that the QR code was exclusively encoded by a cell phone, when right-handed circularly polarized light was used.

3. Materials and methods

3.1. CNCs production

The preparation of CNCs was based on the experimental method used by Hamad *et al.* [52] with adaptations from Fernandes et al [35]. It was used micronized cellulose (CM500, supplied by The Navigator Company, ~500 μm particle size), who underwent mechanical treatment of defibrillation. Scanning Electron Microscopy (SEM) performed by the company presented an average particles length and width dimensions of 359.4 μm and 13.7 μm respectively.

The cellulose was hydrolyzed in sulfuric acid (95-98% purity, Sigma-Aldrich) diluted at a concentration of 64% w/w, with an acid/solid ratio of 8:1, at 45 ºC, for 25 minutes while under continuous mechanical stirring. The cellulose was added to the sulfuric acid and hydrolyzed at a medium speed (300 rpm). The resulting suspension was washed with ultrapure water type II (~10 times the volume of the acid solution used) to stop the hydrolysis and allowed to settle overnight. The process was repited until a pH of approximately 0.70 were reached, the white remaining layer was submitted to subsequent wash by centrifugation cycles (at 12 000 rpm for 20 minutes, using a Thermo Scientific Heraeus Multifuge X1R Centrifuge Series). The CNCs suspends when the pH is between 1.9-3.9 and the supernatant was collected. This suspension was placed into cellulose films (Spectrum Spectra/Por® 4 dialysis films) and then dialyzed with ultrapure water for a minimum of one month, with daily water changes until the pH remained constant, to ensure the elimination of the remaining sulfuric acid and other sub-products of the reaction.

A CNCs-CM500 suspension with 7 ± 0.6% w/w concentration was obtained by osmotic bath with polyethylene glycol (PEG) established by Frka *et al.* [53]. The initial CNCs suspension at 3.4 ± 0.08% w/w was placed in dialysis membrane (Thermo Scientific SnakeSkin™ Dialysis Tubing) and dialyzed, for 12 h, in a 15% w/w aqueous PEG solution. The suspension was then sonicated with 3 consecutives cycles of 20 min over an ice bath using a Hielscher UP400S ultrasonic homogenizer (460 W, 24 kHz, at 0.85 of the cycle and 80% amplitude which corresponds to an energy input of 10 kJ g^{-1}).

The same process, following the method of Fernandes *et al.* [35], was used for the preparation of cellulose microcrystalline (CMC; Avicel® PH-101, ~50 μm particle size, lot #BCBJ0229V), derived from cotton and purchased from Sigma-Aldrich. It was used an acid concentration of 64% w/w, at 45 ºC for 45 minutes while under continuous mechanical stirring. A CNCs-CMC suspension with 3.81 ± 0.08% w/w. concentration was obtained.

Ultrapure water used in the process was purified using a Millipore Elix Advantage 3 water purification system.

3.2. CNCs-CM500

3.2.1. Liquid crystalline phase as a function of CNCs concentration

To attain the phase diagram of the lyotropic aqueous suspension of CNCs as a function of nanoparticles concentration, the dilution was proceeded using the concentrated suspension of 7% w/w from micronized CNCs. The resulting concentrations were: 2.5, 3.0, 3.5, 4, 4.5, 5 and 6% w/w of CNCs. After homogenization by sonication, these were placed in vial tubes with 1.5 ml capacity and allowed to relax for about 3 weeks until no variation in the percentage of anisotropic fraction was observed.

3.3. CNCs-CMC

3.3.1. Ion Exchange

Based on article by Dong and Gray [42], ion-exchange resin (Amberlite® IR120 hydrogen, Sigma-Aldrich) and a 20% w/w aqueous potassium chloride solution were used to replace the protons of the original CNCs-CMC crystallites (CNCs-H) by potassium (CNCs-K). The same procedure with 10% w/w aqueous sodium chloride solution was used to produce CNCs-Na, in which the counter-ion of the CNCs chain was replaced by sodium.

3.3.2. Films from drop-casting method: effect of the CNCs's counterion from H_+ to K_+

Films with a dome-like shape were produced from drop-casting method onto a 100 Ω/sq Indium Tin Oxide (ITO) coated square glass substrates (15x15x0.7 mm), using different fractions of the original CNCs (CNCs-H) and activated CNCs (CNCs-K) to study the color pallet evolution. The mixture between the CNCs-H, that originate films with red coloration, and CNCs-K, originating films with blue coloration, was performed using ratios of 0:1, 1:3, 1:1, 3:1 and 1:0. The glass substrates went through a UVO treatment, where they were exposed to UV light and Ozone (O_3), using a Novascan PSD-UV in a procedure developed within the research group and the droplet allowed to dry at low temperature [54]

3.3.3. CNCs-K/HPC suspension and drop-casted films

To the aqueous suspension of CNCs-K (~ 3.81% w/w CNCs) HPC was added with different molecular weights (Sigma-Aldrich, $\overline{M_w}$= 100 000, 300 000, 600 000) in different ratios (5% w/w 10% w/w, 20% w/w, 30% w/w, 40% w/w and 50% w/w) and homogenized in an Analog Shaker for a week until full dissolution. Droplets of these various mixtures were deposited (following the description in sub chapter 2.3.2 in ITO subtracts), the films studied and then chosen the most favorable combination to produce films. Part of this suspension was placed in vials tubes with 1.5 ml capacity and the presence of the liquid crystalline phase is verified after 4 weeks and observed between crossed polarizers.

CNCs-K/HPC films were produced by the solvent evaporation technique where the suspension (with 2 ml of volume) is deposited into polystyrene Petri dishes, with 35 mm diameter, under controlled environment, until all the solvent evaporated. The evaporation occurred at ~ 4°C for approximately three weeks, thus allowing formation of iridescent films. Replicas of these films with 1.5 mL were also produced. Their thicknesses, 70 ± 10 µm, were determined averaging 10 measurements using the Mitutoyo digital micrometer and are presented at supporting information **7.e**.

3.4. Characterization

Standard characterizations techniques were performed on the cellulosic samples such as Fourier-transformed infrared (FTIR), scanning calorimetry with thermogravimetric analysis (DSC-TG), x-ray diffraction (XRD), Elemental analysis (EA), polarized opticl microscopy (POM), Atomic Force Microscopy (AFM), circular dichroism (CD), test bending, profilometry and general photography, and the detailed description can be found, in the supporting information **7.a**.

4. Results and Discussion

The main goal of this thesis was to produce iridescence and flexible CNCs/HPC composite films, inspired by the optical properties present in the beetles' exoskeleton, from a cellulose nanocrystals lyotropic aqueous suspension. Films obtained from solvent evaporation are intended to display selectively reflection of left circularly polarized (LCP) light, within the visible range, and responsiveness to external stimuli.

The present work also studies the production of CNCs from a micronized cellulose source, obtained by eucalyptus, instead of the regular commercially available cotton source. These later give rise to rice-like nanoparticles, while is expected to obtained needle-like nanoparticles with the micronized cellulose source which have a higher aspect ratio. It is known that the size of nanoparticles influences the properties of the liquid crystalline phase obtained by the self-assembly CNCss [55], [56]. And this source might enable us, when polymers are added to this CNCss lyotropic suspension, to obtain films that reflect structural colored with wavelengths within the visible range of the electromagnetic spectrum. Indeed Yao *et al*., presented an example of this problem when they tried to use a mixture of CNCss, prepared from cellulose microcrystalline (short-length cellulose fiber source, Avicel® PH100) with PEG. The authors claimed that they could not obtain composite films with structural coloration within the visible range. This problem was overcome when the authors moved to a longer source that enabled a better control of particles, its size, and changes in surface charge which consequently differentiate the pitch value of the composite suspension [48].

Firstly, on the following chapter, some structural and chemical properties of the obtained products are presented, comparing the raw material to the cellulose nanocrystals of both micronized and microcrystalline cellulose sources. The results of the characterization techniques include FTIR, XRD diffractograms, elemental analysis, DSC-TGA analysis, POM and AFM.

The influence of the nanoparticles counter-ion CNCs-H and CNCs-K on the structural color palette is also studied by producing films from drop-casting technique with different ratios of each suspension. The micro and macro scale characterization of these dome-shaped like films is accomplished with photography and POM. The same study was made for the CNCs-K/HPC films obtained from drop-casting method using HPC with different percentages in respect with the CNCs content and molecular weights.

The CNCs-K/HPC films produced by solvent evaporation were photographed, its thickness measured, characterized using POM, Vis spectrometry, FTIR, XRD and DSC-TG. Mechanical testing was also performed to verify whether the films flexibility is enhanced by the presence of HPC.

4.1. CNCs Characterization

4.1.1. CM500 and CNCs-CM500

Cellulose nanocrystals, from CM500, designated as CNCs-CM500, were produced based on the methodology presented by Hamad *et al*. [52]. The hydrolysis was performed using a concentration of 64% w/w diluted sulfuric acid, at 45 ºC, for 25 minutes while under continuous mechanical stirring. A yield of 50% ± 0.06 was achieved, which is a much higher value when compared to the one presented by the literature (of 22.4% process yield), for bleached softwood KRAFT pulp using the same hydrolyses conditions [18]. The divergence in these values, and since both sources were somehow fibrillated prior hydrolyses, might rely on the composition of the KRAFT pulp, since we do not know the composition of our source (this is, we do not know if our KRAFT pulp is mainly derived from *Eucalyptus globulus* wood or a mixture of different type of

woods, as the one used by Hamad is 60% western red cedar and 40% spruce, fir, and pine). The different might also be attributed to the differences in the methodology to collect the CNCss from the reaction medium.

Figure 4.1 illustrates the chemical reaction of the cellobiose unit when the cellulose fibers undergoes acid hydrolysis.

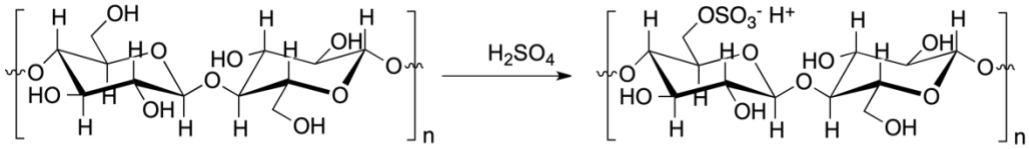

Figure 4.1 Schematic representation of the acid hydrolysis reaction of cellulose using sulfuric acid to produce cellulose nanocrystals.

Hydrolysis with sulfuric acid results in the introduction of sulfate esters at the surface of the cellulose crystallites, leading to added electrostatic stabilization of the suspensions [18]. CNCs samples as well as its precursor from a micronized cellulose (CM500) source were optically, chemically, morphologically, and structurally characterized in order to assess whether the acid hydrolysis reaction carried out resulted in the successfully production of cellulose nanocrystals.

Chemical analysis was done by means of Attenuated Total Reflectance Fourier Transform Infrared ATR-FTIR (**Figure 4.2**) where the black and purple spectra represent the CM500 and the CNCs, respectively, where several absorption bands associated with molecular vibrations of cellulose bonds stand out. Both spectra display coincident vibration bands, as for instance the ones approximately at 3300 cm^{-1}, 2900 cm^{-1} and 1050 cm^{-1} represent the O-H stretching vibration (indicating the presence of hydrogen bonding in the samples), stretching vibrations of C-H and C-O bonds, respectively [57]. The band at 1639.7 cm^{-1} is associated with the vibration of the O-H bond of absorbed water in the cellulose and the vibration band at 890 cm^{-1} is associated with a C-O-C stretching effect on the β(1,4) glycosidic bonds (assigned to the amorphous region) [58], [59]. CNCs spectra band at approximately 817 cm^{-1} is attributed to S-O bond stretching due to the presence of ester-sulfate groups resulting from the acid hydrolysis reaction [60]. This band is nonexistent in the starting material sample (CM500).

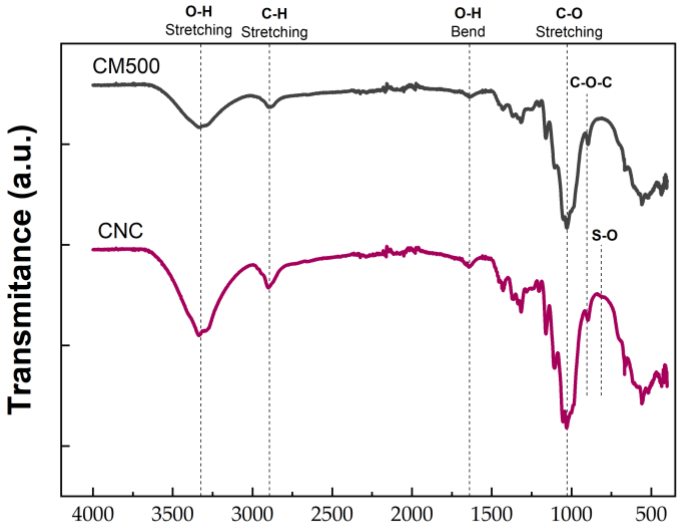

Figure 4.2 ATR-FTIR spectra of CM500 (black line) and CNCs-CM500 (purple line). Each vertical dotted line marks a characteristic absorption band of a cellulose macromolecule binding molecular vibration.

The X-Ray Diffraction structural analysis of both CM500 and CNCs (**Figure 4.3**) allows us to assess the type of cellulose allomorph, to infer the crystallinity index of each sample and to understand if the structural arrangement is affected by the acid hydrolysis procedure.

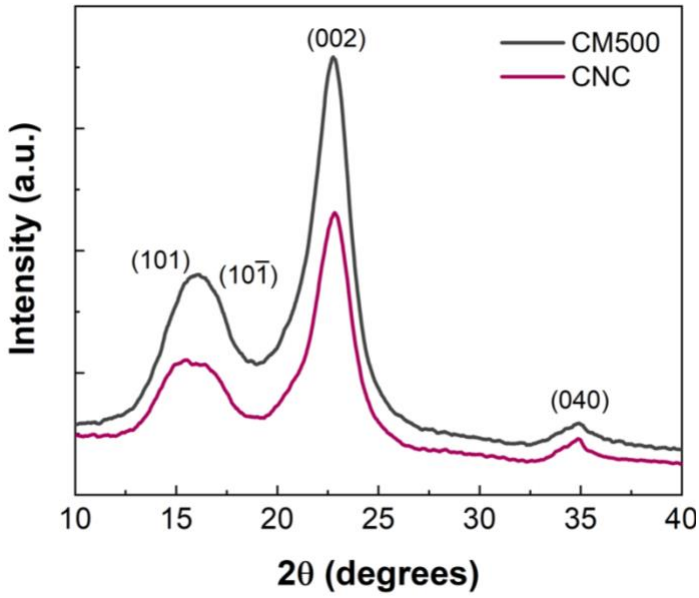

Figure 4.3 XRD diffractograms of CM500 (black line) and CNCs-CM500 (purple line).

XRD diffractograms of CM500 and CNCs samples display peaks around Bragg angle (2θ) of 15.5º, 16.8º and 22.80º characteristics of the 101, 10$\bar{1}$ and 002 (main peak) crystalline planes, respectively [61]. A smother peak of the 040 plane is identified at approximately 34.9º [59], [62]. These diffraction characteristics peaks are associated with cellulose type Iβ [63]. The absence of strong alteration of all peaks means that the structural arrangement of the cellulose is not affected by the performed acid hydrolysis.

The crystallinity index (CrI) was determined with the empirical method presented by Segal *et al*. [64] and using the equation below.

$$CrI = \frac{I_{(002)} - I_{am}}{I_{(002)}} \times 100 \qquad \textbf{Equation 3}$$

In the **Equation 3**, $I_{(002)}$ corresponds to the maximum diffraction intensity of 002 peak, with 2θ between 21 ° and 23 °, and I_{am} corresponds to the diffraction intensity of amorphous material, with 2θ between 18 ° and 20 °, where the intensity is minimal. The CrI results are presented in **Table 1**.

Table 1 Crystallinity Index of CM500 and CNCs-CM500 samples determined by the empirical method presented Segal *et al*. [64].

Sample	CrI (%)
CM500	83.2
CNCS-CM500	88.2

The CNCs have a higher crystalline index when compared to the one obtained for CM500, which was expected since the acid hydrolysis processes mainly attacked the amorphous regions

of the starting material. The CrI values for the CNCs-CM500 samples are approximately similar to the ones reported by Hamad *et al*. [52] (84.6%) for softwood KRAFT pulp using identical conditions (64% w/w acid concentration and 45ºC) and the Segal *et al*. [64] method approach.

Micronized cellulose samples were diluted in water (0.01% w/w) and let in magnetic stirring for 16 hours, before the acid hydrolysis process. From this suspension small droplets were deposit on a glass slide and several images were captured (as **Figure 4.4**) using a polarized optical microscope in order to determine the length of the particles. 100 manual measurements (supporting information **7.b**) were made using ImageJ software to calculate the fibers dimensions. The average length of CM500 was 359 ± 212 µm which corresponds to the length referred by the CM500 supplier company (359.4 µm).

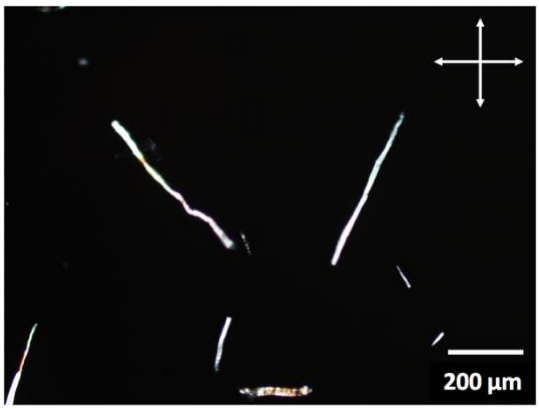

Figure 4.4 Example of a POM image of CM500 fibers captured in transmission mode between crossed polarizers.

In order to assess the size of the obtained CNCs-CM500, the nanoparticles were observed by atomic force microscopy (AFM). CNCs-CM500 particles, diluted in water (0.0025% w/w), were dimensionally characterized using the AFMs topographic images. The obtained images (**Figure 4.5**) were analyzed with the Gwyddion software and 150 measurements (supporting information **7.c**, **Figure 7.2**) of both length and width were taken, following the method described by Honorato-Rios *et al*. [56].

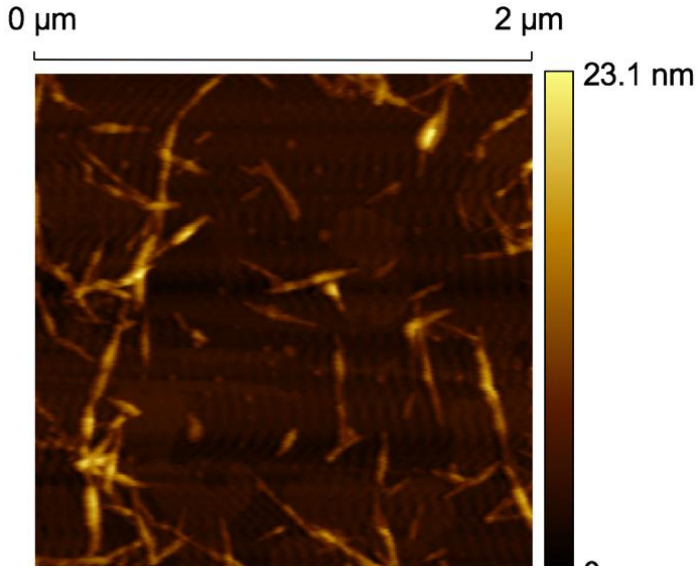

Figure 4.5 TOP view image 2µmx2µm, of an amplitude scan obtained by AFM of CNCs-CM500 fibers deposit in mica.

It is possible to observe that the CNCss morphology is characterized by agglomerates of rice-like structures. The average particle length and width dimensions were 336 ± 92 nm and 9 ± 3 nm, respectively, which estimates a ratio of 37. Acid hydrolysis process proven to be successful and both dimensions are at the nanoscale.

By thermogravimetric analysis coupled with differential scanning calorimetry (TGA-DSC) analysis it was possible to that verify the thermal stability of the produced cellulose nanocrystals CNCs-CM500 (purple line) and compare with the starting material (CM500 black lines) (**Figure 4.6**). The continuous line represents the mass fraction and the dot lines the DSC progression.

The first smooth mass drop on both samples, below 120 ºC, is due to the evaporation of residual water present in the cellulose fibers. The sample CM500 exhibit an abrupt fall in the TG line in the temperature range of 280 to 370 ºC. This fall coincides with a massive endothermic reaction peak thus indicating a presence of a first order pyrolysis reaction common observed for this material [65].

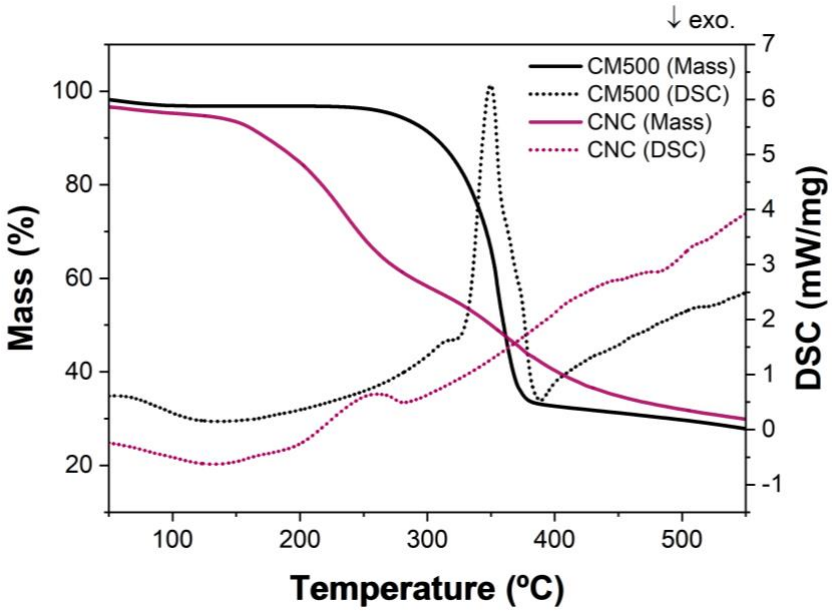

Figure 4.6 DSC-TGA analysis of CM500 (black lines) and CNCs-CM500 (purple line).

From the CNCs thermogravimetric curve (purple lines) it can be seen that their degradation starts at lower temperatures, compared with the raw material, and it's possible to identify other two important occurrences. The first mass loss event occurs at approximately 150º to 250 °C due to the degradation of regions more accessible to sulfate groups [66]. At 350 ºC, the crystalline regions, least affected by the hydrolysis process, decompose. The latest event at about 400 °C indicates the cellulose oxidation related to the solid decomposition [66].

The amount of sulfate groups attached to the cellulose nanocrystals surface can be estimate from elemental analysis (EA). Thus, it is possible to assess the amount of sulfate ester groups introduced by acid hydrolysis in the anhydro-glucopyranose (AGP) units. The surface charge of the samples are detailed in the following table (**Table 2**) as well as the predicted values for pure cellulose [67].

Samples from the raw micronized cellulose lack the sulfur element as it has not undergone acid hydrolysis.

Table 2 C, H, S and estimated Oxygen elemental analysis of the samples CM500 and CNCs-CM500, as well as the predicted values for pure cellulose.

Sample	Carbon (w/w%)	Hydrogen (w/w%)	Sulfur (w/w%)	Oxygen [a] (w/w%)	$-OSO_3H$/ 100
Pure cellulose predicted values [67]	44.44	6.18	-	49.38	-
CNCs from other KRAFT pulp [b]	40.78	5.78	0.92	52.52	4.7
CM500	42.19	5.67	-	52.14	-
CNCs	42.40	6.20	0.41	50.99	2.09

[a] *values obtained by mass difference;*
[b] *elemental analysis data for CNCs derived from Softwood KRAFT pulp using 64% w/w acid concentration at 45 ºC for 25 min* [52].

The degree of substitution (DS) of $-OSO_3H$ per 100 AGP units (n) was determined using the method described by Hamad *et al*. [52] and applying the equation bellow.

$$n = \frac{100 \times 162.141 \times S\,(\%)}{3206.6 - 80.063 \times S\,(\%)} \qquad \textbf{Equation 4}$$

In the **Equation 4**, S (%) corresponds to the sulfur content measured by elemental analysis. The value of n for the CNCs-500 is 2.09 of $-OSO_3H$ groups per 100 AGP units, which is half than those presented by Hamad [52] for the same acid hydrolysis conditions ($-OSO_3H$/100 of 4.7). The difference is these values might be related to the reasons presented above for the difference in reaction yield.

The concentrated suspension of CNCs-CM500 (~ 7% w/w CNCs) was diluted to 2.5, 3.0, 3.5, 4, 4.5, 5 and 6% w/w CNCss concentrations, sonicated and let to rest for 4 weeks. The samples were then observed between cross-polarizers as can be seen in **Figure 4.7 - (a)**. If one looks at suspension with 2 and 2.5 %w/w of CNCss two distinct phases, within one sample, were obtained. The upper isotropic phase, where the nanoparticles with lower sizes are randomly arranged, and the birefringent lower phase corresponding to the anisotropic phase. Generically, anisotropic phase increases with the increment of CNCss nanoparticles in suspension, as expected, however it is not a linear growth. This increase is nonlinear since nanoparticles are electrostatically stabilized, and cannot keep a constant ionic strength as the concentration of CNCs in the suspension increases, so each suspension has different ionic strength that affects the LC phase. [68] [69]

The anisotropic phase fraction of each suspension is graphically represented in **Figure 4.7 - (b)** and is obtained by dividing the height of the anisotropic zone by the suspension total height. The phase separation is detected at 2% and 2.5% w/w CNCs. Although the increase of the anisotropic phase is proportional with the CNCs concentration, as observed, the suspensions above 2.5% w/w concentration have shown to be completely anisotropic.

CNCs produced from a micronized cellulose source, with larger particles dimensions, was intended as a matrix for the addition of HPC so that the CNCs/HPC suspension could be used to produce films with iridescence and coloration within the visible spectrum. However, the process is time consuming and took four months to acquire CNCs-CM500 liquid crystalline phase, which compromised the dissertation time conclusion. For this reason, commercial CNCss (Avicel® PH-101) were synthesized using the methodology developed by Fernandes *et al*. [35]. The same procedure was executed by C. Gouveia [70] in her dissertation thesis to produce CNCs/HPC films.

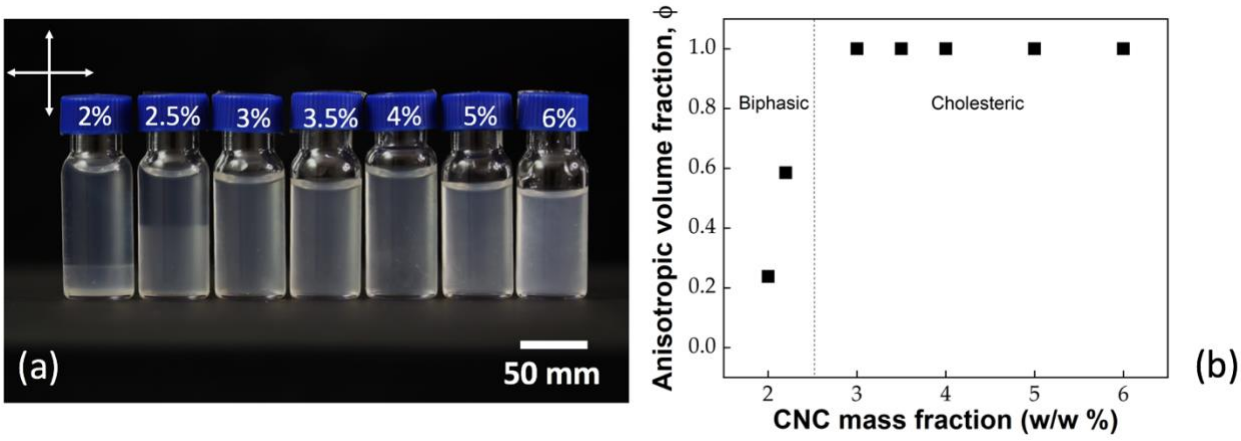

Figure 4.7 Photography taken with crossed polarizers (a) and anisotropic volume fraction of CNCs-CM500 suspension as a function of CNCs concentration (2.5, 3.0, 3.5, 4, 4.5, 5 and 6% w/w) (b).

4.1.2. CMC and CNCs-CMC

Cellulose nanocrystals from microcrystalline cellulose (Avicel® PH-101) (CNCs-CMC) were also produced and used in this dissertation. The acid hydrolysis was performed using an acid concentration of 64% w/w, at 45 ºC for 45 minutes while under continuous mechanical stirring. Therefore both CNCs and its precursor (CMC) were optically, chemically, morphologically, and structurally characterized as well.

Chemical analysis was performed by Attenuated Total Reflectance Fourier Transform Infrared spectroscopy and is presented below (**Figure 4.8**) where the black and purple spectra represents the CMC and the CNCs-CMC, respectively. Several absorption bands associated with molecular vibrations of cellulose bonds can be observed.

The coincident bands of both CMC and CNCs around 3338 cm^{-1}, 2900 cm^{-1} and 1060 cm^{-1} represent the O-H, C-H and C-O stretching vibration correspondingly [57]. The absorption band at 1638 cm^{-1} is associated with the vibration of the O-H bond of water absorption in the cellulose and 890 cm^{-1} is associated with a C-O-C stretching effect on the β(1,4) glycosidic bonds (assigned to the amorphous region) [58] [59]. CNCs spectrum band at approximately 817 cm^{-1} is attributed to S-O bond stretching due to the presence of sulfate groups resulting from acid hydrolysis [60]. This band is nonexistent in the CMC sample.

The obtained spectra exhibit absorption bands similar to the ones found in the FTIR of both CM500 and CNCs-CM500 (**Figure 4.2**), however the ones associated with S-O bonds are slightly more prominent in the CNCs-CMC, probably due to the higher time of the acid hydrolysis process. This information can be verified by elemental analysis presented in **Table 3**, where the content of the samples is detailed as well as the predicted values. Samples from the raw microcrystalline cellulose lack the sulfur element as it has not undergone acid hydrolysis.

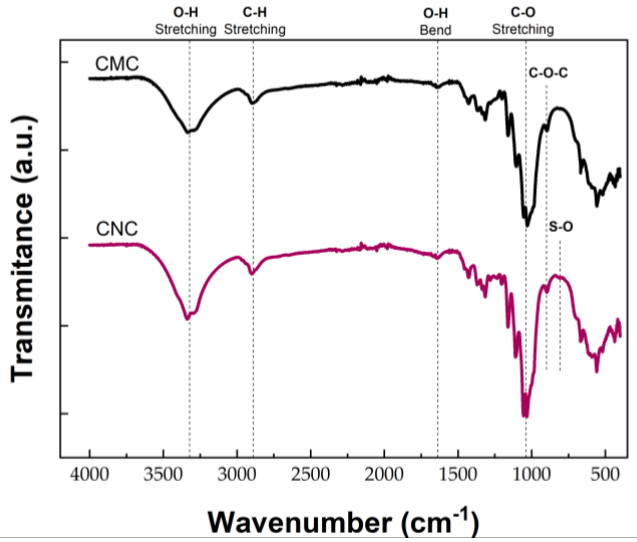

Figure 4.8 ATR-FTIR spectra of CMC (black line) and CNCs (purple line). Each vertical dotted line marks a characteristic absorption band of a cellulose macromolecule binding molecular vibration.

Table 3 C, H, S and estimated Oxygen elemental analysis of the samples CMC and CNCs-CMC, as well as the predicted values for pure cellulose.

Sample	Carbon (w/w%)	Hydrogen (w/w%)	Sulfur (w/w%)	Oxygen * (w/w%)	–OSO_3H/ 100
Pure cellulose predicted values [67]	44.44	6.18	-	49.38	-
CMC	43.51	6.42	-	50.09	-
CNCs	41.03	6.04	0.95	51.98	4.92

** values obtained by mass difference*

The average degree of substitution ($\overline{DS}$) of -OSO_3H per 100 AGP units (n) was determined using the method described by Hamad *et al.* [52] and applying the **Equation 4**. The value of n is 4.92 –OSO_3H groups per 100 AGP for the registered 0.95% sulfur content, which is in good agreement to the value presented by Yao *et al.* (0.90% ± 0.03) using the same starting material and similar reaction time of (30 min) [48].

XRD diffractograms from CMC (black line) and CNCs-CMC (purple line) samples (**Figure 4.9**) display peaks around 2θ=15º, 16.6º and 22.7º attributed to crystallographic planes of 101, $10\bar{1}$ and 002 (which is the main peak and characteristic of the crystalline region), respectively [71]. These diffraction characteristics peaks are associated with cellulose type Iβ [63].

The peak associated with the 040 plane is identified at approximately 34.8º and its perceptible to be smother in the CNCs sample. The absence of strong alteration of all peaks means the structural arrangement of the cellulose is not affected by the performed acid hydrolysis.

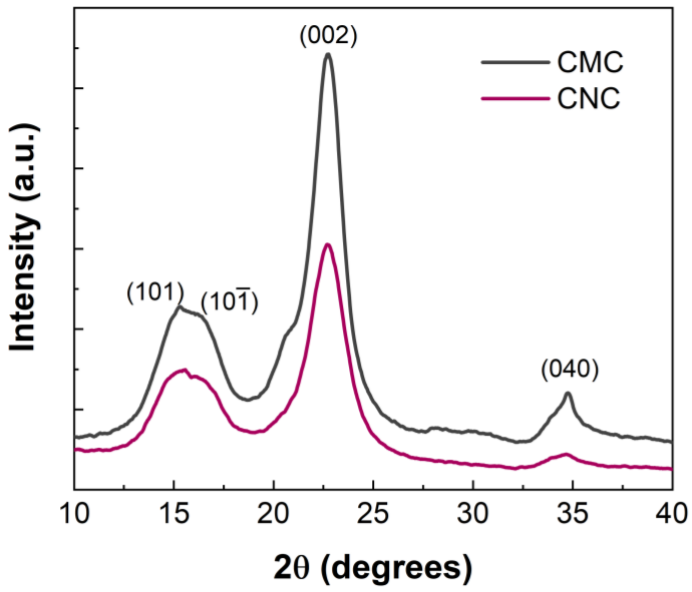

Figure 4.9 XRD diffractograms of CMC (black line) and CNCs (purple line).

The crystallinity index was determined with the empirical method presented by Segal *et al.* [64], using the **Equation 3**, described above. The CrI results are presented in the **Table 4** bellow.

Table 4 Crystallinity Index of CMC and CNCs-CMC samples determined by the empirical method presented by Segal *et al.* [64].

Sample	CrI (%)
CMC	75.7
CNCS-CMC	87.8

The CNCs has a higher crystalline index compared to CMC, which was expected since acid hydrolysis processes mainly attacked the amorphous zones of the starting material. These values are in agreement with the literature for cellulose nanocrystals obtained by acid hydrolysis from CMC (Avicel® PH101) [60], [72].

CNCs-CMC particles, drop-casted from a suspension in water with a low content of nanoparticles (0.01% w/w), were dimensionally characterized using the AFMs topographic images. The obtained images (**Figure 4.10**) were analyzed with Gwyddion software, following the methodology presented by Honorato-Rios *et al.* [56] and 150 measurements of both length and width were taken (supporting information **d**, **Figure 7.3**).

The average particle length and width dimensions were determined as 153 ± 34 nm and 6 ± 2 nm, respectively, which estimates an aspect ratio of approximatively 26. The length values are similar, however the width are slightly lower from the ones reported by Fernandes *et al.* where 152 ± 65 nm and 17 ± 7 nm of length and width, respectively and aspect ratio of 10 ± 3 were obtained [35]. The discrepancy of the width values is related to the difference of the techniques used to obtain the particle images, but also the methodology (the measuring) to obtain the particles dimensions.

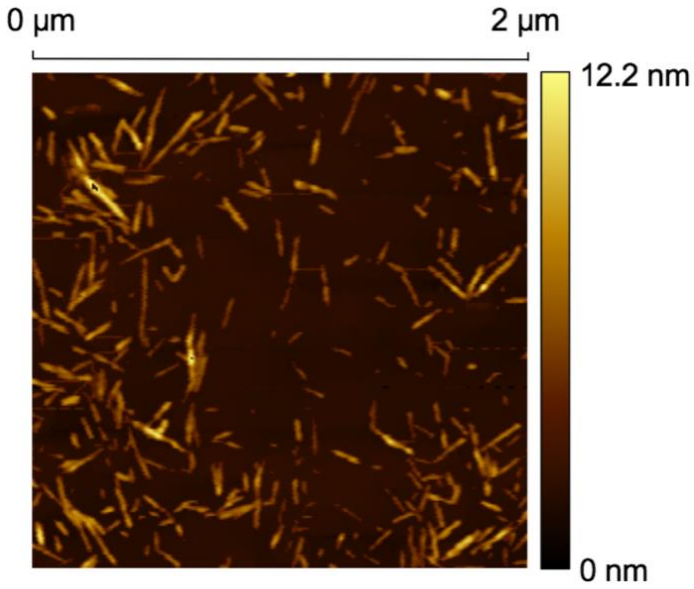

Figure 4.10 TOP view image, 2µmx2µm, of an amplitude scan obtained by AFM of CNCs-CMC fibers deposited in mica.

The thermal stability of both CMC (black lines) and CNCs-CMC (purple lines) from a microcrystalline source is analyzed in **Figure 4.11**.

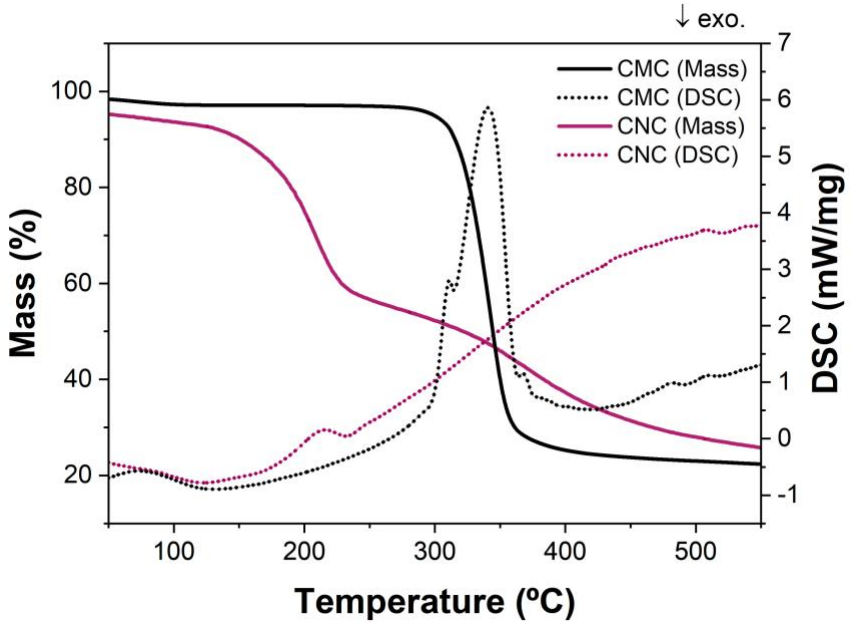

Figure 4.11 DSC-TGA analysis of CMC (black lines) and CNCs-CMC (purple line).

The scanning calorimetry with thermographic analysis of CMC and CNCs-CMC have a similar behavior when compared to CM500 and CNCs-CM500 samples at **Figure 4.6**. The smooth mass drop, on both samples, bellow 120 ºC is related to moisture evaporation. The CMC curve (black line) indicates a first order pyrolysis reaction, with a mass loss of 86.91%, from 300 ºC to 370 °C [65]. This event is associated with a high mass loss of cellulosic material and its

characterized by a series of degradation reactions, including dehydration, decomposition, and depolymerization of the glycosidic units [71].

On the CNCs curves (purple lines) the degradation starts at lower temperatures, fact probably attributed to smaller fiber dimensions as compared to the original raw material [60]. A first mass change, of 39.39%, occurs between 150 ºC to 240 °C and corresponded to the degradation of regions more accessible to the sulfate groups. The second mass loss event at 390 ºC is attributed to the breakdown of the more refractory crystalline fraction, which was less susceptible to hydrolysis leading to the formation of carbon-based residues of the samples [71].

A photograph taken between cross-polarizes of vials with CNCs-CMC suspension with different concentrations (2.2%, 2.6%, 3.0%, 3.5%, 3.8%, 4.5%, 5.5%, 6.5% and 8.5% w/w) is shown at **Figure 4.12** - **(a)** where the isotropic and anisotropic phases can be observed.

The anisotropic phase fraction of each suspension is graphically represented in **Figure 4.12** - **(b)**. One can observe that 2.2% w/w of CNCs is completely isotropic while both 6.5% and 8.5% w/w concentrations are found to be completely anisotropic. As commented before in this document, the anisotropic phase increase is not linearly with the increment of CNCss percentage.

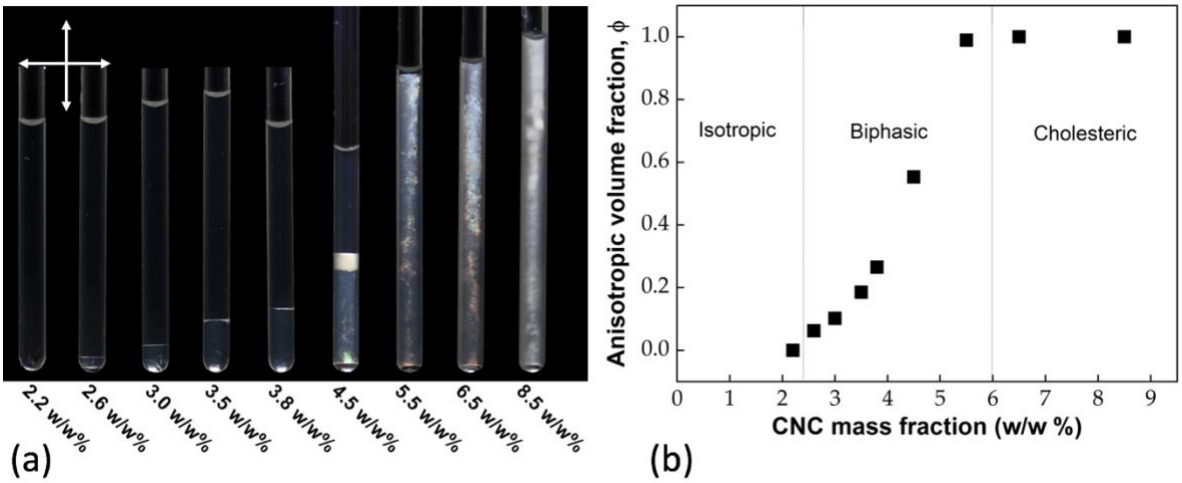

Figure 4.12 Photography taken with crossed polarizers (a) and anisotropic volume fraction of CNCs-CMC suspension as a function of CNCs concentration (b) with 2.2%, 2.6%, 3.0%, 3.5%, 3.8%, 4.5%, 5.5%, 6.5% and 8.5% w/w concentration.

The CNCs-CMC were used to produce CNCs/HPC composite films in order to obtain iridescent films that reflect structural coloration with wavelengths in the visible range of the electromagnetic spectrum. Since CNCs films tend to be brittle it is important to add HPC as a reinforcement to improve their mechanical properties.

4.2. CNCs-K/HPC composites

Based on the work developed by C. Gouveia [70] described in her Master dissertation thesis, the produced composite films of CNCs/HPC shown selective left-handed circularly polarized light reflection and right-handed circularly polarized light transmission. The observed iridescence is due to the structural organization impart by the cholesteric arrangement of the precursor suspensions, **Figure 4.13**. Although the pristine CNCs film exhibited iridescence, only the sample with 10% w/w HPC reflected structural coloration in the visible range of the electromagnetic spectrum, and the coloration tend to be lost with the increase of HPC in the composite system (supplement information **7.e**). By SEM images and UV-VIR-NIR spectroscopy

the author was able to show that the cholesteric organization was maintained even on the sample with the higher concentration of HPC and was able to determine the pitch value for each sample. Nevertheless, determination of the helicity of the CNCs organization was yet to be accessed.

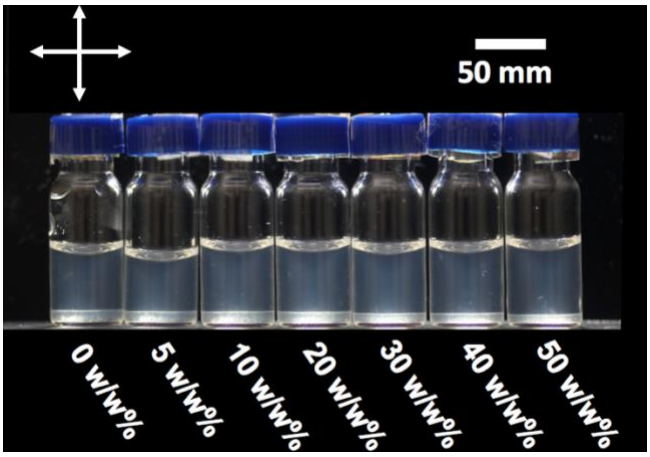

Figure 4.13 Photography taken between crossed polarizers of CNCs-CMC/HPC suspension, with 0, 5, 10, 20, 30, 40 and 50% w/w of HPC concentration in relation to the CNCs content.

The Circular Dichroism is a spectroscopy technique that allows to access the rotational direction of the polarized light, whether is clockwise (RCP), showing negative values, or counterclockwise (LCP) showing positive values. CD analysis of the CNCs/HPC films (**Figure 4.14- (a)**) confirms that 0, 10, 20 and 30% w/w HPC concentrations, although colorless, present LCP handedness. This technique only analyses wavelengths until 800 nm, for that reason, and even thought 40 and 50% w/w HPC indicated positives values, is not conclusive the same LCP light direction. Nevertheless, the SEM images of the cross-section obtained for the composite films with 40% HPC:CNCs showed a left-handed helicoidal arrangement.

Resistance to cracking of CNCs/HPC films was verified using bend test procedure in which a surface strain was applied to the sample without adding overall tensile load (**Figure 4.14 – (b)**) [73]. The strain necessary to induce surface cracking was determined by bending the samples over mandrels. Note that the films became exponentially more flexible for concentrations above 20% w/w HPC and that the 50% w/w HPC/CNCs composite sample bend without breaking for the maximum strain. The error bars indicate the standard errors associated with repetitions.

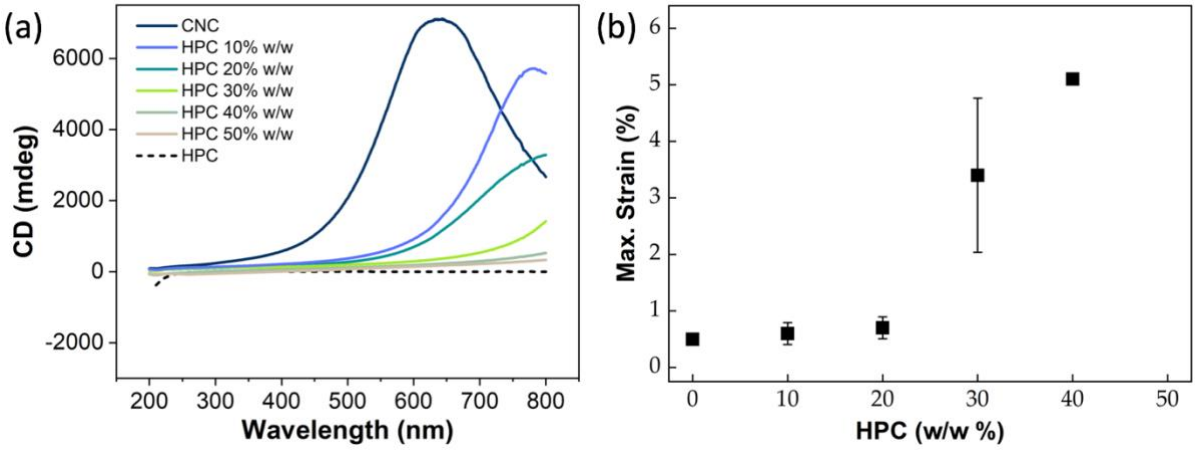

Figure 4.14 Circular dichroism (a) and mandrels bend test (b) results of CNCs/HPC films with 0, 10, 20, 30, 40, 50 and 100% w/w of HPC.

The sonication, performed during the cellulose nanocrystals production, increases the suspension cholesteric pitch and leads to a red coloration of the CNCss films after solvent evaporation [74], [75]. In addition, increasing the HPC concentration in the CNCs/HPC composite system seems to promote the increase of the pitch value of the suspensions. For these reasons, the introduction of HPC in the CNCs matrix proved not to be effective to produce iridescent and colorful CNCs/HPC composite films, as this addiction induced the wavelength shift to the near-infrared region of the electromagnetic spectrum.

Following the article published by Dong and Gray [42] it was used ion-exchange resin and a 20% w/w aqueous potassium chloride solution to induce the blue shift of the CNCs coloration. **Figure 4.15** illustrates the substitution reaction of the hydrogen, present in the sulfate groups of the CNCs chain (CNCs-H), by potassium (CNCs-K). The intention was to reduce the pitch value of the CNCss suspension so that it could increase, promoted by the addition of HPC, and could be maintained within the visible spectrum. The same substitution procedure was used with sodium, originating CNCs-Na, for the sake of comparison.

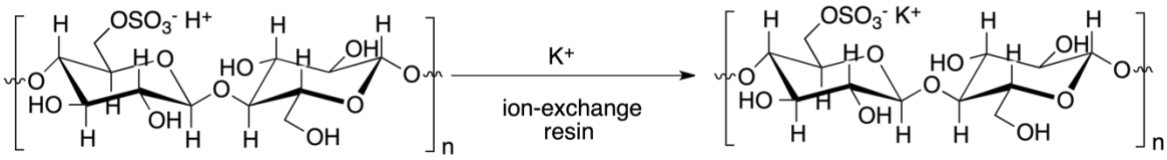

Figure 4.15 Schematic representation of the ion-exchange effect on the surface charge of the cellobiose unit.

The ICP-AES technique performed to the CNCs-K and CNCs-Na samples, described at supporting information **7.a**, revealed 77.68 mg/l of potassium and 63.10 ml/l of sodium, respectively, which proves the effectiveness of the substitution. Note that this technique is expensive and more precise than elemental analysis and that the values obtained by both methodologies should not be compared.

The ion substitution is also visually observed in **Figure 4.16**, where both CNCs-H and CNCs-K films from drop-casting method were produced and studied using POM and profilometry. Analyzing the spectrum of CNCs-H its perceptible that the maximum reflected wavelength is at 640nm (**Figure 4.16 – (c)**) which correspond to the red color of the visible spectrum (a). Both droplet casted films present LCP light reflection and RCP light transmission. After changing its counter-ion to potassium (b) a blue shift is induced in the CNCss coloration (CNCs-K, **Figure 4.16 – (b)**), to 426 nm (**Figure 4.16 – (d)**). The color change of these films, for the same suspension concentration, happens because the introduction of the counterion influences the critical concentration at which the phase separation occurs. I.e, counterion properties such as ion size, dissociation constant, hydration number, and hydrophilic/hydrophobic balance will influence the interparticle forces (as steric repulsion, electrostatic repulsion, hydration, and hydrophobic interactions) responsible for the phase separation [42]. Dong and Gray examined that when hydrated inorganic cations bind to the negatively charged particle surface a hydration force would be generated between particles and If the repulsive force between particles decreases, the critical concentration would increase [42].

The films color uniformity can be explained by the nonexistence of the so called coffee-ring effect, (**Figure 4.16 – (e), (f)**), confirmed by profilometry (attributed to the UVO treatment performed on the substrates and to the lower the solvent evaporation rate). After the substitution preceded, the registered pH increased from 1.95 for the CNCs-H, to 4.80 for the CNCs-K, as confirmed in the literature by MacLachlan *et al.* [76].

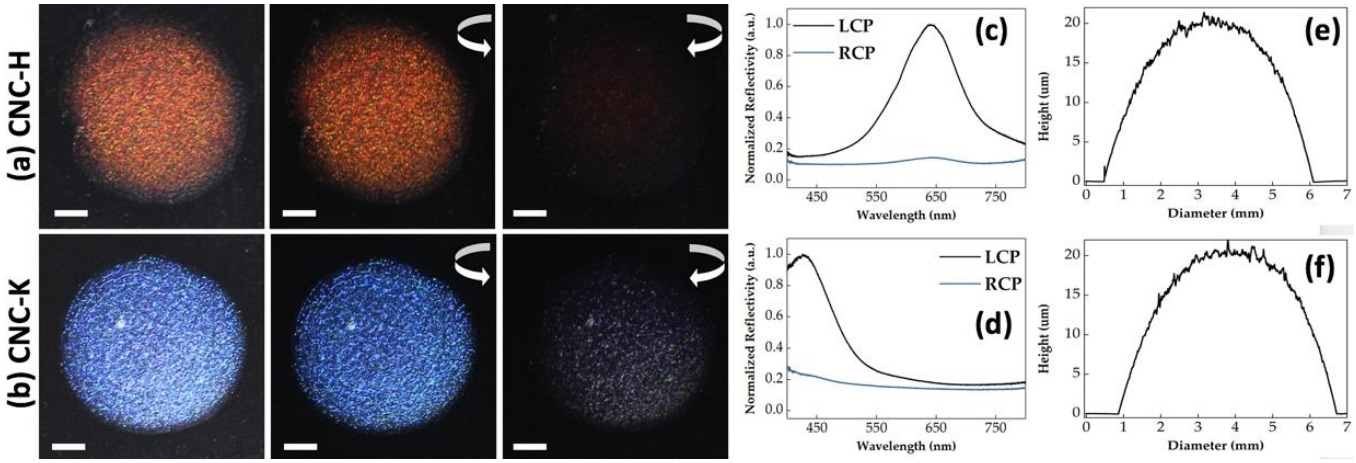

Figure 4.16 Photographic images of CNCs-H (a) and CNCs-K (b) drop-casted films observed under visible light, left and right circularly polarized light (indicated by the direction of the arrows); the obtained visible spectra (c) (d), respectively, were acquired with a spectrophotometer accoupled to the POM and the correspondingly profilometry. The scale bar corresponds to 1 mm.

DSC-TGA analysis of both CNCs-H (black lines) and CNCs-K (purple lines) (**Figure 4.17**), were proceeded to verify whether the ion exchange would affect their degradation process.

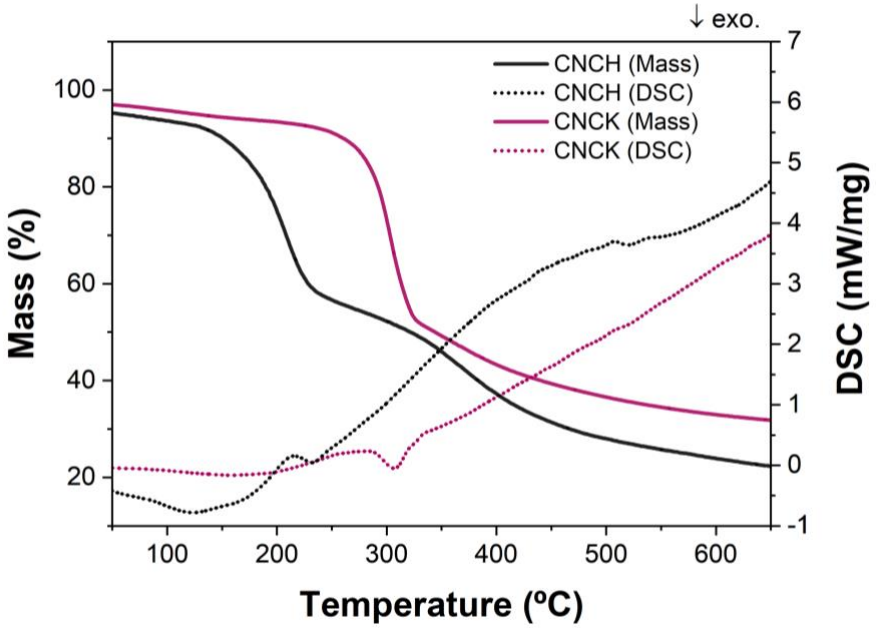

Figure 4.17 DSC-TGA analysis of CNCs-H and CNCs-K.

CNCs-H from a microcrystalline cellulose source was already analyzed in this document (sub chapter **4.1.2**). Its degradation process occurs in two steps, the first at 150 ºC to 240 ºC and the second at around 390 ºC. Meaning the CNCs-H degradation is a second order pyrolysis reaction [65]. For CNCs-K, the degradation process occurs with only one step that starts at a temperature two times higher than the one registered for CNCs-H, at 280 ºC. The ion exchange of the CNCs-H to potassium leads to an improvement of thermal properties and the transformation of the process to a first order reaction.

The ion exchange process has proven to be effective promoting the blue shift of the CNCs films, as expected, and improving its thermal properties. Dong and Gray proved that the suspensions were less temperature dependent when the counter-ion was added. The authors

explained this with the relative insensitivity of ionic and steric interactions of this nanoparticles when exposed to temperature [42].

In order to study the color potential of both CNCs-H and CNCs-K, positioned at extremes of the visible spectrum, films from drop-casted methods with different ratios of each suspension were produced. These films with 0:1, 1:3, 1:1, 3:1 and 1:0 ratios of CNCs-K/CNCs-H are registered in **Figure 4.18**, as well as the one obtained with CNCs-Na.

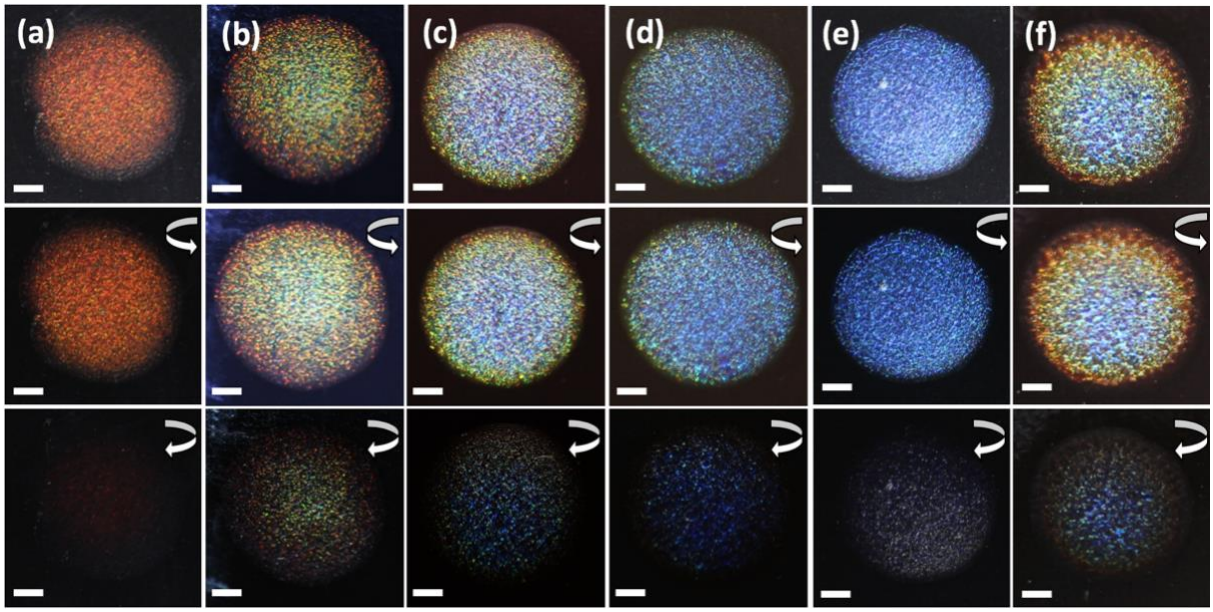

Figure 4.18 Photographic images of CNCs-K/CNCs-H films derived drop-casting method from different suspensions of: mixtures of CNCs-H and CNCs-K in different ratios 1:0 (a), 1:3 (b), 1:1 (c), 3:1 (d), 0:1 (e) and CNCs-Na (f), respectively. They were obtained under visible light and left-handed and right-handed circularly polarized light (indicated by the direction of the arrows). The scale bar corresponds to 1 mm.

The films were photographed under visible light using a left circularly polarized (LCP) and a right circularly polarized (RCP), as indicated by the direction of the arrows, with a 18º angle. It's perceptible at the macro-scale that starting with the same CNCs content in suspension, different counter-ions lead to different final coloration, since CNCs-H give rises to orange films, CNCs-K originates totally blue films and the CNCs-Na has a greenish tint. Dong and Gray stablished that as the particle size decreases, their excluded volume is reduced, and a higher suspension concentration is required to form an ordered phase. Thus, the critical concentration increases with the atomic number of the counterions and the tendency to form ordered phase formation is CNCs-H > CNCs-Na > CNCs-K [42].

In addition, a color gradient throughout the different ratios is visibly verified. These results were verified at the micro-scale using POM and the reflection spectra of the spectra recorded on the center of each film (**Figure 4.19**). The images and spectra were obtained with circular crossed polarization, left circular polarization and right circular polarization, LCP (black line) and RCP (blue line) light.

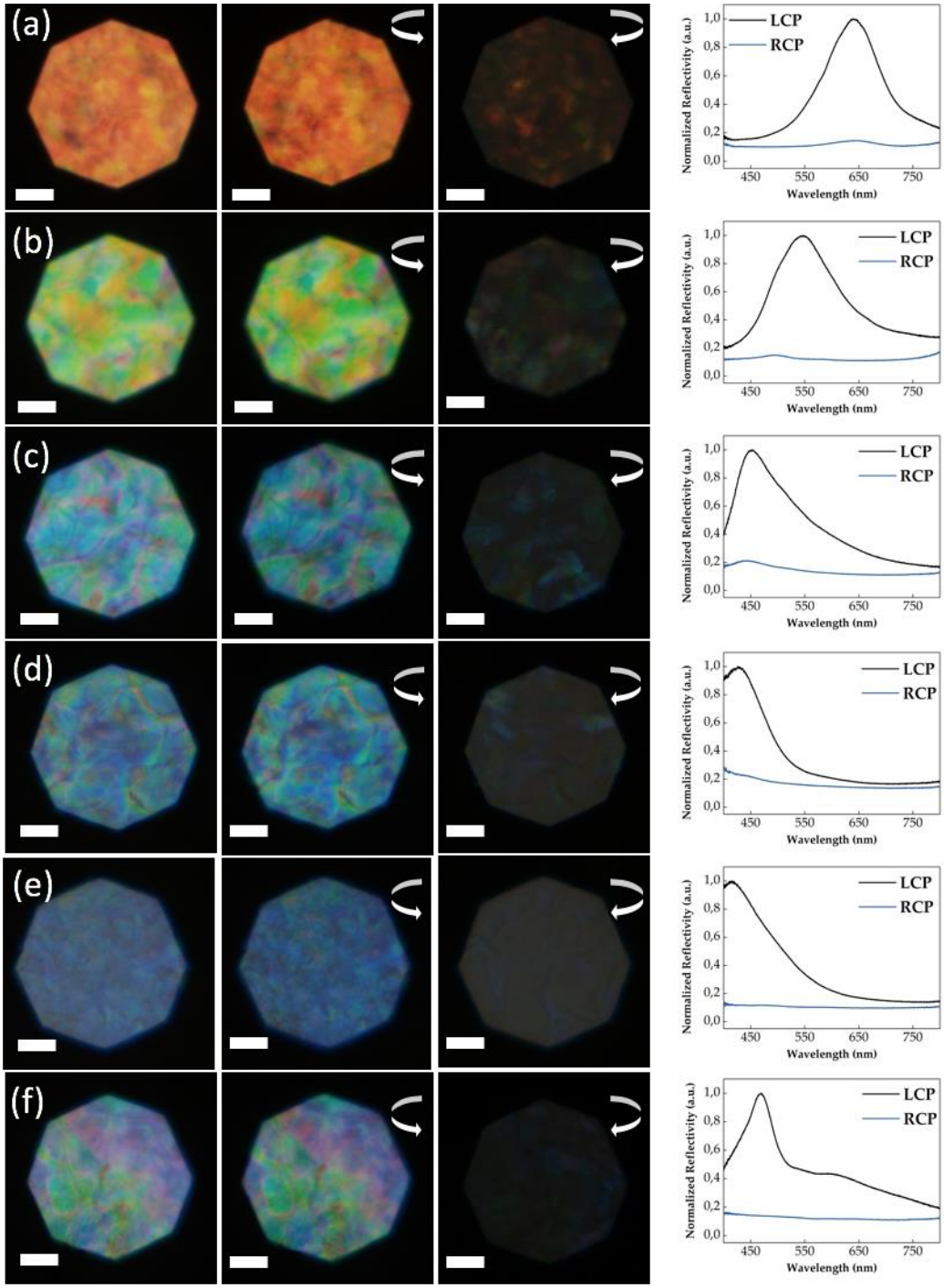

Figure 4.19 POM images, obtained in reflection mode of drop-casting films from mixtures of CNCs-K/CNCs-H in different ration, 1:0 (a), 1:3 (b), 1:1 (c), 3:1 (d), 0:1 (e) and Na (f), respectively. They were observed with circular cross polarization, left circular polarization and right polarization. The obtained spectra was acquired with LCP and RCP and the scale bar corresponds to 50 µm.

By analyzing the macro and micro images it's possible to verify that all films reflect structural coloration with wavelengths within the visible range and that the original CNCs-H (a) has a red coloration with a maximum of 640 nm. The substitution of the counter-ion to potassium (e) promotes a uniform blue shift throughout the droplet, to a maximum of 426 nm, while the substitution to sodium (f) promotes a less uniform coloration between a green and blue shade with a maximum at around 470 nm. Having in mind the de Vries equation (**Equation 1**) and considering that the refractive index of CNCs is 1.56 an estimation of the pitch value of the helicoidal arrangement at the center of the films can be estimated, as demonstrated by Dumanli

et al. [33]. **Table 5** specifies the maximum wavelength, the estimated pitch and the wavelength variation (determined by the full width at half maximum, FWHM) of the spectrum of each drop-casted film. Note that the films maximum wavelength reflection increases with the CNCs-K concentration and that the pitch value is directly proportional to the wavelength. The wavelength variation ($\Delta\lambda$) values are relatively small, between 83 to 149, but higher in the mixtures of the suspensions. Although far from an ideal cholesteric organization, where these values should be of the order of just some tens nm, the reflected color, within the observed area of the films, are well defined.

The films obtained from the mixture of CNCs-K and CNCs-H with ratios of 1:3 (b), 1:1 (c) and 3:1 (d) of CNCs-K shows a color gradient at macro (**Figure 4.18**) and micro-scale (**Figure 4.19**) that is confirmed by the obtained spectra. The mixture between both CNCss with only 25% w/w of CNCs-K displays a maximum wavelength reflection of 547 nm, which corresponds to the transition from the red original CNCs-H to a greenish coloration. For higher ratios the obtained films present a blue coloration in the center, as in the 1:1, and eventually spreads throughout the diameter of the film, as in 3:1, until it becomes completely blue, as in the film derived from 100% CNCs-K. Thus, the reflected wavelength decreases as the content in CNCs-K in the mixture increases. All films show iridescence, selective left-handed circularly polarized light reflection and right-handed circularly polarized light transmission. Although the coloration in these films is not totally uniform, which might be further controlled with the evaporation conditions, these results can be seen as a different methodology to tune structural coloration by combining suspensions with CNCs with different counter-ions, maintaining a low viscosity of the suspension. Nevertheless, the obtained films are still very brittle, but this study give us a CNCs suspension derived from CMC (Avicel® PH101) that allow to obtain iridescent films with the lower pitch value derived from LC suspensions with low content of CNCss.

Table 5 Maximum wavelength peak determined from spectra maximum reflectivity value, the cholesteric pitch value using the de Vries expression and the $\Delta\lambda$ wavelength variation (FWHM value, related to the spectral width) determined from each spectrum. Films by drop-casting method of CNCs-H, CNCs-K, CNCs-Na and different ratios of 1:3, 1:1 and 3:1 from the CNCs-K/CNCs-H mixtures. Data acquired from **Figure 4.19**.

Films	λ_{MAX} (nm)	Estimated pitch value (nm)	$\Delta\lambda$ (FWHM)
CNCS-H	640	410	110
1:3	547	351	133
1:1	454	291	117
3:1	426	273	149
CNCS-K	426	273	110
CNCs-Na	470	301	83

It is important to use hydroxypropylcellulose as a reinforcement to compensate the brittleness of the systems by increasing the flexibility while maintaining the optical characteristics of the CNCs films. HPC with an average molecular weight of 80000 was tested in order to improve the mechanical properties of the films produced by Gouveia, and the bending tests demonstrate that the addition of HPC in different ratios allowed the obtained films to be bend without breaking, as shown in **Figure 4.14**. However, this film did not present iridescence since an increase in the suspension pitch value was obtained which gave rise to a maximum reflection to wavelengths in the near-infra-red region.

HPC with average molecular weights of 100 000, 300 000 and 600 000 were added to the CNCs-K suspension in different percentages, 5, 10, 20, 30, 40 and 50% w/w of HCP in relation to the CNCs-K content. The mixtures were sonicated for a few seconds to ensure that the mixture

is homogenized and let in an Analog Shaker for a few days until full dissolution. Films of each suspension were produced, by slow evaporation of the solvent from droplets, and photographed as can be seen in **Figure 4.20**.

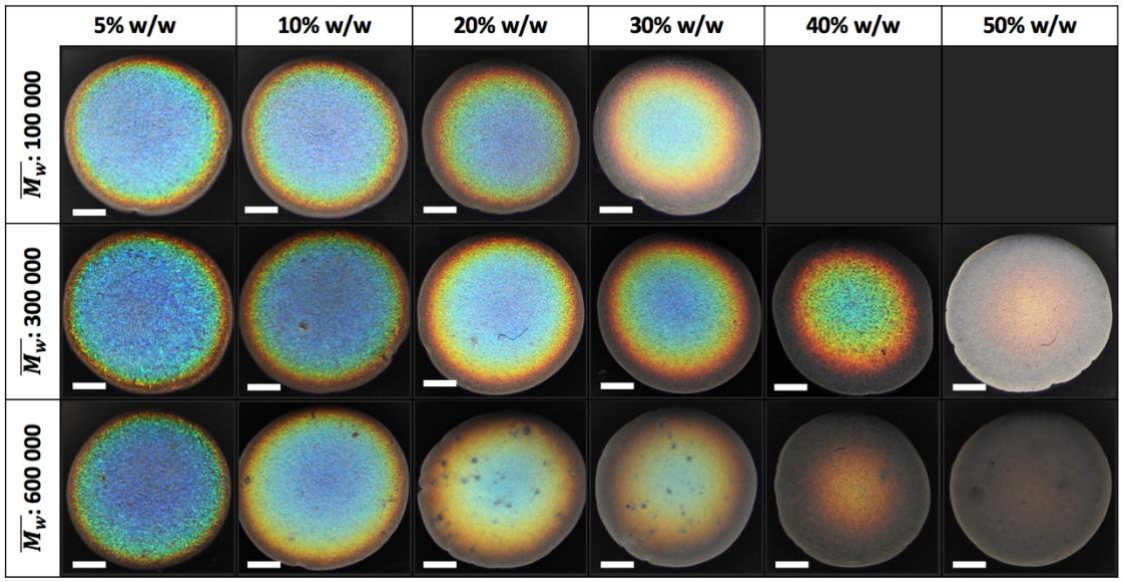

Figure 4.20 Photographic images of CNCs-K/HPC films derived from mixtures of LC CNCs-K aqueous (3.81% w/w) suspensions with different percentages of HPC (5, 10, 20, 30, 40 and 50% w/w, relative to CNCs content) and different average molecular weights (100 000, 300 000 and 600 000), taken under visible light. The scale bar corresponds to 1mm.

Although films of $\overline{M_w}$ 100 000 seem more flexible, than the ones obtained from mixtures with the HPC with $\overline{M_w}$ 80 000, the improvements were not significant, so only films from the mixtures of 5, 10, 20 and 30% w/w HPC were produced for color comparison reasons. The films obtained from the mixture of HPC with $\overline{M_w}$ of 300 000 show a color evolution as the percentage of HPC increases, starting with a blue iridescence (at 5% w/w) until the color appears only in the center with a red coloration (at 50% w/w). In the samples derived from HPC with an $\overline{M_w}$ of 600 000 the color evolution is quicker, starting with a blue coloration in the center of the 5% w/w HPC droplet and fading close to 40% w/w of HPC, where due to the lack of structural coloration at the periphery one can assume that the helicoidal pitch of the structure is in the order of magnitude of the wavelength of the near-infrared. Films obtained from mixtures with the higher molecular weight became blurred, without shimmer, to values above 20% w/w of HPC and appeared to have present particles aggregate.

The CNCs-K/HPC composite films were analyzed with Vis spectroscopy in reflection mode and their spectra were acquired at the center of the film (Supporting information **7.f**, **Figure 7.5**, **Figure 7.6**, **Figure 7.7**). **Figure 4.21 (a-c)** illustrates the maximum wavelength obtained for each film (black line) as the function of content of HPC in the sample, for each composite system. In these graphs are also plotted the wavelength variation determined as the full width at half maximum (FWHM) (blue line) as a function of the HPC content. One can see that the increment of HPC content gave rises to an increase in the reflected wavelength and is more noticeable in the sample of HPC with $\overline{M_w}$ of 600 000. In this later composite system, the film with 30% w/w of HPC presents, more than 70% of area with structural coloration and a further increase in HPC lead to a loss in visible coloration. From the same figure one can also see that the wavelength variation is larger than that observed for the other composite systems. This might imply the existence of a large number of domains with different colors, that are translated in helical structures with different pitch values. Combining this with the poor dispersibility observed

macroscopically we decided to not continue with the use of the HPC with such a high molecular weight. Although composite systems derived from the HPC present similar response to the increase of HPC content, samples with 30% w/w of HPC became more matte, less brilliant, when compared with the ones obtained with the system with HPC with $\overline{M_w}$ of 300 000.

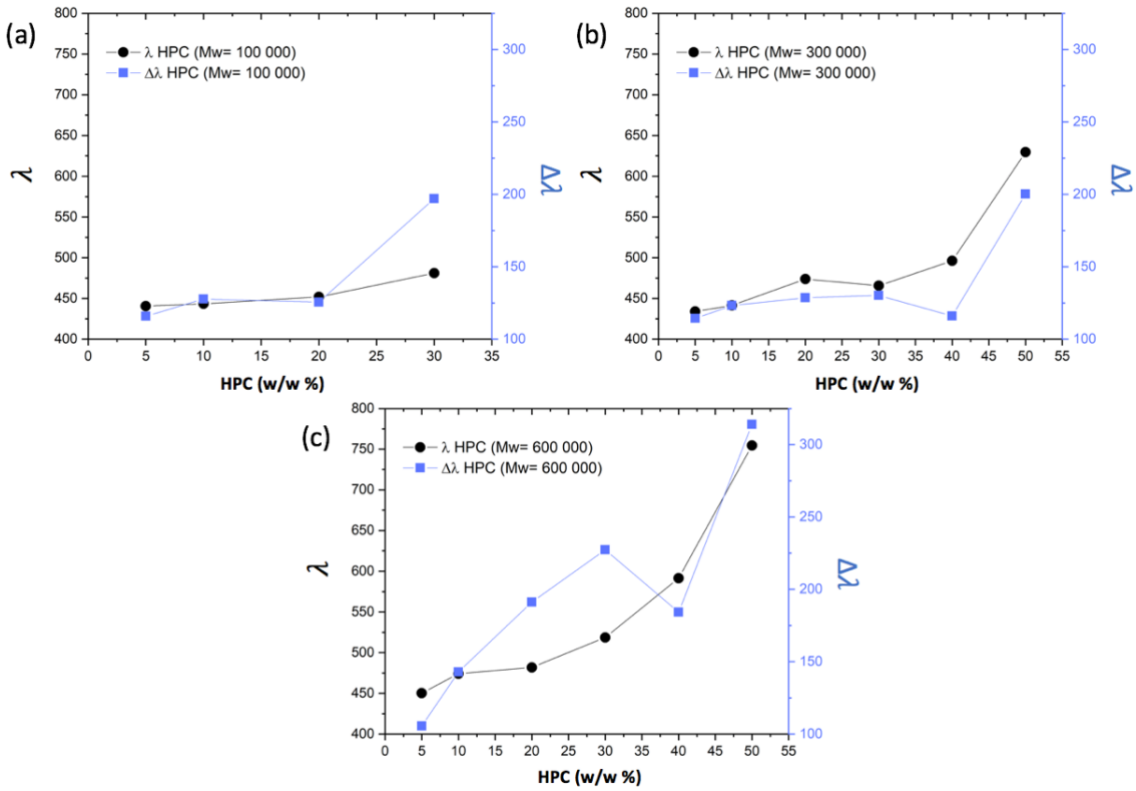

Figure 4.21 Wavelength evolution of CNCs-K/HPC droplets as a function of HPC content, with average molecular weight of 100 000 (a), 300 000 (b) and 600 000 (c). The black line represents the maximum wavelength determined at the center of the film, and the blue line represents the wavelength variation (FWHM of reflection spectrum).

The suspensions with CNCss concentrations capable of forming liquid crystal phase present tactoids when observed by POM under crossed polarizers. Tactoids are ellipsoidal shaped anisotropic droplets with parallel birefringent bands that appear in isotropic dispersions [77]. As the concentration of CNCs suspensions is increased, bigger tactoids with more periodic bands tend to appear. After depositing the films, obtained from the drop-casting method, the water from the suspensions evaporates and the tactoids have time to grow by a coalescence mechanism (where smaller tactoids fuse to form larger tactoids). Due to the gelation state, the solid film retains the cholesteric organization and some of the tactoids orientate perpendicular to the cross section, which can be observed, forming fingerprints patterns [38], [77].

The cholesteric structure in the CNCs-K/HPC films can be confirmed by the presence of fingerprints, observed in **Figure 4.22**.

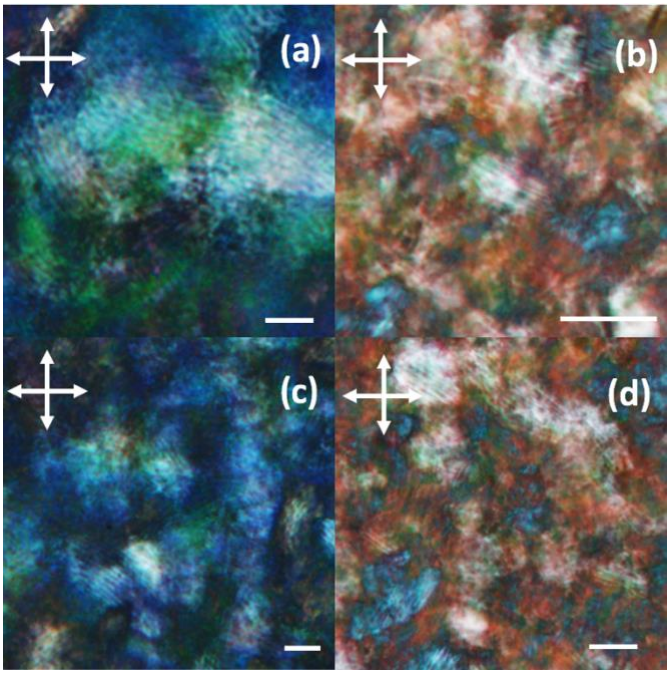

Figure 4.22 POM images of CNCs-K/HPC films textures obtained in transmission mode from 10% w/w HPC ($\overline{M_w}$ =300 000) (a), 50% w/w HPC ($\overline{M_w}$ =300 000) (b), 10% w/w HPC ($\overline{M_w}$ =600 000) (c) and 40% w/w HPC ($\overline{M_w}$ =600 000) (d). The scale bar corresponds to 20 µm.

Considering the addition of HPC in the color evolution and appearance, it was decided to proceed with the study of the composites system with HPC with $\overline{M_w}$ 300 000. The films were photographed, a 18º angle, under visible light (first row of photographs), using a left-handed circular polarizer (LCP) and with a right circular polarizer (RCP), as indicated by the direction of the arrows (**Figure 4.23**). The profilometry technique was also performed to the CNCs-K/HPC films in order to obtain their topographic profile, **Figure 4.24**.

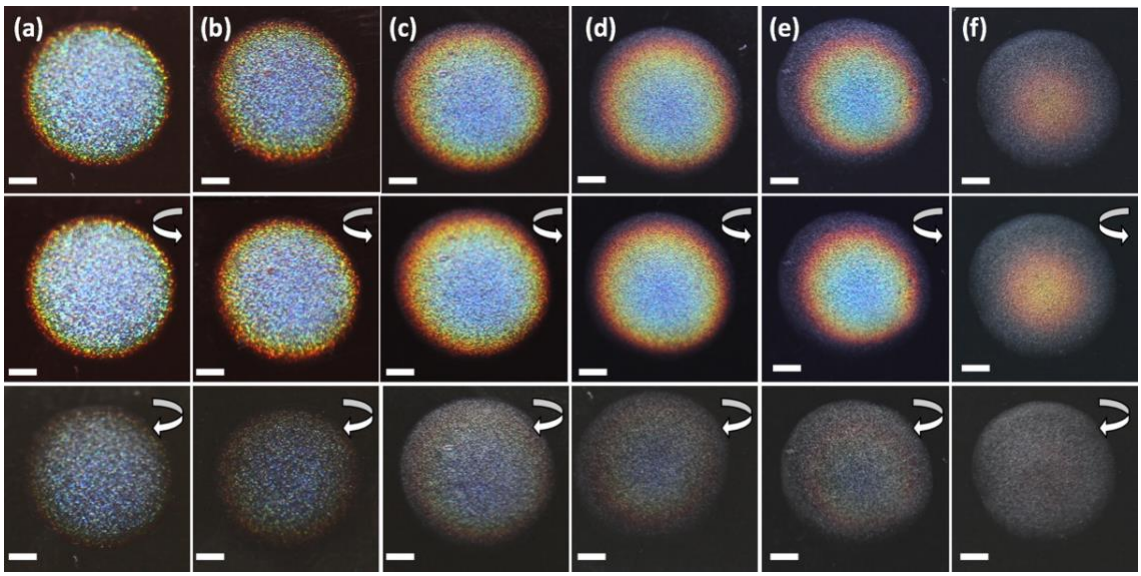

Figure 4.23 Photographic images of CNCs-K/HPC $\overline{M_w}$= 300 000 films with different percentages, 5% (a), 10% (b), 20% (c), 30% (d) 40% (e) and 50% (f) w/w of HPC, respectively. They were observed under visible light and using the left- and right-handed circular polarizer. The scale bar corresponds to 1 mm.

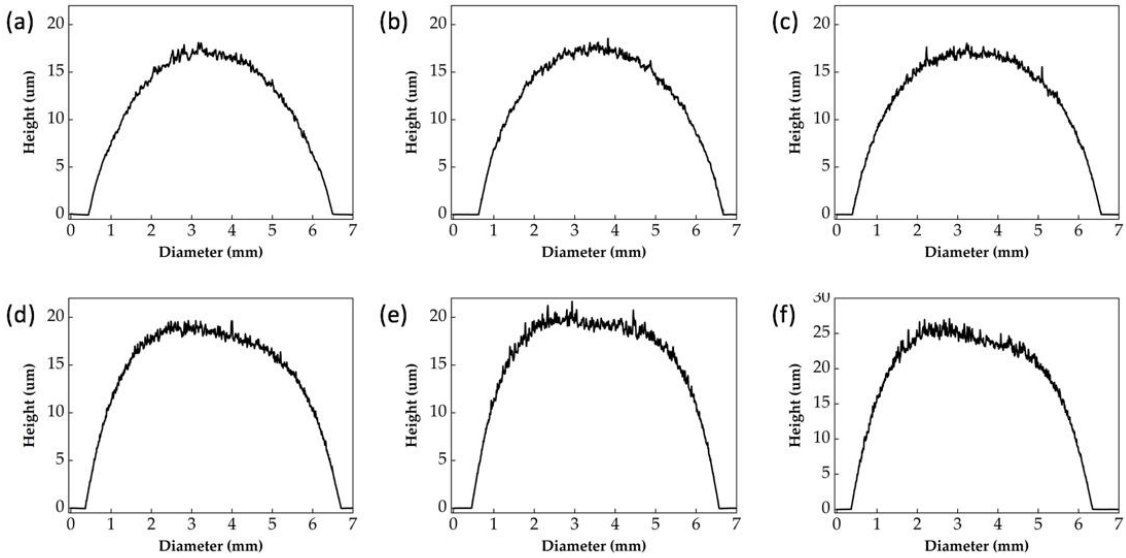

Figure 4.24 Profilometry scan across the diameter of the CNCs-K/HPC $\overline{M_w}$= 300 000 films with different percentages, 5% (a), 10% (b), 20% (c), 30% (d) 40% (e) and 50% (f) w/w of HPC, respectively.

It's noticeable on a macroscopic scale that the films present selective left circularly polarized light reflection and right circularly polarized light transmission. By analyzing **Figure 4.24** one can conclude that the coffee stain effect is faded in all CNCs-K/HPC films due to the UVO treatment performed on the subtract, and the slow evaporation of the solvent.

Figure 4.23 also shows the presence of a color gradient within each film, not observed in the pristine CNCs, which tends to increase with the HPC concentration. Starting with the sample with 5% w/w HPC (a), that presents a large blue structural coloration, this region tends to be reduced and becoming gradually smaller when the percentage of HPC is increased. By contrast, the regions with yellowish/greenish and red color tends to increase. The perimeter of the colored areas tends to decrease from 30% w/w HPC (d), from which a colorless zone begins to appear on the outer edge of the film, leading to 50% w/w HPC (f), with only a red coloration area in the center. The presence of HPC in the suspensions seems to induce a separation of cholesteric domains with different pitch values within the films. This might be related with the increase of viscosity as the HPC concentration rises, however further studies should be performed in order to understand this effect.

The change in maximum reflected wavelength can be verified at the micro-scale using POM and the characteristic wavelengths determined at the center of each film (**Figure 4.25**). The films were observed with left- (black line) and right-handed (blue line) circular polarization. By analyzing these POM images, it is possible to confirm that at the center of all the films strong coloration with wavelength within the visible range are obtained. The addition of HPC promoted the gradual increase of the wavelength, with a red-shift transition from 434 nm, for 5% w/w HPC (a), to 630 nm, for 50% w/w HPC (f). The 10% w/w HPC (b), shows a blue coloration in the center, that transitions to a greenish coloration in the samples with 20% (c) and 30% (d) w/w HPC. The 40% w/w HPC (e) appeared to have a green coloration with yellow and red notes and 50% w/w HPC (f) displayed a uniform red coloration.

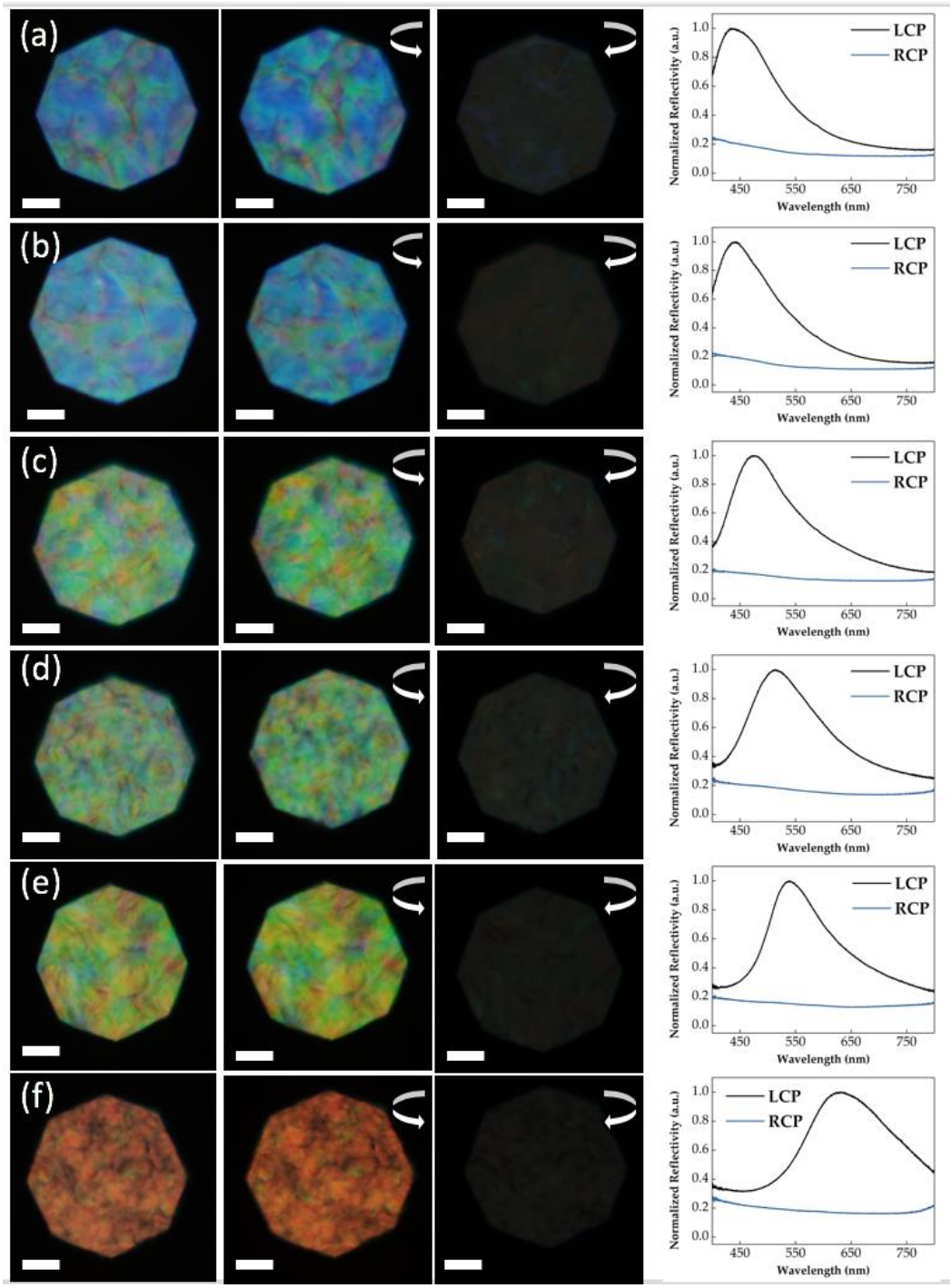

Figure 4.25 POM images, obtained in reflection mode of drop-casting films from mixtures of CNCs-K/HPC $\overline{M_w}$ = 300 000 in different percentages, 5% (a), 10% (b), 20% (c), 30% (d) 40% (e) and 50% (f) w/w of HPC, respectively. They were observed with circular cross polarization, left circular polarization and right circular polarization. The obtained spectra were acquired under LCP and RCP light and the scale bar corresponds to 50 µm.

Table 6 specifies the wavelength peak, the estimated pitch values (from **Equation 1**) and wavelength variation (by the FWHM of each spectrum) of each drop-casted film.

Table 6 Maximum wavelength peak determined from spectra maximum reflectivity value, the cholesteric pitch value using the de Vries expression and the Δλ wavelength variation (FWHM value, related to the spectral width) determined from each spectrum, of the CNCs-K/HPC films by drop-casting method with different concentrations (5, 10, 20, 30, 40, 50% w/w HPC). Data acquired from **Figure 4.25**.

w/w of HPC	λ_{MAX} (nm)	Estimated pitch value (nm)	Δλ (FWHM)
5%	434	278	433
10%	441	283	441
20%	466	299	475
30%	474	304	465
40%	496	318	496
50%	630	404	629

4.3. CNCs-K/HPC films

Based on the POM and Vis-spectroscopy results and CNCs-K/HPC films photographs, it was found that it would be possible to produce films with structural coloration with maximum wavelength reflection within the visible range of the electromagnetic spectrum, between blue and red. At the same time, 100% HPC (3% in water) films with different molecular weights were produced by the solvent evaporation process. By handling the 80 000 and 300 000 molecular weight films, it was noticed that these latter were more flexible than those of lower molecular weight. Thus, by adding HPC with $\overline{M_w}$ = 300 000, it is expected to obtain CNCs-K/HPC composite films with better optical and mechanical properties that the ones previously produced by Gouveia.

Films with 3.5 cm diameter were produced by solvent casting from a polystyrene petri dishes using 2 ml of CNCs-K/HPC suspension, CNCs (a), CNCs-K (b), 10% (c), 20% (d), 30% (e), 40% (f) and 50% (g) w/w of HPC. Photography's were taken and can be observed in **Figure 4.26**. The films with about 120 ± 10 µm (supporting information **7.g**) of thickness were photographed under visible light using a left circular polarizer (LCP) and a right circular polarizer (RCP), as indicated by the direction of the arrows.

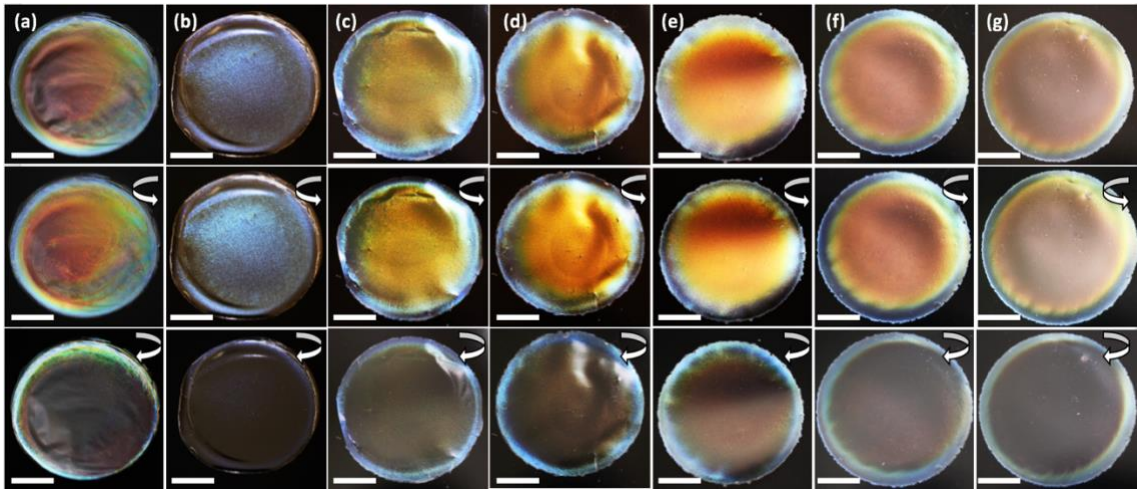

Figure 4.26 Photographic images of CNCs-H (a), CNCs-K (b), 10% (c), 20% (d), 30% (e), 40% (f) and 50% (g) w/w of HPC films, respectively. They were observed under visible light and using the left and right circular polarizers. The scale bar corresponds to 1cm.

It's evident by the photographic register that the films exhibited iridescence, selective left-handed circularly polarized light reflection, with the observation of a strong bright coloration and right-handed circularly polarized light transmission, where the films became almost colorless.

Although the optical response of these CNCs-K/HPC composite systems was better than the ones observed for the droplet-method films, obtained by 10 µl droplet evaporation, a uniform coloration throughout the entire film was not achieved. It is noteworthy that all films presented a blue outer ring, probably due to the evaporation rate process. For concentrations above 30% w/w HPC concentrations the obtained films exhibited a brightness decrease, as the shining appearance tends to fade, and from 40% w/w of HPC the films presented a matte finish.

The CNCs film (**Figure 4.26-(a)**) exhibits a bright iridescent red coloration while the blue CNCs-K (b) is the only membrane with a uniform coloration. These optical characteristics were similar to the ones presented by the films derived from droplets with the same suspensions. The 10% w/w HPC (c) film shown a predominant green iridescent coloration that becomes reddish in the 20% w/w HPC (d) film. Films with 30% (e), 40% (f) and 50% w/w HPC (g) revealed color variation in three distinct areas, the red center, that tends to become gradually wider when the HPC percentages increases, a blue periphery and a green area in between. The structural coloration of the center of the films were confirmed using POM reflection images. These were observed under visible light, left-handed circular polarization and right-handed circular polarization and its characteristic wavelengths determined by spectroscopy (**Figure 4.27**). The LCP spectra were used to determinate the maximum wavelength peak, and the wavelength variation (by the FWHM value) and the estimated pitch value, using the Vries equation (**Equation 1**) for each film, which is specified at **Table 7.**

Table 7 Maximum wavelength peak determined from spectra maximum reflectivity value, the cholesteric pitch value using the de Vries expression and the $\Delta\lambda$ wavelength variation (FWHM value, related to the spectral width) determined from each spectrum, of the CNCs-K/HPC composite films (CNCs-H, CNCs-K, and 10, 20, 30, 40, 50% w/w HPC concentrations). Data acquired from **Figure 4.27**.

Samples	λ_{MAX} (nm)	Estimated pitch value (nm)	$\Delta\lambda$ (FWHM)
CNCS-H	665	426	230
CNCS-K	426	273	116
10% w/w HPC	544	349	172
20% w/w HPC	554	355	168
30% w/w HPC	621	398	179
40% w/w HPC	686	440	194
50% w/w HPC	742	476	234

Based on **Figure 4.27**, its noticeable that all CNCs-K/HPC composite films present structural coloration within the visible range of the electromagnetic spectrum and that the maximum wavelength tends to increase with the addition of HPC, also perceptible at **Table 7**, as already verified in the films obtained from droplets. For that reason, 10% w/w of HPC film (**Figure 4.25**- **(c)**) evident a green coloration, with 544 nm, where its starts to appear a yellow tint for the 20% w/w HPC (d) film, with a maximum of 554 nm and a 355 nm pitch value. The film with 30% w/w of HPC (e), with a maximum wavelength value of 621 nm presents a 398 nm pitch, is completely red. The 40% (f) and 50% (g) w/w of HPC films present a maximum wavelength of 686 nm and 742 nm respectively, showing a trend to an increase of wavelength towards the near-infrared region of the electromagnetic spectrum. Note that the CNCs-H film presents a higher number of multicolored domains and the highest value of wavelength variation of 230 nm, twice the value of CNCs-K and reflects a strong coloration in the red wavelength, with 665 nm, while CNCs-K has a well-defined peak, with 116 nm of $\Delta\lambda$ and a maximum wavelength in the blue visible range, with 426 nm.

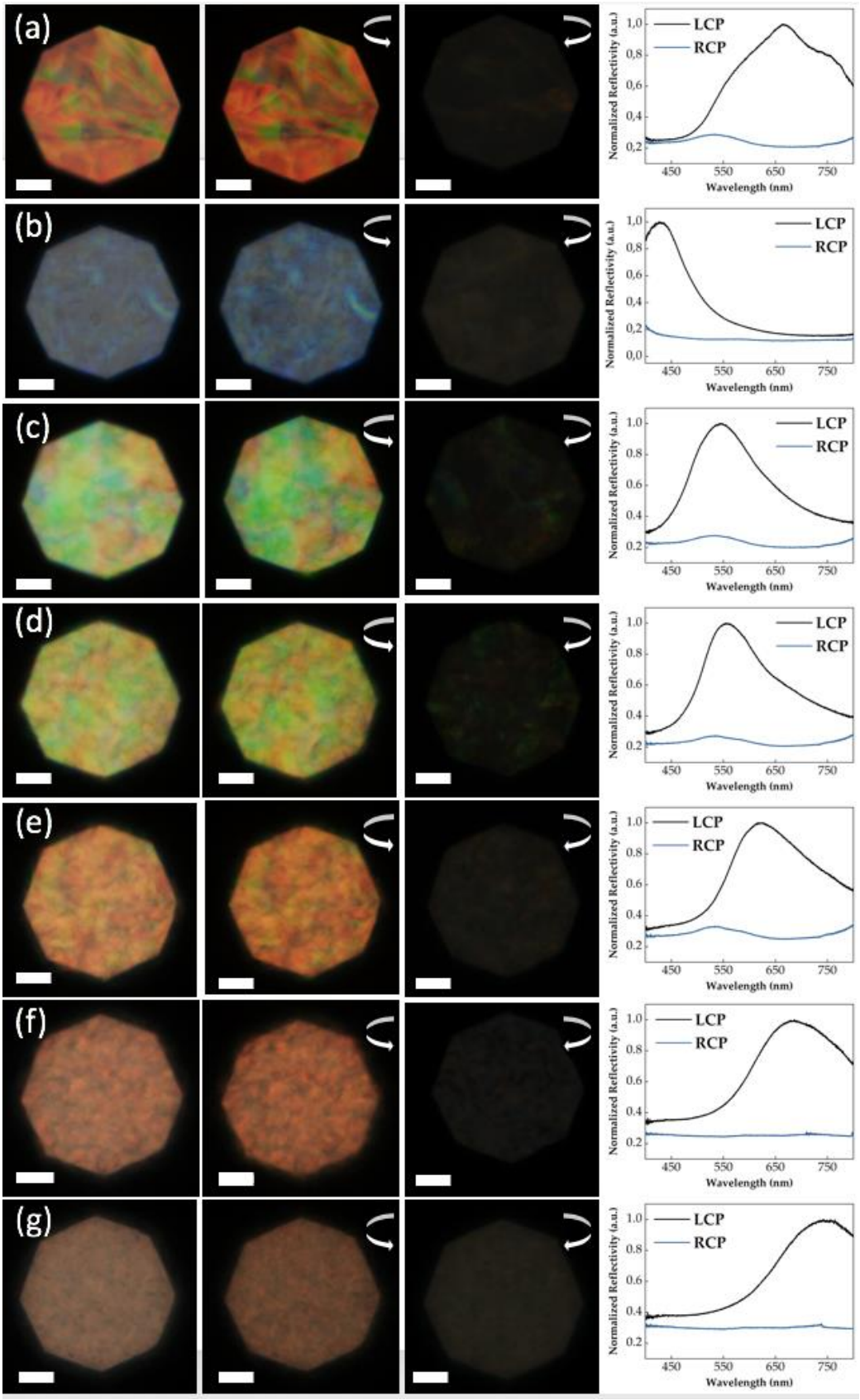

Figure 4.27 POM images, obtained in reflection mode of CNCs (a), CNCs-K (b) and different percentages of 10% (c), 20% (d), 30% (e), 40% (f) and 50% (g) w/w of HPC, respectively. They were observed with visible light, left circular polarization and right circular polarization. The obtained spectra were acquired with LCP and RCP and the scale bar corresponds to 50 μm.

The FTIR spectra of CNCs, CNCs-K, HPC and CNCs-K/HPC system with 300 000 molecular weight are presented in **Figure 4.28**. It is evident that the CNCs and CNCs-K are identical which indicates that the ion exchange does not interfere with the absorbance of the characteristic bonds of cellulose. Also, the difference between the CNCs and the HPC spectra are not significant since hydroxypropylcellulose is derived from cellulose with addition of 2-hydroxypropyl groups [78], therefore, it has similar characteristics chemical bonds. Note that these have common bands such as O-H, C-H and C-O at around, 3330 cm^{-1}, 2900 cm^{-1} and 1069 cm^{-1}, respectively [79]. For that reason, the films with 20% and 50% w/w of HPC are very similar as well, nevertheless the C-H and C-O bonds become more pronounced with the increased of HPC percentages.

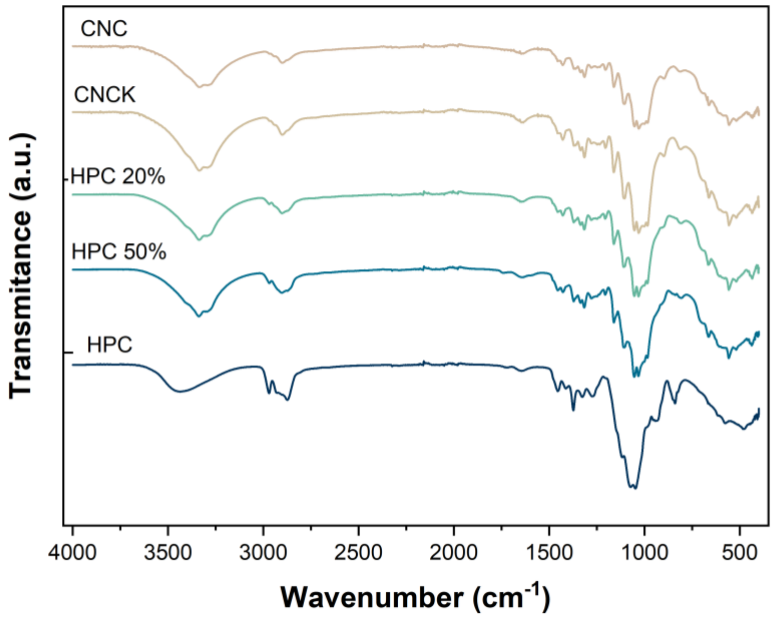

Figure 4.28 FTIR spectra of CNCs-K/HPC ($\overline{M_w}$= 300 000) films of CNCs, CNCs-K, 20%, 50% and 100% w/w of HPC, respectively.

XRD diffractograms of CNCs-K and 20%, 50% and 100% w/w of HPC with 300 000 molecular weight are presented in **Figure 4.29**. The first displays the characteristic peaks of cellulose nanocrystals with peaks at 2θ=15º, 16.6º and 22.7º attributed to crystallographic planes of 101, $10\bar{1}$ and 002 (which is the main peak and characteristic of the crystalline region), respectively [71]. The hydroxypropylcellulose film exhibit a peak at 2θ=8º corresponding to the HPC crystallographic plane 100 and another at 2θ= 20,3º which is a slightly oriented amorphous halo [80]. The presence of the HPC as a reinforcement in the CNCs-K/HPC composite films is proven by the appearance of these characteristics' peaks in the 20% and 50% w/w HPC, where the 100 plane is most evident for the higher concentration.

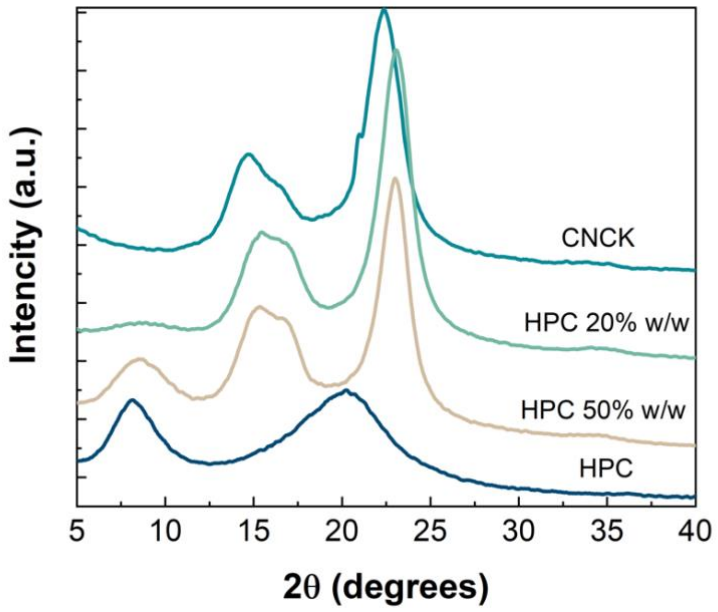

Figure 4.29 XRD diffractograms of CNCs-K/HPC ($\overline{M_w}$= 300 000) films with 0%, 20%, 50% and 100% w/w of HPC, respectively.

Thermal stability is of critical importance for optical materials, since oxidation will influence the inherent colors and water absorption capacity [48]. For that reason, thermogravimetric analysis of CNCs, 50% and 100% w/w HPC were accomplished to verify the stability acquired by the composite films when hydroxypropylcellulose is used as reinforcement of the CNCs-K matrix (**Figure 4.30**).

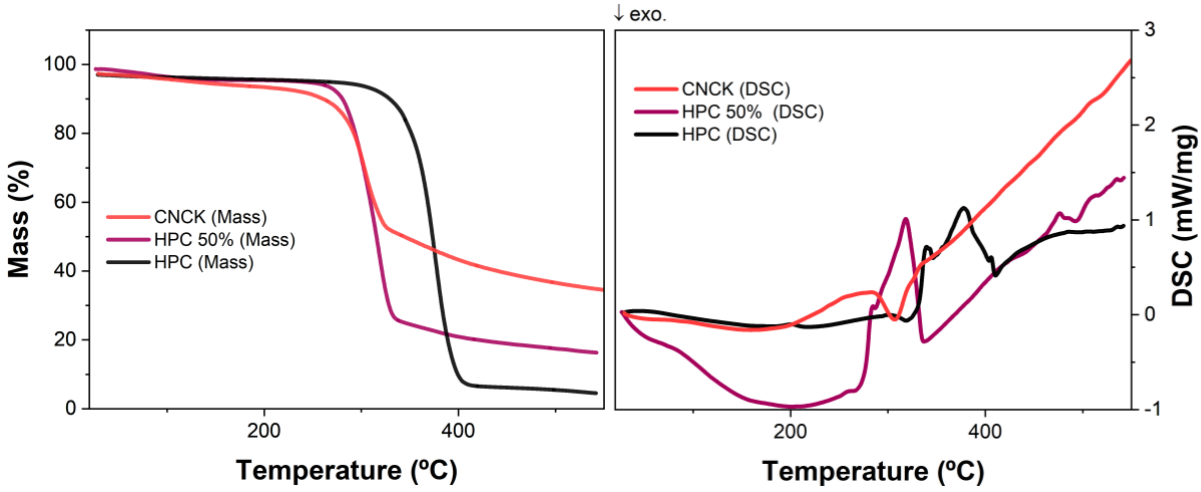

Figure 4.30 DSC-TGA analysis of CNCs-K, 50% and 100% w/w of HPC films (red, purple and black lines respectively).

As demonstrated before, the ion exchange of the protonated CNCs from H_+ to K_+ leads to a first order reaction, **Figure 4.17**. The degradation process of the CNCs-K, **Figure 4.30** red line, displays a mass change of 45.95% between 270 ºC to 320 ºC. In the HPC film (black line), the degradation process occurs also in one single stage and starts at a higher temperatures, at 300 ºC, with a mass drop of 92.69%. It appears to have an endothermic peak at 378 ºC. The film with 50% w/w of HPC, represented by the purple line, is a first order degradation reaction where

only one massive drop appears, between the ones registered for CNCs-K and HPC diffractogram, this is between 290 ºC and 335 ºC, with an 82.46% mass variation. Meaning that the introduction of hydroxypropylcellulose in the composite system causes an improvement in the mass degradation making the CNCs-K/HPC composite films more thermally stable [23].

4.4. CNCs-K/HPC films mechanical tests

Although the flexibility of the films were visibly enhanced while handling the films, it is important to quantify the mechanical improvements when hydroxypropylcellulose was added as a reinforcement in the CNCs-K matrix. Several experiences were done in order to attain such results however, numerous problems were encountered during mechanical testing. In the first tries the film slip from the equipment clamps. In order to overcome this problem CNCs-K/HPC films were placed between two acetate frames, where each one contained double-sided adhesive tape to bond both frames and the film.

It was noted that when closing the clamps, the film slip due to the glide of the tape, or one end of the film was dragged and did not break, **Figure 4.31 (a)** and **(b)**, respectively. So, mounting the sample in the equipment was a great problem and the best results were obtained when the test was performed without frames. Although we could obtain some data the samples always broke exactly on the equipment clamps. These results induce a lot of uncertainty as to whether the break was due to the test itself or due to the force exerted by the grips, **Figure 4.31 (c)**. The images of some of these tests are presented below, **Figure 4.31**. Due to the lack of time no other methodology was tested.

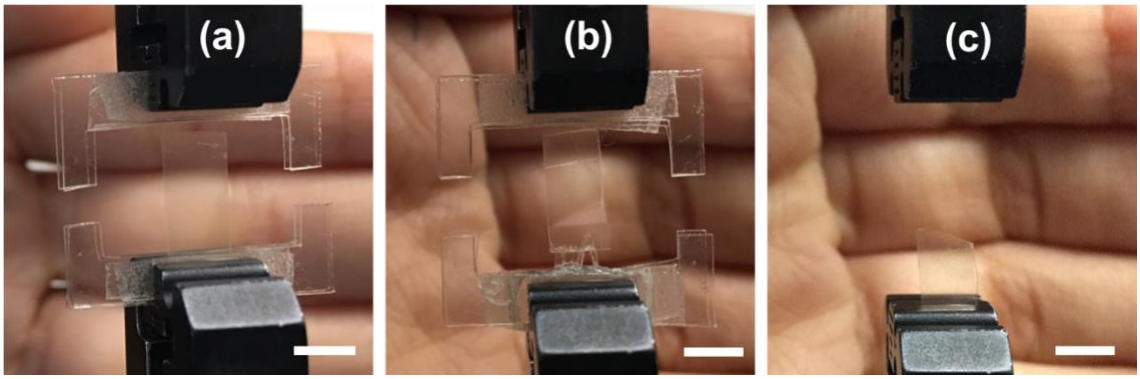

Figure 4.31 Images taken after the mechanical test procedure with frame, (a) and (b), and without frame (c) using the 50% w/w of HPC concentration.

5. Conclusion and future perspectives

The main goal of this work was to produce cellulose nanocrystalline composite films with the addition of hydroxypropylcellulose, as a reinforcement, in order to improve the flexibility of CNCs films while maintaining their typical structural coloration, when obtained from a lyotropic aqueous diluted CNCs suspension.

CM500 from a eucalyptus source with particles lengths of 359 ± 212 µm, measured using POM, went through an acid hydrolysis process with a 50% yield and originated needle-like particles with average particle length and width dimensions of 336 ± 92 nm and 9 ± 3 nm, respectively, with an aspect ratio of 37 ratio. The crystalline index, measured using the empirical Segal method from XRD data, was registered as 88.2%, which corresponds to a 5% increase compared with the raw material (CM500). The degree of substitution was calculated as 2.09 - OSO_3H groups per 100 AGP units using elemental analysis. The separation between isotropic to anisotropic phase of this CNCs when suspended in water was found to occur between 2% and 2.5% w/w of CNCs content. CNCs-CM500 hold great potential, due to their high aspect ratio, to produce CNCs/HPC composites films with iridescence and visible coloration. However, the process was time-consuming and impossible to carry out further studies in this dissertation time.

In parallel, studies using CNCs-CMC were performed in order to understand the effect of the counter-ion in the CNCs coloration pallet as well as its introduction in the CNCs-K/HPC composite system. For that reason, the protons present on ester sulfate groups were substituted to potassium and sodium and suspensions with 0:1, 1:3, 1:1, 3:1 and 1:0 ratios of CNCs-K/CNCs-H were produced. Droplets were deposited on a pre-treated substrate with UVO treatment, by drop-casting method, to create a hydrophobic zone and promote the planar anchoring of the CNCs suspension. It was confirmed that the substitutions enabled the blue shift of the CNCss coloration, using POM, and that CNCs-K is thermally more stable than the protonated CNCs, proven by DSC-TGA analysis. The different ratios shown a gradual wavelength evolution from red to blue and all droplets exhibited iridescence, selective left circularly polarized light reflection and right circularly polarized light transmission.

To improve the mechanical properties of the brittle CNCs films, hydroxypropylcellulose ($\overline{M_w}$= 300 000) was added to the CNCs-K suspension in different percentages, 5%, 10%, 20%, 30%, 40%, 50% w/w of HPC. Films with these suspensions were obtained by the solvent evaporation technique. It was proven that the addition of HPC increases the wavelength leading to the infrared spectrum, however POM images proved that the films presented coloration in the visible range even for the higher concentration. CNCs-K, with a blue coloration, proved to be a great starting point for the addition of HPC to the system, preserving wavelength from passing to infrared. The color evolution was gradual, and the increase of the pitch value was proportional to the addition of hydroxypropylcellulose, having been obtained films with blue, green and red coloration. These composite films although presenting structural coloration lose its brilliance above 30% w/w HPC transitioning to a matte finish.

In conclusion, it was possible to control the color pallet of the films of CNCss with ion exchange and mimic the nanostructures present in nature, as an example of the *Cetonia aurata* beetle, since the CNCs-K/HPC films also displayed LCP light reflection and RCP light transmission using 100% cellulosic products.

An enhanced of the mechanical properties seems to be achieved with addition of plasticizer polymer, HPC with 300 000 molecular weight, since the films are less brittle (however mechanical testing should be done to confirm this observation) without compromising the structural coloration.

In the future, it would be interesting to produce CNCs/HPC composite systems obtained from eucalyptus (Micronized Cellulose) and study the films color evolution potential. It is attractive

to try different times for the acid hydrolysis to examine its influence in the yield, liquid crystalline phase separation and coloration. These colored CNCs-K/HPC films have potential to be used in inkjet or other printing methods and tested in different substrates. They can also be used as ink and so it is noteworthy to study and control the viscosity and rheology of the mixtures. Therefore, in order to continue this study, draw more conclusions and improve the product, I propose the following tests:

- Study the organization at the nanoscale, with SEM or TEM techniques;
- Study the influence of HPC addition on the suspension properties by, for instance, rheology;
- Determine the ionic strength of the different suspensions by DLS, zeta potential stability and see if the presence of HPC affects their stability;
- Determine the film's mechanical properties;
- Determine the composite mixtures rheological properties;
- Determine the brightness and opacity of films;

In the long run it would be interesting to study the possible addition of a fluorescent element in order to mimic the multiple structural characteristics of the *Hoplia coerulea* beetle, thus produce a cellulose-based OVD with several safety levels.

6. References

[1] B. Baloukas, “Thin Film-Based Optically Variable Security Devices : From Passive to Active,” *PhD Dissertation*, no. École Polytechnique de Montréal. p. 220, 2012.

[2] Bank of england, “Banknote statistics | Bank of England,” 2019. [Online]. Available: https://www.bankofengland.co.uk/statistics/banknote. [Accessed: 08-Feb-2019].

[3] “• Counterfeit euro banknotes in Europe 2012-2018 | Statistic.” [Online]. Available: https://www.statista.com/statistics/412739/europe-euro-banknotes-counterfeit-removed/. [Accessed: 08-Feb-2019].

[4] Y. P. Zhang, “Anti-counterfeiting method using synthesized Nanocrystalline Cellulose Taggants,” no. Diss. Ph. D. Thesis, McGill University, Montreal. 2012.

[5] J. Sun, B. Bhushan, and J. Tong, “Structural coloration in nature,” *RSC Adv.*, vol. 3, no. 35, pp. 14862–14889, 2013.

[6] S. Tadepalli, J. M. Slocik, M. K. Gupta, R. R. Naik, and S. Singamaneni, “Bio-Optics and Bio-Inspired Optical Materials,” *Chem. Rev.*, vol. 117, no. 20, pp. 12705–12763, 2017.

[7] S. R. Mouchet *et al.*, “Photonic scales of Hoplia coerulea beetle: Any colour you like,” *Mater. Today Proc.*, vol. 4, no. 4, pp. 4979–4986, 2017.

[8] M. Giese, M. K. Khan, W. Y. Hamad, and M. J. MacLachlan, “Imprinting of photonic patterns with thermosetting amino-formaldehyde- cellulose composites,” *ACS Macro Lett.*, vol. 2, no. 9, pp. 818–821, 2013.

[9] M. Giese and M. Spengler, “Cellulose nanocrystals in nanoarchitectonics-towards photonic functional materials,” *Mol. Syst. Des. Eng.*, vol. 4, no. 1, pp. 29–48, 2019.

[10] M. Mitov, “Cholesteric liquid crystals in living matter,” *Soft Matter*, vol. 13, no. 23, pp. 4176–4209, 2017.

[11] J. A. Kelly, M. Giese, K. E. Shopsowitz, W. Y. Hamad, and M. J. MacLachlan, “The development of chiral nematic mesoporous materials,” *Acc. Chem. Res.*, vol. 47, no. 4, pp. 1088–1096, 2014.

[12] Y. Geng, P. L. Almeida, S. N. Fernandes, C. Cheng, P. Palffy-Muhoray, and M. H. Godinho, “A cellulose liquid crystal motor: a steam engine of the second kind,” *Sci. Rep.*, vol. 3, no. 1, p. 1028, Dec. 2013.

[13] K. Shuichi, “Structural Colors in the Realm of Nature,” in *World Scientific*, W. Scientific, Ed. Singapure: World Scientific Publishing Co. Pte., 2008, pp. 1–145.

[14] T.-D. Nguyen, E. Sierra, H. Eguiraun, and E. Lizundia, “Iridescent cellulose nanocrystal films: the link between structural colour and Bragg’s law.,” *Eur. J. Phys.*, vol. 39, no. 4, 2018.

[15] C. Chindawong, “Drying-Induced Structure Formation in Polymer Films,” Ph. D, Natural and Material Science at Clausthal University of Technology, 2015.

[16] S. Vignolini and N. Bruns, “Bioinspiration Across All Length Scales of Materials,” *Adv. Mater.*, vol. 30, no. 19, pp. 2018–2020, 2018.

[17] M. K. Khan, M. Giese, M. Yu, J. A. Kelly, W. Y. Hamad, and M. J. Maclachlan, “Flexible mesoporous photonic resins with tunable chiral nematic structures,” *Angew. Chemie - Int. Ed.*, vol. 52, no. 34, pp. 8921–8924, 2013.

[18] W. Y. Hamad, “Cellulose nanocrystals: Properties, production and applications,” in *Cellulose Nanocrystals: Properties, Production and Applications*, First., C. V. Stevens, Ed. Chichester, West Sussex: 2017 John Wiley & Sons Ltd, 2017, pp. 1–289.

[19] J. George and S. N. Sabapathi, “Cellulose nanocrystals: synthesis, functional properties, and applications.,” *Nanotechnol. Sci. Appl.*, vol. 8, pp. 45–54, 2015.

[20] S. Tongye, P. Langan, A. D. French, G. P. Johnson, and S. Gnanakaran, “Conformational flexibility of soluble cellulose oligomers: Chain length and temperature dependence,” *J. Am. Chem. Soc.*, vol. 131, no. 41, pp. 14786–14794, 2009.

[21] J. P. Borges, J. P. Canejo, S. N. Fernandes, P. Brogueira, and M. H. Godinho, “Cellulose-Based Liquid Crystalline Composite Systems,” in *Nanocellulose Polymer Nanocomposites*, vol. 9781118871, Hoboken, NJ, USA: John Wiley & Sons, Inc., 2014, pp. 215–235.

[22] A. P. C. Almeida, J. P. Canejo, S. N. Fernandes, C. Echeverria, P. L. Almeida, and M. H. Godinho, “Cellulose-Based Biomimetics and Their Applications,” *Adv. Mater.*, vol. 30, no. 19, 2018.

[23] O. W. Guirguis and M. T. H. Moselhey, “Thermal and structural studies of poly (vinyl alcohol) and hydroxypropyl cellulose blends,” *Nat. Sci.*, vol. 04, no. 01, pp. 57–67, 2012.

[24] R. S. Werbowyj and D. G. Gray, “Ordered Phase Formation in Concentrated Hydroxypropylcellulose Solutions,” *Macromolecules*, vol. 13, no. 1, pp. 69–73, 1980.

[25] C. Echeverria, P. L. Almeida, G. Feio, J. L. Figueirinhas, and M. H. Godinho, “A cellulosic liquid crystal pool for cellulose nanocrystals: Structure and molecular dynamics at high shear rates,” *Eur. Polym. J.*, vol. 72, pp. 72–81, 2015.

[26] S. N. Fernandes *et al.*, “Structural color and iridescence in transparent sheared cellulosic films,” *Macromol. Chem. Phys.*, vol. 214, no. 1, pp. 25–32, 2013.

[27] P. G. Gennes and J. Prost, “Liquid crystals: main types and properties, The Physics of Liquid Crystals,” in *Oxford University Press, Oxford, U.K*, Second., vol. 2, J. Birman, S. F. Edwards, C. H. Llewellyn Smith, and M. Rees, Eds. Paris, 1993, pp. 1–40.

[28] I.-C. Khoo, *Liquid Crystals*, Second. Hoboken, NJ, USA: John Wiley & Sons, Inc., 2007.

[29] S. N. Fernandes, L. F. Lopes, and M. H. Godinho, “Recent advances in the manipulation of circularly polarised light with cellulose nanocrystal films,” *Curr. Opin. Solid State Mater. Sci.*, vol. 23, no. 2, pp. 63–73, Apr. 2019.

[30] L. Wang, A. M. Urbas, and Q. Li, “Nature-Inspired Emerging Chiral Liquid Crystal Nanostructures: From Molecular Self-Assembly to DNA Mesophase and Nanocolloids,” *Adv. Mater.*, vol. 1801335, pp. 1–42, 2018.

[31] V. Sharmaa, M. Crneb, J. O. Parkc, and M. Srinivasaraoc, “Unusual coloration in scarabaeid beetles,” *Mater. Today Proc. 1*, no. 1, pp. 161–171, 2014.

[32] S. R. Mouchet *et al.*, “Liquid-induced colour change in a beetle: the concept of a photonic cell.,” *Sci. Rep.*, vol. 6, no. 1, pp. 1–10, Jan. 2016.

[33] A. G. Dumanli *et al.*, “Digital color in cellulose nanocrystal films,” *ACS Appl. Mater. Interfaces*, vol. 6, no. 15, pp. 12302–12306, 2014.

[34] T. H. Zhao, R. M. Parker, C. A. Williams, K. T. P. Lim, B. Frka-Petesic, and S. Vignolini, “Printing of Responsive Photonic Cellulose Nanocrystal Microfilm Arrays,” *Adv. Funct. Mater.*, vol. 29, no. 21, 2019.

[35] S. N. Fernandes *et al.*, “Mind the Microgap in Iridescent Cellulose Nanocrystal Films,” *Adv. Mater.*, vol. 29, no. 2, p. 1603560, 2017.

[36] T. Wu, J. Li, J. Li, S. Ye, J. Wei, and J. Guo, “A bio-inspired cellulose nanocrystal-based nanocomposite photonic film with hyper-reflection and humidity-responsive actuator properties,” *J. Mater. Chem. C*, vol. 4, no. 41, pp. 9687–9696, 2016.

[37] W. Li *et al.*, “The liquid crystalline order, rheology and their correlation in chitin whiskers suspensions,” *Carbohydr. Polym.*, vol. 209, pp. 92–100, 2019.

[38] J. F. Revol, H. Bradford, J. Giasson, R. H. Marchessault, and D. G. Gray, “Helicoidal self-ordering of cellulose microfibrils in aqueous suspension,” *Int. J. Biol. Macromol.*, vol. 14, no. 3, pp. 170–172, 1992.

[39] J. F. Revol, L. D. Godbout, and D. G. Gray, “Solidified liquid crystals of cellulose with optically variable properties,” 1997.

[40] J. Leng *et al.*, “Flexible latex photonic films with tunable structural colors templated by cellulose nanocrystals,” *J. Mater. Chem. C*, vol. 6, no. 9, pp. 2396–2406, 2018.

[41] A. Sydney Gladman, E. A. Matsumoto, R. G. Nuzzo, L. Mahadevan, and J. A. Lewis, “Biomimetic 4D printing,” *Nat. Mater.*, vol. 15, no. 4, pp. 413–418, 2016.

[42] X. M. Dong and D. G. Gray, “Effect of counterions on ordered phase formation in suspensions of charged rodlike cellulose crystallites,” *Langmuir*, vol. 13, no. 8, pp. 2404–2409, 1997.

[43] C. C. Y. Cheung, M. Giese, J. A. Kelly, W. Y. Hamad, and M. J. Maclachlan, “Iridescent chiral nematic cellulose nanocrystal/polymer composites assembled in organic solvents,” *ACS Macro Lett.*, vol. 2, no. 11, pp. 1016–1020, 2013.

[44] B. Natarajan *et al.*, “Binary Cellulose Nanocrystal Blends for Bioinspired Damage Tolerant Photonic Films,” *Adv. Funct. Mater.*, vol. 28, no. 26, pp. 1–11, 2018.

[45] Y. P. Zhang, V. P. Chodavarapu, A. G. Kirk, and M. P. Andrews, “Nanocrystalline cellulose for covert optical encryption,” *J. Nanophotonics*, vol. 6, no. 1, p. 063516, Jul. 2012.

[46] C. Chindawong and D. Johannsmann, “An anisotropic ink based on crystalline nanocellulose: Potential applications in security printing,” *J. Appl. Polym. Sci.*, vol. 131, no. 22, pp. 1–6, 2014.

[47] Y. D. He *et al.*, “The Angular Size and Proper Motion of the Afterglow of GRB 030329,” *ACS Appl. Mater. Interfaces*, vol. 10, no. 6, pp. 5805–5811, 2004.

[48] K. Yao, Q. Meng, V. Bulone, and Q. Zhou, “Flexible and Responsive Chiral Nematic Cellulose Nanocrystal/Poly(ethylene glycol) Composite Films with Uniform and Tunable Structural Color,” *Adv. Mater.*, vol. 29, no. 28, pp. 1–8, 2017.

[49] H. Wan *et al.*, “Rapidly Responsive and Flexible Chiral Nematic Cellulose Nanocrystal Composites as Multifunctional Rewritable Photonic Papers with Eco-Friendly Inks,” *ACS Appl. Mater. Interfaces*, vol. 10, no. 6, pp. 5918–5925, 2018.

[50] J. A. Kelly, A. M. Shukaliak, C. C. Y. Cheung, K. E. Shopsowitz, W. Y. Hamad, and M. J. MacLachlan, “Responsive photonic hydrogels based on nanocrystalline cellulose,” *Angew. Chemie - Int. Ed.*, vol. 52, no. 34, pp. 8912–8916, 2013.

[51] J. Chen *et al.*, “Self-healing responsive chiral photonic films for sensing and encoding,” *J. Mater. Chem. C*, vol. 6, no. 29, pp. 7767–7775, 2018.

[52] W. Y. Hamad and T. Q. Hu, “Structure-process-yield interrelations in nanocrystalline cellulose extraction,” *Can. J. Chem. Eng.*, vol. 88, no. 3, pp. 392–402, 2010.

[53] B. Frka-Petesic, G. Guidetti, G. Kamita, and S. Vignolini, “Controlling the Photonic Properties of Cholesteric Cellulose Nanocrystal Films with Magnets,” *Adv. Mater.*, vol. 29, no. 32, pp. 1–7, 2017.

[54] D. Saraiva, “Electro-optical devices based on cellulose nanocrystals,” Faculdade de Ciências e Tecnologia da Universidade Nova de Lisboa, 2018.

[55] X. M. Dong, J. F. Revol, and D. G. Gray, “Effect of microcrystallite preparation conditions on the formation of colloid crystals of cellulose,” *Cellulose*, vol. 5, no. 1, pp. 19–32, 1998.

[56] C. Honorato-Rios *et al.*, “Fractionation of cellulose nanocrystals: enhancing liquid crystal ordering without promoting gelation,” *NPG Asia Mater.*, vol. 10, no. 5, pp. 455–465, 2018.

[57] J. L. Huang, C. J. Li, and D. G. Gray, “Functionalization of cellulose nanocrystal films via ‘thiol-ene’ click reaction,” *RSC Adv.*, vol. 4, no. 14, pp. 6965–6969, 2014.

[58] V. Hospodarova, E. Singovszka, and N. Stevulova, “Characterization of Cellulosic Fibers by FTIR Spectroscopy for Their Further Implementation to Building Materials,” *Am. J. Anal. Chem.*, vol. 09, no. 06, pp. 303–310, 2018.

[59] D. Ciolacu, F. Ciolacu, and V. I. Popa, “Amorphous cellulose - Structure and characterization,” *Cellul. Chem. Technol.*, vol. 45, no. 1–2, pp. 13–21, 2011.

[60] D. Gaspar *et al.*, “Nanocrystalline cellulose applied simultaneously as the gate dielectric and the substrate in flexible field effect transistors,” *Nanotechnology*, vol. 25, no. 9, 2014.

[61] C. M. Popescu, C. M. Tibirna, I. E. Raschip, M. C. Popescu, P. Ander, and C. Vasile, “Bulk and surface characterization of unbleached and bleached softwood kraft pulp fibres,” *Cellul. Chem. Technol.*, vol. 42, no. 9–10, pp. 525–547, 2008.

[62] E. de Morais Teixeira, A. C. Corrêa, A. Manzoli, F. de Lima Leite, C. de Ribeiro Oliveira, and L. H. C. Mattoso, “Cellulose nanofibers from white and naturally colored cotton fibers,” *Cellulose*, vol. 17, no. 3, pp. 595–606, 2010.

[63] S. Nam, A. D. French, B. D. Condon, and M. Concha, “Segal crystallinity index revisited by the simulation of X-ray diffraction patterns of cotton cellulose Iβ and cellulose II,” *Carbohydr. Polym.*, vol. 135, pp. 1–9, Jan. 2016.

[64] L. Segal, J. J. Creely, A. E. Martin, and C. M. Conrad, “An Empirical Method for Estimating the Degree of Crystallinity of Native Cellulose Using the X-Ray Diffractometer,” *Text. Res. J.*, vol. 29, no. 10, pp. 786–794, 1959.

[65] D. Y. Kim, Y. Nishiyama, M. Wada, and S. Kuga, “High-yield carbonization of cellulose by sulfuric acid impregnation,” *Cellulose*, vol. 8, no. 1, pp. 29–33, 2001.

[66] G. H. D. Tonoli *et al.*, “Cellulose micro/nanofibres from Eucalyptus kraft pulp: Preparation and properties,” *Carbohydr. Polym.*, vol. 89, no. 1, pp. 80–88, 2012.

[67] J. L. Huang, C. J. Li, and D. G. Gray, “Cellulose nanocrystals incorporating fluorescent methylcoumarin groups,” *ACS Sustain. Chem. Eng.*, vol. 1, no. 9, pp. 1160–1164, 2013.

[68] C. Honorato-Rios, A. Kuhnhold, J. R. Bruckner, R. Dannert, T. Schilling, and J. P. F. Lagerwall, “Equilibrium Liquid Crystal Phase Diagrams and Detection of Kinetic Arrest in Cellulose Nanocrystal Suspensions,” *Front. Mater.*, vol. 3, no. 21, pp. 1–13, May 2016.

[69] M. D. Xue, T. Kimura, J. F. Revol, and D. G. Gray, “Effects of ionic strength on the isotropic-chiral nematic phase transition of suspensions of cellulose crystallites,” *Langmuir*, vol. 12, no. 8, pp. 2076–2082, 1996.

[70] C. Gouveia, “Elementos oticamente variáveis para sistemas de anti falsificação originários de celulose nanocristalina,” Faculdade de Ciências e Tecnologia da Universidade Nova de Lisboa, 2018.

[71] N. F. Vasconcelos *et al.*, “Bacterial cellulose nanocrystals produced under different hydrolysis conditions: Properties and morphological features,” *Carbohydr. Polym.*, vol. 155, pp. 425–431, 2017.

[72] S. Park, J. O. Baker, M. E. Himmel, P. A. Parilla, and D. K. Johnson, “Cellulose crystallinity index: Measurement techniques and their impact on interpreting cellulase performance,” *Biotechnol. Biofuels*, vol. 3, pp. 1–10, 2010.

[73] A. G. Hernández *et al.*, *Protection of Materials and Structures From the Space Environment*, vol. 32, no. Chapter 12. Ibaraki: Springer, 2013.

[74] S. Beck, J. Bouchard, and R. Berry, “Controlling the reflection wavelength of iridescent solid films of nanocrystalline cellulose,” *Biomacromolecules*, vol. 12, no. 1, pp. 167–172, 2011.

[75] R. M. Parker *et al.*, “The Self-Assembly of Cellulose Nanocrystals : Hierarchical Design of Visual Appearance,” *Adv. Mater.*, vol. 1704477, no. 30.19, pp. 1–13, 2018.

[76] Y. T. Xu, Y. Dai, T. D. Nguyen, W. Y. Hamad, and M. J. MacLachlan, “Aerogel materials with periodic structures imprinted with cellulose nanocrystals,” *Nanoscale*, vol. 10, no. 8, pp. 3805–3812, 2018.

[77] P. X. Wang, W. Y. Hamad, and M. J. MacLachlan, “Structure and transformation of tactoids in cellulose nanocrystal suspensions,” *Nat. Commun.*, vol. 7, no. May, pp. 1–8, 2016.

[78] C. Echeverria, P. L. Almeida, G. Feio, J. L. Figueirinhas, and M. H. Godinho, “A cellulosic liquid crystal pool for cellulose nanocrystals: Structure and molecular dynamics at high shear rates,” *Eur. Polym. J.*, vol. 72, pp. 72–81, Nov. 2015.

[79] T. Huq *et al.*, “Nanocrystalline cellulose (NCC) reinforced alginate based biodegradable nanocomposite film,” *Carbohydr. Polym.*, vol. 90, no. 4, pp. 1757–1763, 2012.

[80] R. J. Samuels, “Solid-state characterization of the structure and deformation behavior of water-soluble hydroxypropylcellulose,” *J. Polym. Sci. Part A-2 Polym. Phys.*, vol. 7, no. 7, pp. 1197–1258, 1969.

[81] ASTM, “Standard Test Methods for Bend Testing of Material for Ductility 1,” 1998.

[82] P. Oswald, “Phase transitions and unwinding of cholesteric liquid crystals,” *Org. Electron. Optoelectron. F.*, vol. 661, no. 2, pp. 47–78, 2006.

7. Supporting information

a. Characterization

Characterization via Fourier Transform Infrared (FTIR) spectroscopy was obtained using a PerkinElmer Spectrum Two spectrometer equipped with a universal attenuated total reflectance ATR element (Perkin Elmer Ltd, Bucks, UK). Spectra were acquired at room temperature, with data between 4000 to 400 cm^{-1} with a 4 cm^{-1} resolution.

X-Ray diffraction (XRD) spectra were acquired using a PANalytical X'pert PRO model diffractometer with Bragg-Brentano (θ/2θ coupled) geometry with CuK (λ = 1.5406 Å) radiation at 45 KV and 40 mA. The XRD patterns were obtained with a scanning step of 2θ=0.033°, from 5º to 40° C.

Thermogravimetric analysis coupled with Scanning calorimetry with (TGA-DSC) was performed using a STA 449 F3 Jupiter® simultaneous thermal analyzer. Each sample was heated at a heating rate of 10 ºC/min from 25 to 900 ºC, in an inert nitrogen atmosphere.

Elemental analysis (EA) was performed using a Thermo-Finnigan-CE Instruments Flash EA 1112 CHNS series model element analyzer, based on the combustion method of vanadium pentoxide catalyzed material.

ICP-AES technique was performed by digesting 2.7 mg of the CNCs-K and CNCs-Na in 500 µl of nitric acid (p.a.). The process was carried out at 60 ° to 70 ° C for 1 hour or until complete dissolution.

In order to determine the average length and diameter dimensions of the produced CNCs, Atomic Force Microscopy (AFM) data acquired using an Asylum Re-search MFP-3D tapping mode system with commercial silicon probes (scanning frequency of 300 kHz, k=26 N/m). The analyzed CNCs particles were prepared by depositing 1 µl droplets of an extremely diluted CNCs suspension in water onto a mica substrate (Muscovite Mica, V-5 from Electron Microscopy Sciences). Just prior to deposition, the suspension was sonicated in an ice bath with a Hielscher UP400S ultrasonic tip (460 W, 24 kHz, 0.85 cycle and 80% amplitude) for two consecutive 20 minute periods. AFM images were analyzed with Gwyddion software (version 2.50, http://gwyddion.net) and the process consisted of 150 manual measurements of CNCs particles length and width.

Polarized Optical Microscopy (POM) images were obtained using a polarized optical microscope (Olympus BX-51) connected to a cold light source (Olympus KL2500). An equipped camera (Olympus DP73) and Olympus Stream Basic 1.9 software were used for image capture. Reflectance spectrometry analysis of the produced CNCs films was measured with a Sarspec spectrometer (using the software LightScan 1.1.17, in Sense+ mode)

Photographs taken from the films were captured with the Canon EOS 550D camera coupled to an EF-S60 mm macro lens under visible radiation and using left and right circular rotation polarizers or cross polarizers.

Circular dichroism (CD) experiments were performed using an Applied Photophysics Chirascan™ CD spectrometer. The scanned wavelengths ranged from 200 and 800 nm, with a bandwidth of 1 nm and scanning rate of 200 nm/s.

Bend-testing of the CNCs/HPC films were conducted using cylindrical mandrels apparatus with a semi-suspended pliable platform (BRAIVE Instruments), and a set of mandrels varying in diameter. A total of 10 mandrels were used, ranging in diameter from 25 to 2 mm. Briefly, within 1 second, each film was folded to 180° to form an inverted "U" (**Figure 7.1**) shaped angle over the mandrel, maintaining close contact with it [81] The shape was maintained for 2 seconds before release. Each sample was bend-tested using successively smaller mandrels, with

the sample being inspected after being bent around each mandrel. The bend procedure was continued until cracks were visible or until the sample did not experience any cracking with the smallest mandrel, in which case the sample was recorded as having not cracked (NC).

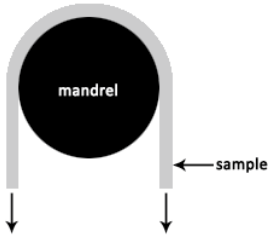

Profilometry was used to map the surface of solid CNCs films derived from droplets using

Figure 7.1 Schematic representation of the bend-test configuration showing a sample bent around a mandrel.

a KLA Tencor D-600 stylus profilometer. Scanning speed was 0.05 mm/s, while stylus weight applied was 2 mg.

b. POM measurements of CM500 fibers length

Table 8 POM measurements of CM500 fibers length.

	Measurements										
CM500 Fibers Length (µm)	170.368	551.752	228.571	229.198	692.912	49.762	373.623	591.939	117.855	150.111	637.486
	194.53	194.706	255.687	143.542	817.056	373.623	315.231	190.313	462.316	694.644	372.814
	406.185	229.014	117.539	266.64	400.272	315.231	172.756	105.787	205.116	263.123	173.069
	679.837	259.251	437.567	331.985	745.671	172.756	153.764	132.628	242.842	740.447	357.429
	244.136	130.953	851.085	65.41	573.693	153.764	533.698	148.746	181.789	225.572	437.657
	268.646	340.068	195.197	297.37	586.808	533.698	434.104	224.104	189.349	235.338	334.173
	387.015	405.201	199.588	439.817	279.307	434.104	774.966	611.462	509.887	230.893	465.48
	300.605	950.223	183.473	465.17	90.835	774.966	115.515	168.874	90.767	284.702	656.333
	299.919	180.894	532.414	143.916	572.343	115.515	673.846	494.264	727.81	563.478	650.605
	503.26	134.56	794.761	168.8	49.762	673.846	342.406	225.925	77.383	459.795	494.52

c. AFM Measurements of CNCs-CM500 fibers length and width

Table 9 AFM Measurements of CNCs-CM500 fibers length and width.

	CNCs – CM500 Measurements									
Length (nm)	598.27	397.46	461.99	206.61	330.09	332.13	266.46	326.37	287.79	428.63
	311.84	470.06	483.73	213.17	455.97	216.08	285.12	276.61	183.47	359.01
	304.47	502.20	403.94	338.15	417.75	354.80	343.42	486.10	241.33	306.54
	283.58	394.38	288.22	343.89	438.24	326.90	291.68	427.77	209.17	400.27
	436.18	256.27	389.36	299.84	348.47	324.28	327.06	381.99	399.30	231.44
	323.75	379.05	273.45	203.85	557.41	339.16	388.35	212.10	238.33	430.04
	149.07	343.42	371.25	324.72	274.42	262.92	253.85	279.21	284.70	526.42
	271.82	197.54	344.30	239.68	268.86	550.36	259.88	274.66	441.43	371.36
	395.78	500.00	375.90	265.14	315.98	247.96	279.48	351.53	285.01	240.20
	373.28	238.27	327.01	212.54	364.01	232.47	289.26	257.19	239.18	282.92
	381.34	551.62	310.43	423.63	403.19	301.12	289.52	219.12	272.04	282.54
	469.19	310.43	284.06	185.42	203.04	537.64	301.12	485.26	238.51	268.83
	476.25	313.47	376.48	584.61	260.60	317.19	269.44	415.65	312.73	321.74
	495.08	330.51	435.69	383.43	236.55	281.76	273.45	434.27	316.90	393.55
	496.72	291.04	247.28	458.21	278.86	292.19	399.44	281.80	300.24	428.63
Width (nm)	5.352	2.253	7.356	7.075	7.752	9.59	10.33	12.27	8.631	18.25
	7.34	5.865	10.57	9.158	6.275	7.79	10.05	10.56	8.234	21.21
	7.466	8.278	4.433	8.149	8.123	7.205	13.77	8.075	6.946	14.94
	7.048	6.391	8.56	10.07	9.3	4.615	15.88	13.68	8.264	13.73
	10.24	6.927	8.635	9.333	10.47	8.777	9.317	9.6	7.469	16.96
	4.526	9.941	9.288	8.46	10.24	1.261	10.06	8.675	5.041	9.049
	7.365	7.826	7.318	3.677	7.375	4.084	10.32	12.79	9.129	10.68
	6.06	5.013	7.854	8.109	7.32	6.453	10.36	12.73	7.19	12.43
	3.316	5.908	10.86	10.68	7.324	5.475	9.214	9.953	7.958	20.44
	8.963	6.25	11.01	9.575	7.572	4.23	11.13	9.498	10.75	11.89
	6.676	6.191	11	8.158	4.966	5.661	12.42	9.12	13.49	9.22
	9.029	10.24	9.816	8.183	9.429	4.549	8.356	8.557	14.59	6.984
	5.679	6.753	6.547	11.33	5.473	2.695	6.91	9.138	10.63	10.59
	7.697	8.052	11.26	10.74	7.901	1.668	6.662	10.11	9.343	11.3
	7.039	7.088	12.33	7.941	5.633	11.22	14.81	8.949	12.87	18.25

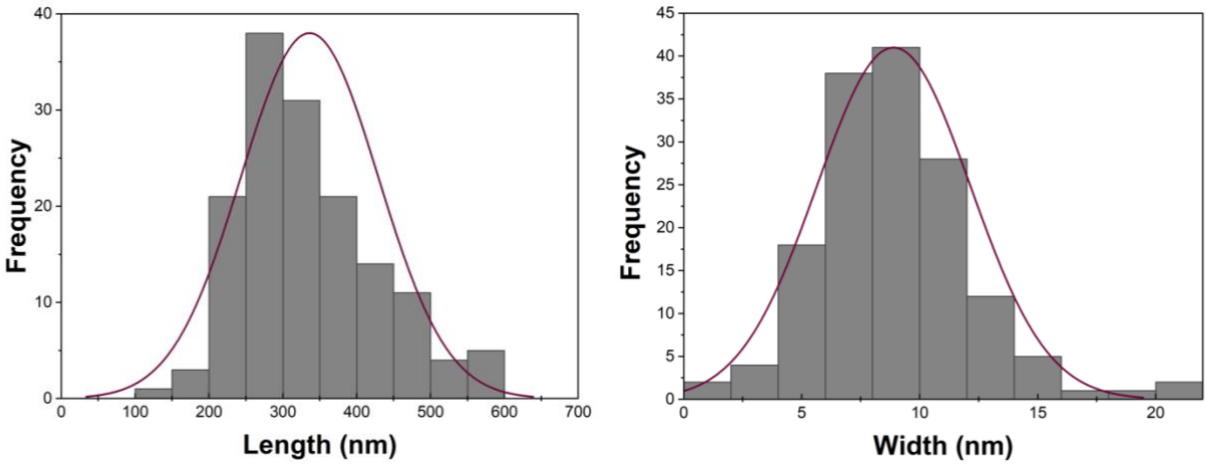

Figure 7.2 CNCs-CM500 histograms representing particles length and diameter distribution.

d. AFM Measurements of CNCs-CMC fibers length and width

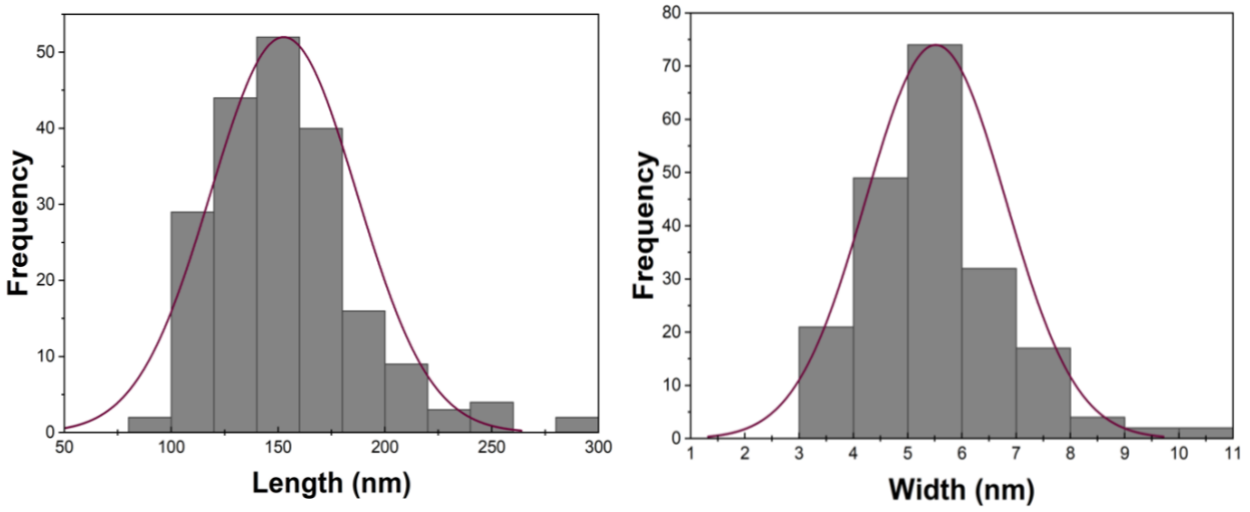

Figure 7.3 CNCs-CMC histograms representing particles length and diameter distribution.

Table 10 AFM Measurements of CNCs-CMC fibers length and width.

	CNCs – CM500 Measurements									
Length (nm)	115.92	168.65	173.33	121.71	114.18	117.14	146.25	185.57	165.25	139.10
	244.58	109.09	185.78	164.28	137.72	137.04	161.56	140.90	177.28	133.53
	295.67	169.21	155.88	110.71	209.58	108.44	156.08	131.08	163.96	144.51
	180.06	210.65	178.75	150.76	152.72	154.60	205.58	140.05	198.06	162.00
	192.54	150.56	184.99	106.79	144.14	116.03	240.15	152.52	180.75	127.93
	148.98	149.07	122.14	114.06	126.43	171.89	169.91	206.61	166.67	181.94
	131.38	143.31	174.42	154.91	156.20	103.93	137.17	107.41	149.31	142.28
	179.98	138.87	126.57	162.63	143.03	161.56	186.00	129.34	101.68	162.98
	249.69	136.00	147.91	123.98	171.96	170.72	165.23	126.39	164.93	138.20
	134.06	158.34	148.75	150.29	161.86	235.95	110.83	164.53	148.00	164.09
	161.48	220.74	164.18	241.07	134.72	122.29	154.57	120.09	168.65	170.62
	208.22	168.63	135.87	127.51	165.17	215.32	138.01	164.53	106.79	153.21
	163.85	141.31	133.83	141.91	118.27	148.98	143.77	156.08	132.73	134.06
	123.91	152.05	104.44	167.49	125.44	185.59	202.60	130.13	185.21	125.58
	159.12	179.98	115.69	105.33	140.62	182.12	128.24	199.27	123.59	105.33
Width (nm)	6.10	5.10	4.41	5.36	4.63	5.83	5.37	5.60	6.36	4.16
	6.22	4.53	5.45	5.46	3.94	4.54	4.70	4.87	5.36	4.88
	4.27	5.67	5.22	3.03	5.61	5.99	4.68	4.14	6.47	7.84
	7.12	6.50	3.99	4.00	6.00	3.99	5.04	7.58	4.89	6.33
	8.71	5.47	5.03	4.56	6.33	3.36	6.99	4.12	4.89	5.95
	5.79	5.59	4.23	3.08	4.25	5.15	5.01	6.71	5.41	8.50
	5.38	5.19	4.41	3.41	4.78	6.05	5.53	4.84	4.78	10.21
	4.87	4.37	5.40	4.70	6.13	5.79	5.39	5.02	6.60	7.14
	5.60	4.01	4.61	4.05	4.96	4.85	4.98	5.09	5.10	8.42
	6.16	5.66	3.32	5.19	3.88	3.87	6.74	4.36	6.13	10.31
	5.83	6.73	3.60	5.72	3.60	6.32	4.67	4.71	6.41	7.37
	5.45	3.59	4.80	5.82	4.36	3.47	4.37	7.45	5.05	7.64
	6.04	3.92	3.60	5.04	3.38	5.28	5.38	5.26	5.02	9.01
	6.10	5.66	4.21	5.69	4.18	5.78	4.24	6.57	5.09	8.70
	5.78	3.70	3.46	4.91	5.47	4.62	5.53	5.19	5.29	9.95

e. CNCs/HPC composite films

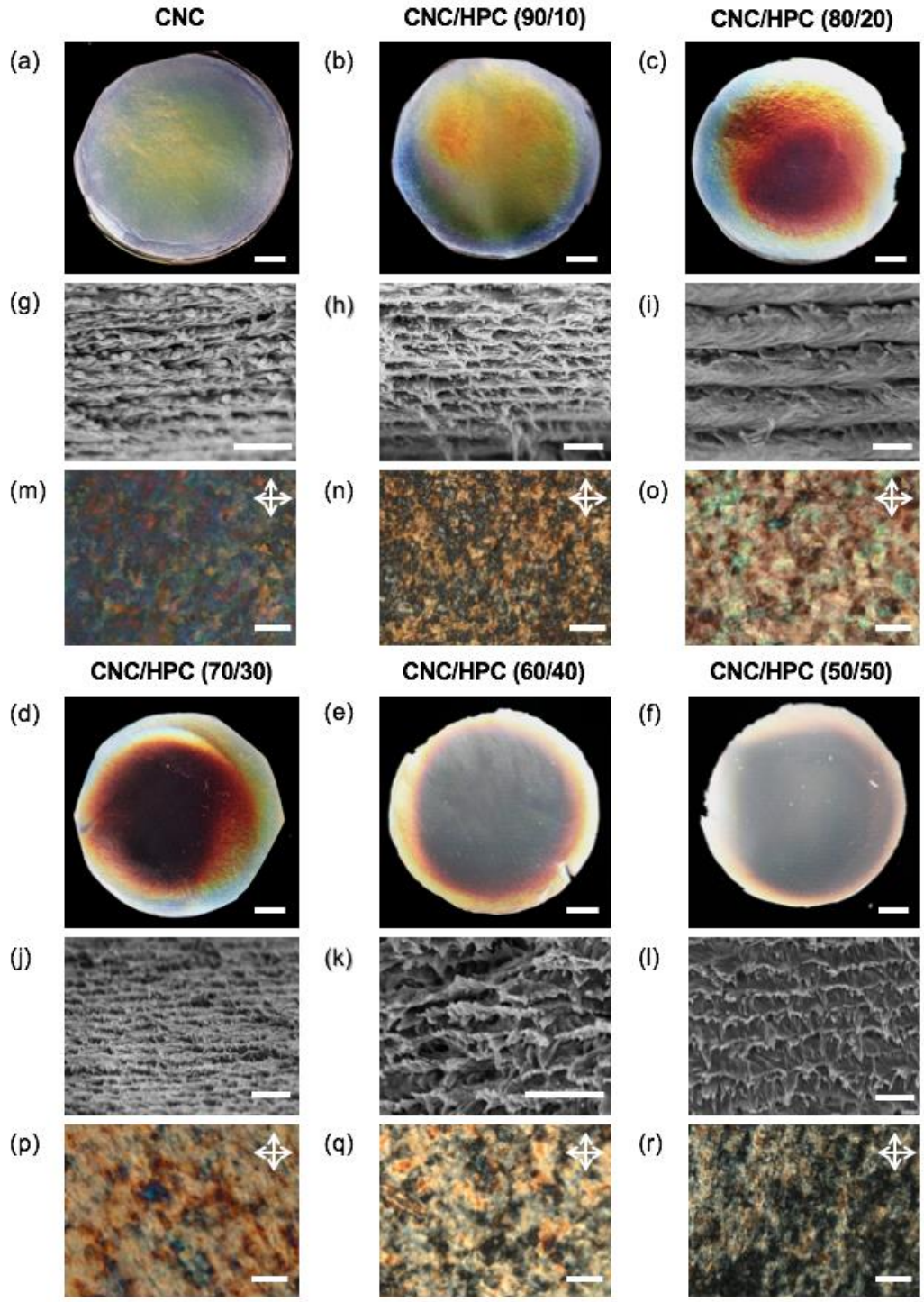

Figure 7.4 Photography taken with LCP polarizers (a) to (f), SEM (g) to (l) and POM (m) to (r) of CNCs/HPC films, with 0, 10, 20, 30, 40, 50% w/w HPC concentration. Scales: 5 mm for (a) to (f), 500 nm for (g) to (i) and 100 μm POM images.

f. CNCs-K/HPC films ($\overline{M_w}$= 100 000, 300 000 and 600 000), Photographs under visible light and left-handed and right-handed circularly polarized light and spectra analyzes

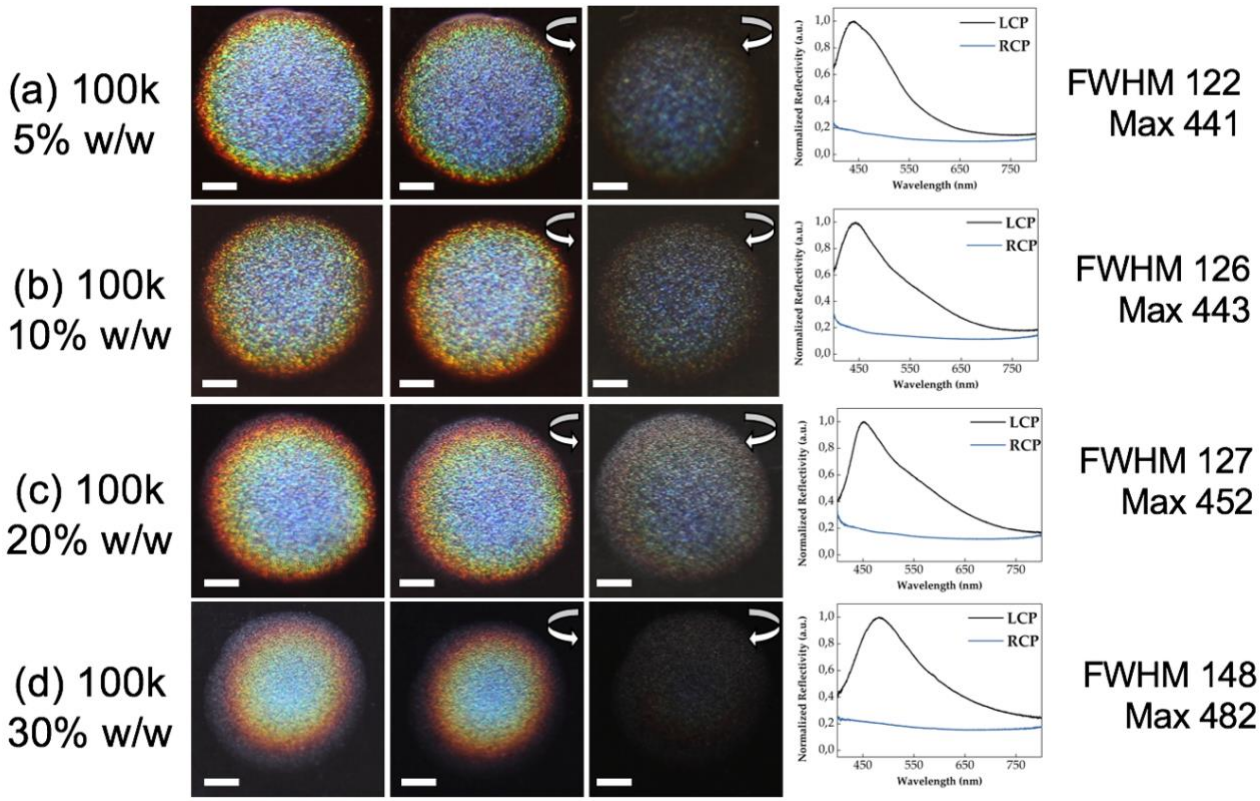

Figure 7.5 Photographic images of CNCs-K/HPC composite films, using different percentages 5% (a), 10% (b), 20% (c) and 30% (d) w/w of HPC $\overline{M_w}$= 100 000, respectively, observed under visible light, left and right circular polarize light (indicated by the direction of the arrows); the obtained Vis spectra respectively was acquired with a spectrophotometer accoupled to the POM and the correspondingly profilometry. The scale bar corresponds to 1mm.

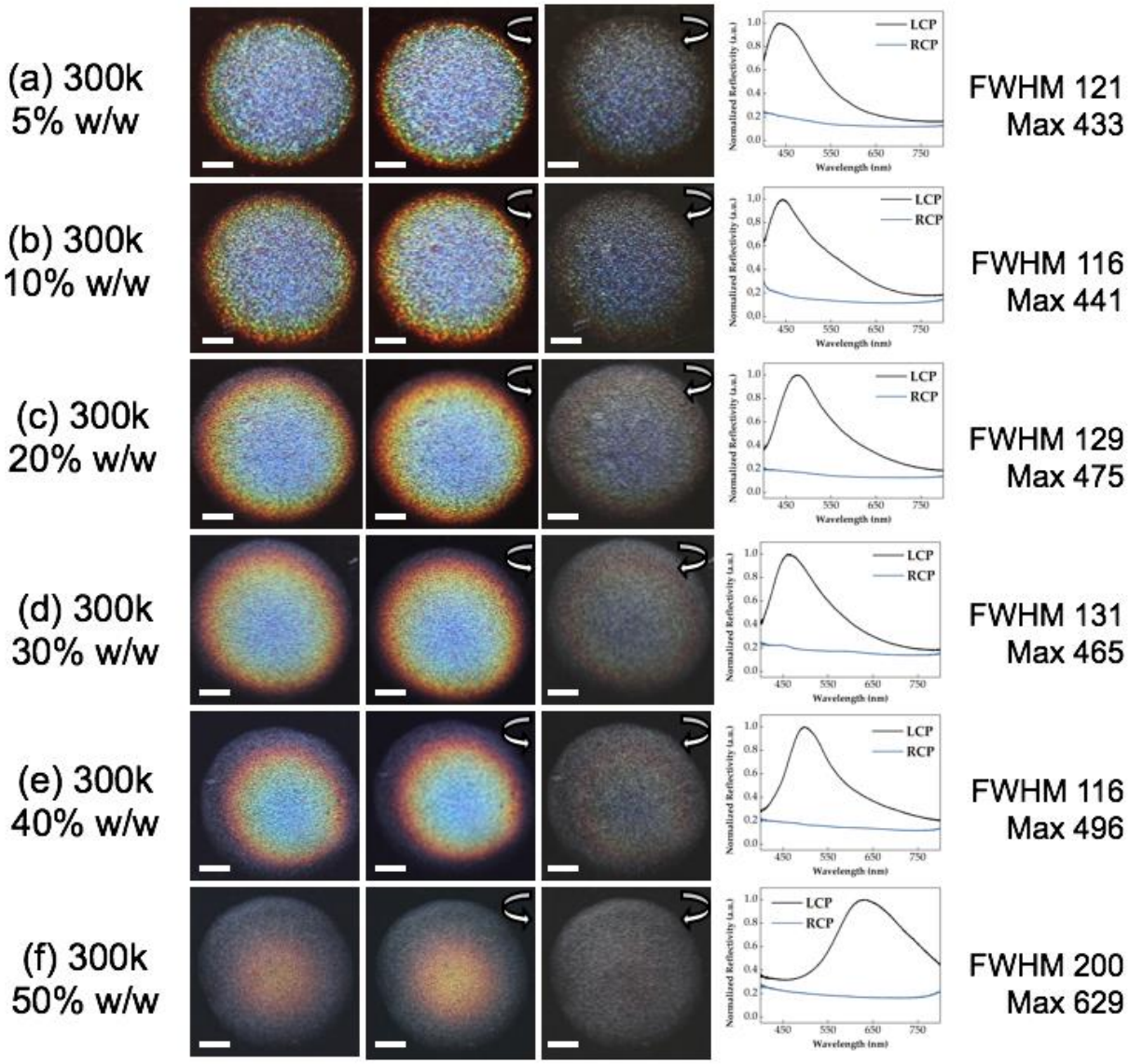

Figure 7.6 Photographic images of CNCs-K/HPC composite films, using different percentages 5% (a), 10% (b), 20% (c), 30% (d), 40% (e) and 50% (f) w/w of HPC $\overline{M_w}$= 300 000, respectively, observed under visible light, left and right circular polarize light (indicated by the direction of the arrows); the obtained Vis spectra respectively was acquired with a spectrophotometer accoupled to the POM and the correspondingly profilometry. The scale bar corresponds to 1mm.

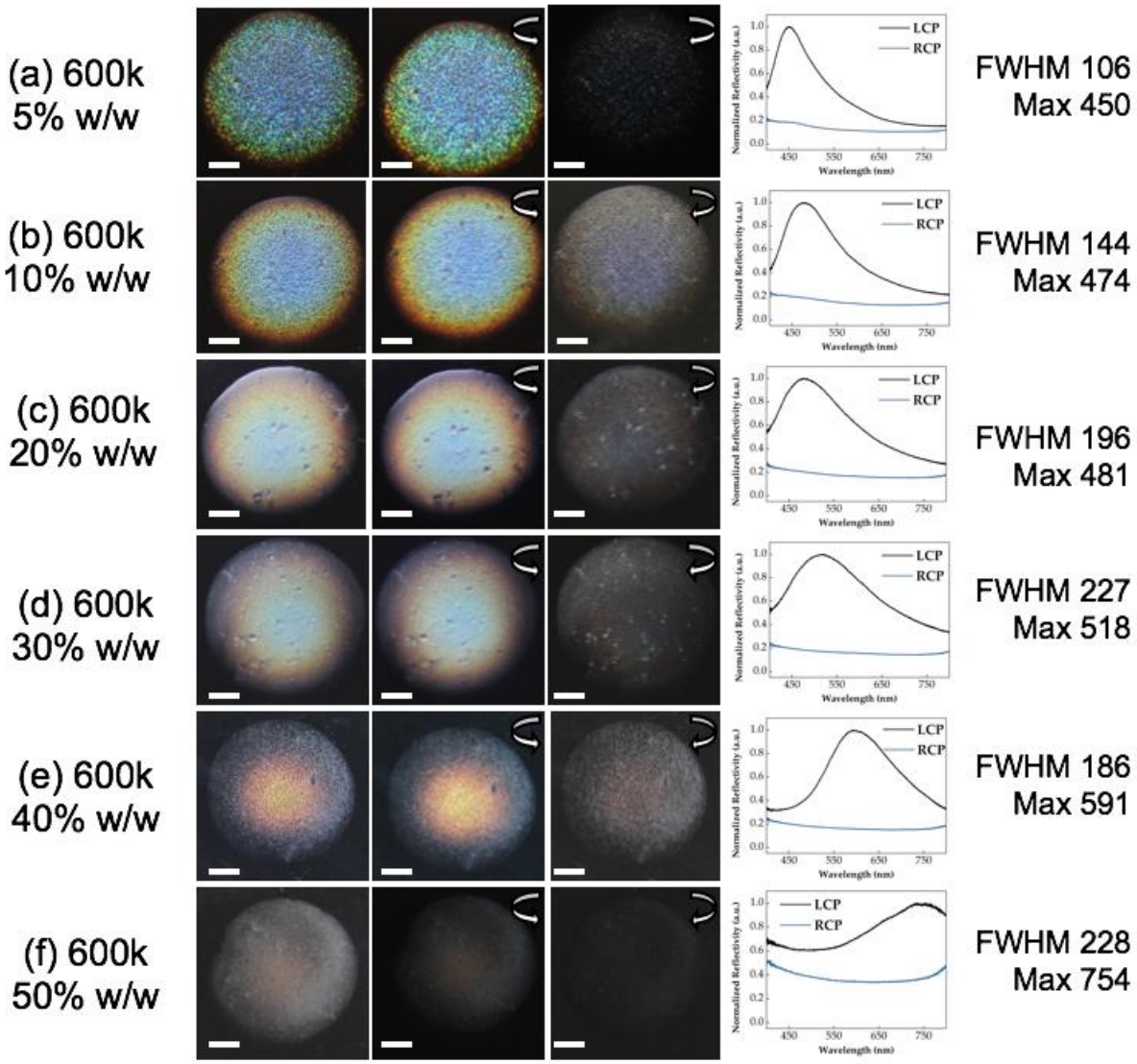

Figure 7.7 Photographic images of CNCs-K/HPC composite films, using different percentages 5% (a), 10% (b), 20% (c), 30% (d), 40% (e) and 50% (f) w/w of HPC $\overline{M_w}$= 600 000, respectively, observed under visible light, left and right circular polarize light (indicated by the direction of the arrows); the obtained Vis spectra respectively was acquired with a spectrophotometer accoupled to the POM and the correspondingly profilometry. The scale bar corresponds to 1mm.

g. Thickness measurements of the CNCs-K/HPC films

Table 11 Thickness measurements of the CNCs-K/HPC films

	HPC (w/w %)				
	10%	20%	30%	40%	50%
Measurements (mm)	0.168	0.151	0.067	0.099	0.067
	0.198	0.204	0.071	0.101	0.065
	0.159	0.197	0.082	0.092	0.060
	0.178	0.193	0.073	0.094	0.081
	0.196	0.211	0.076	0.086	0.059
	0.176	0.180	0.075	0.097	0.076
	0.185	0.215	0.084	0.085	0.078
	0.182	0.106	0.057	0.095	0.074
	0.161	0.199	0.084	0.061	0.068
	0.209	0.202	0.072	0.076	0.075

ELSEVIER LICENSE
TERMS AND CONDITIONS

Jan 07, 2020

This Agreement between FCT-UNL ("You") and Elsevier ("Elsevier") consists of your license details and the terms and conditions provided by Elsevier and Copyright Clearance Center.

License Number	4743840066199
License date	Jan 07, 2020
Licensed Content Publisher	Elsevier
Licensed Content Publication	Current Opinion in Solid State & Materials Science
Licensed Content Title	Recent advances in the manipulation of circularly polarised light with cellulose nanocrystal films
Licensed Content Author	S.N. Fernandes,L.F. Lopes,M.H. Godinho
Licensed Content Date	Apr 1, 2019
Licensed Content Volume	23
Licensed Content Issue	2
Licensed Content Pages	11
Start Page	63
End Page	73
Type of Use	reuse in a thesis/dissertation

Portion	figures/tables/illustrations
Number of figures/tables/illustrations	2
Format	electronic
Are you the author of this Elsevier article?	No
Will you be translating?	No
Title	Bio-inspired nanocellulose composites systems with structural coloration as optical security features
Institution name	Faculdade de Ciências e Tecnologia da Universidade Nova de Lisboa
Expected presentation date	Feb 2020
Portions	Figure 2.3
Requestor Location	FCT-UNL Faculdade de Ciências e Tecnologia Caparica, Lisboa 2829-516 Portugal Attn: FCT-UNL
Publisher Tax ID	GB 494 6272 12
Total	0.00 EUR
Terms and Conditions	

INTRODUCTION

1. The publisher for this copyrighted material is Elsevier. By clicking "accept" in connection with completing this licensing transaction, you agree that the following terms and conditions apply to this transaction (along with the Billing and Payment terms and conditions established by Copyright Clearance Center, Inc. ("CCC"), at the time that you opened your Rightslink account and that are available at any time at http://myaccount.copyright.com).

GENERAL TERMS

2. Elsevier hereby grants you permission to reproduce the aforementioned material subject to the terms and conditions indicated.

3. Acknowledgement: If any part of the material to be used (for example, figures) has appeared in our publication with credit or acknowledgement to another source, permission must also be sought from that source. If such permission is not obtained then that material may not be included in your publication/copies. Suitable acknowledgement to the source must be made, either as a footnote or in a reference list at the end of your publication, as follows:

"Reprinted from Publication title, Vol /edition number, Author(s), Title of article / title of chapter, Pages No., Copyright (Year), with permission from Elsevier [OR APPLICABLE SOCIETY COPYRIGHT OWNER]." Also Lancet special credit - "Reprinted from The Lancet, Vol. number, Author(s), Title of article, Pages No., Copyright (Year), with permission from Elsevier."

4. Reproduction of this material is confined to the purpose and/or media for which permission is hereby given.

5. Altering/Modifying Material: Not Permitted. However figures and illustrations may be altered/adapted minimally to serve your work. Any other abbreviations, additions, deletions and/or any other alterations shall be made only with prior written authorization of Elsevier Ltd. (Please contact Elsevier at permissions@elsevier.com). No modifications can be made to any Lancet figures/tables and they must be reproduced in full.

6. If the permission fee for the requested use of our material is waived in this instance, please be advised that your future requests for Elsevier materials may attract a fee.

7. Reservation of Rights: Publisher reserves all rights not specifically granted in the combination of (i) the license details provided by you and accepted in the course of this licensing transaction, (ii) these terms and conditions and (iii) CCC's Billing and Payment terms and conditions.

8. License Contingent Upon Payment: While you may exercise the rights licensed immediately upon issuance of the license at the end of the licensing process for the transaction, provided that you have disclosed complete and accurate details of your proposed use, no license is finally effective unless and until full payment is received from you (either by publisher or by CCC) as provided in CCC's Billing and Payment terms and conditions. If full payment is not received on a timely basis, then any license preliminarily granted shall be deemed automatically revoked and shall be void as if never granted. Further, in the event that you breach any of these terms and conditions or any of CCC's Billing and Payment terms and conditions, the license is automatically revoked and shall be void as if never granted. Use of materials as described in a revoked license, as well as any use of the materials beyond the scope of an unrevoked license, may constitute copyright infringement and publisher reserves the right to take any and all action to protect its copyright in the materials.

9. Warranties: Publisher makes no representations or warranties with respect to the licensed material.

10. Indemnity: You hereby indemnify and agree to hold harmless publisher and CCC, and their respective officers, directors, employees and agents, from and against any and all claims arising out of your use of the licensed material other than as specifically authorized pursuant to this license.

11. No Transfer of License: This license is personal to you and may not be sublicensed, assigned, or transferred by you to any other person without publisher's written permission.

12. No Amendment Except in Writing: This license may not be amended except in a writing signed by both parties (or, in the case of publisher, by CCC on publisher's behalf).

13. Objection to Contrary Terms: Publisher hereby objects to any terms contained in any purchase order, acknowledgment, check endorsement or other writing prepared by you, which terms are inconsistent with these terms and conditions or CCC's Billing and Payment terms and conditions. These terms and conditions, together with CCC's Billing and Payment terms and conditions (which are incorporated herein), comprise the entire agreement between you and publisher (and CCC) concerning this licensing transaction. In the event of any conflict between your obligations established by these terms and conditions and those established by CCC's Billing and Payment terms and conditions, these terms and conditions shall control.

14. Revocation: Elsevier or Copyright Clearance Center may deny the permissions described in this License at their sole discretion, for any reason or no reason, with a full refund payable to you. Notice of such denial will be made using the contact information provided by you. Failure to receive such notice will not alter or invalidate the denial. In no event will Elsevier or Copyright Clearance Center be responsible or liable for any costs, expenses or damage incurred by you as a result of a denial of your permission request, other than a refund of the amount(s) paid by you to Elsevier and/or Copyright Clearance Center for denied permissions.

LIMITED LICENSE

The following terms and conditions apply only to specific license types:

15. **Translation**: This permission is granted for non-exclusive world **English** rights only unless your license was granted for translation rights. If you licensed translation rights you may only translate this content into the languages you requested. A professional translator must perform all translations and reproduce the content word for word preserving the integrity of the article.

16. **Posting licensed content on any Website**: The following terms and conditions apply as follows: Licensing material from an Elsevier journal: All content posted to the web site must maintain the copyright information line on the bottom of each image; A hyper-text must be included to the Homepage of the journal from which you are licensing at http://www.sciencedirect.com/science/journal/xxxxx or the Elsevier homepage for books at http://www.elsevier.com; Central Storage: This license does not include permission for a scanned version of the material to be stored in a central repository such as that provided by Heron/XanEdu.

Licensing material from an Elsevier book: A hyper-text link must be included to the Elsevier homepage at http://www.elsevier.com . All content posted to the web site must maintain the copyright information line on the bottom of each image.

Posting licensed content on Electronic reserve: In addition to the above the following clauses are applicable: The web site must be password-protected and made available only to bona fide students registered on a relevant course. This permission is granted for 1 year only. You may obtain a new license for future website posting.

17. **For journal authors:** the following clauses are applicable in addition to the above:

Preprints:

A preprint is an author's own write-up of research results and analysis, it has not been peer-reviewed, nor has it had any other value added to it by a publisher (such as formatting, copyright, technical enhancement etc.).

Authors can share their preprints anywhere at any time. Preprints should not be added to or enhanced in any way in order to appear more like, or to substitute for, the final versions of articles however authors can update their preprints on arXiv or RePEc with their Accepted Author Manuscript (see below).

If accepted for publication, we encourage authors to link from the preprint to their formal publication via its DOI. Millions of researchers have access to the formal publications on ScienceDirect, and so links will help users to find, access, cite and use the best available version. Please note that Cell Press, The Lancet and some society-owned have different preprint policies. Information on these policies is available on the journal homepage.

Accepted Author Manuscripts: An accepted author manuscript is the manuscript of an article that has been accepted for publication and which typically includes author-incorporated changes suggested during submission, peer review and editor-author communications.

Authors can share their accepted author manuscript:

- immediately
    - via their non-commercial person homepage or blog
    - by updating a preprint in arXiv or RePEc with the accepted manuscript
    - via their research institute or institutional repository for internal institutional uses or as part of an invitation-only research collaboration work-group
    - directly by providing copies to their students or to research collaborators for their personal use
    - for private scholarly sharing as part of an invitation-only work group on commercial sites with which Elsevier has an agreement
- After the embargo period
    - via non-commercial hosting platforms such as their institutional repository
    - via commercial sites with which Elsevier has an agreement

In all cases accepted manuscripts should:

- link to the formal publication via its DOI
- bear a CC-BY-NC-ND license - this is easy to do
- if aggregated with other manuscripts, for example in a repository or other site, be shared in alignment with our hosting policy not be added to or enhanced in any way to appear more like, or to substitute for, the published journal article.

Published journal article (JPA): A published journal article (PJA) is the definitive final record of published research that appears or will appear in the journal and embodies all value-adding publishing activities including peer review co-ordination, copy-editing, formatting, (if relevant) pagination and online enrichment.

Policies for sharing publishing journal articles differ for subscription and gold open access articles:

Subscription Articles: If you are an author, please share a link to your article rather than the full-text. Millions of researchers have access to the formal publications on ScienceDirect, and so links will help your users to find, access, cite, and use the best available version.

Theses and dissertations which contain embedded PJAs as part of the formal submission can be posted publicly by the awarding institution with DOI links back to the formal publications on ScienceDirect.

If you are affiliated with a library that subscribes to ScienceDirect you have additional private sharing rights for others' research accessed under that agreement. This includes use for classroom teaching and internal training at the institution (including use in course packs and courseware programs), and inclusion of the article for grant funding purposes.

Gold Open Access Articles: May be shared according to the author-selected end-user license and should contain a CrossMark logo, the end user license, and a DOI link to the formal publication on ScienceDirect.

Please refer to Elsevier's posting policy for further information.

18. **For book authors** the following clauses are applicable in addition to the above: Authors are permitted to place a brief summary of their work online only. You are not allowed to download and post the published electronic version of your chapter, nor may you scan the printed edition to create an electronic version. **Posting to a repository:** Authors are permitted to post a summary of their chapter only in their institution's repository.

19. **Thesis/Dissertation**: If your license is for use in a thesis/dissertation your thesis may be submitted to your institution in either print or electronic form. Should your thesis be published commercially, please reapply for permission. These requirements include permission for the Library and Archives of Canada to supply single copies, on demand, of the complete thesis and include permission for Proquest/UMI to supply single copies, on demand, of the complete thesis. Should your thesis be published commercially, please reapply for permission. Theses and dissertations which contain embedded PJAs as part of the formal submission can be posted publicly by the awarding institution with DOI links back to the formal publications on ScienceDirect.

Elsevier Open Access Terms and Conditions

You can publish open access with Elsevier in hundreds of open access journals or in nearly 2000 established subscription journals that support open access publishing. Permitted third party re-use of these open access articles is defined by the author's choice of Creative Commons user license. See our open access license policy for more information.

Terms & Conditions applicable to all Open Access articles published with Elsevier:

Any reuse of the article must not represent the author as endorsing the adaptation of the article nor should the article be modified in such a way as to damage the author's honour or reputation. If any changes have been made, such changes must be clearly indicated.

The author(s) must be appropriately credited and we ask that you include the end user license and a DOI link to the formal publication on ScienceDirect.

If any part of the material to be used (for example, figures) has appeared in our publication with credit or acknowledgement to another source it is the responsibility of the user to ensure their reuse complies with the terms and conditions determined by the rights holder.

Additional Terms & Conditions applicable to each Creative Commons user license:

CC BY: The CC-BY license allows users to copy, to create extracts, abstracts and new works from the Article, to alter and revise the Article and to make commercial use of the Article (including reuse and/or resale of the Article by commercial entities), provided the user gives appropriate credit (with a link to the formal publication through the relevant DOI), provides a link to the license, indicates if changes were made and the licensor is not represented as endorsing the use made of the work. The full details of the license are available at http://creativecommons.org/licenses/by/4.0.

CC BY NC SA: The CC BY-NC-SA license allows users to copy, to create extracts, abstracts and new works from the Article, to alter and revise the Article, provided this is not done for commercial purposes, and that the user gives appropriate credit (with a link to the formal publication through the relevant DOI), provides a link to the license, indicates if changes were made and the licensor is not represented as endorsing the use made of the

work. Further, any new works must be made available on the same conditions. The full details of the license are available at http://creativecommons.org/licenses/by-nc-sa/4.0.

CC BY NC ND: The CC BY-NC-ND license allows users to copy and distribute the Article, provided this is not done for commercial purposes and further does not permit distribution of the Article if it is changed or edited in any way, and provided the user gives appropriate credit (with a link to the formal publication through the relevant DOI), provides a link to the license, and that the licensor is not represented as endorsing the use made of the work. The full details of the license are available at http://creativecommons.org/licenses/by-nc-nd/4.0. Any commercial reuse of Open Access articles published with a CC BY NC SA or CC BY NC ND license requires permission from Elsevier and will be subject to a fee.

Commercial reuse includes:

- Associating advertising with the full text of the Article
- Charging fees for document delivery or access
- Article aggregation
- Systematic distribution via e-mail lists or share buttons

Posting or linking by commercial companies for use by customers of those companies.

20. **Other Conditions**:

v1.9

Questions? customercare@copyright.com or +1-855-239-3415 (toll free in the US) or +1-978-646-2777.